

**LG Chem, Ltd.**

LG Twin Tower, 128 Yeoui-daero, Yeongdeungpo-gu, Seoul 07336, Korea  
T. +82-2-3773-1114 F. +82-2-3773-7935 www.lgchem.com

Kyunghyun Nahm  
Deputy General Counsel  
[khnahm@lgchem.com](mailto:khnahm@lgchem.com)

July 30, 2020

Arizona Corporation Commission  
1200 W. Washington Street  
Phoenix, AZ 85007

**RE: In the Matter of the Commission's Inquiry of Arizona Public Service Battery Incident at McMicken Energy Storage Facility Pursuant to AZ Administrative Code R14-2-101. (Docket No. E-01345A-19-0076)**

LG Chem, Ltd. provides these comments in response to APS' July 27, 2020 submission "McMicken Battery Energy Storage Event Technical Analysis and Recommendations." All industry stakeholders share the goal of reducing safety risks associated with BESS installations so that the promise of this technology can be fully realized in the future. This Commission, the public, and the first responders who were injured at the McMicken facility deserve a complete analysis.

Many parties invested extensive resources in trying to understand all aspects of the event. LG Chem notes, however, that DNV-GL, the author of the "final" report submitted by APS, did not directly participate in the key investigations (site visits with the other parties and their experts, direct forensic examination of artifacts, etc.), although its report does summarize selected findings of APS' retained consultants. DNV-GL explicitly admits that despite the involvement of many other failure analysis firms and experts, its report reflects DNV-GL's views alone -- not a consensus view. This may, in part, explain why many of the opinions set forth in the report cannot be squared with the findings of the independent experts retained by LG Chem to investigate the cause of the failure -- experts who directly participated in the many site visits and direct analysis of the evidence.

In fact, as explained below, the independent experts retained by LG Chem believe that the evidence rules out DNV-GL's theory regarding the cause of the initial thermal runaway event. However, DNV-GL ignored other experts' views and key evidence without any explanation. So to provide a more complete record, LG Chem is submitting to the ACC a report prepared by Exponent, a recognized expert in the relevant subject matter. Exponent's report includes an executive summary of its key findings and comments on the various shortcomings of the DNV-GL report.

**LG Chem, Ltd.**

LG Twin Tower, 128 Yeoui-daero, Yeongdeungpo-gu, Seoul 07336, Korea  
T. +82-2-3773-1114 F. +82-2-3773-7935 [www.lgchem.com](http://www.lgchem.com)

Based upon the Exponent report, and LG Chem's own analysis of the five factors that DNV-GL concluded contributed to the ultimate event, LG Chem offers the following comments.

**Cause of the thermal runaway**

Based on the available evidence, metallic lithium plating did not cause an internal cell failure leading to the initial thermal runaway event at McMicken. The facts of the incident that have been established to a reasonable degree of scientific rigor, together with relevant peer reviewed literature, rule out the initiating cause proposed by DNV-GL. The analysis performed by APS and their experts could not produce evidence of metallic lithium plating as the cause of thermal runaway, and their test experiments could not produce test results that showed internal cell failure was a viable cause. Rather, the data collected and analyzed point to initiation of cell thermal runaway through intense heating of the incident cells caused by an external heat source such as external electrical arcing on Rack 15. The two primary bases for this conclusion, explained below, are substantiated by the available evidence, but the DNV-GL report ignores them without any explanation.

First, Exponent tested the internal cell failure theory by forcing a parallel cell configuration into thermal runaway. Exponent then compared the resulting voltage profile to the voltage profile recorded during the incident, and found that the two did not match. Hence it is unlikely that an internal short within a single cell caused the observed voltage excursion. Exponent's report includes a detailed discussion on this critical point.

Second, the data recorded shows that, during the incident, there was a discharging current of 4.9A (amps) present during the voltage excursion. Considering that the current sensor was placed in between modules 7 and 8, this could be explained by two electrical isolation failures which came to exist simultaneously within the subject rack; therefore, the rack's DC current could have been associated with arcing and subsequent temperature rise which is observed via the power conversion system's (PCS) temperature sensors. DNV-GL's own report acknowledges that "the current flipped from -27.9A charging to 4.9 A discharging," but offered no explanation for it. The fact that the discharging current was recorded at 4.9A, instead of 0A, means the current indeed flowed to somewhere else, supporting a double point electrical isolation failure – not an internal cell short. Exponent's report also discusses the evidence supporting this critical point in detail.

**LG Chem, Ltd.**

LG Twin Tower, 128 Yeoui-daero, Yeongdeungpo-gu, Seoul 07336, Korea  
T. +82-2-3773-1114 F. +82-2-3773-7935 [www.lgchem.com](http://www.lgchem.com)

Exponent also addresses the reasoning set forth in the DNV-GL report regarding the cause of the thermal runaway event. DNV-GL's report relies primarily on findings of deposits containing lithium in other (presumably similarly situated) battery cells. DNV-GL also relies on its understanding that voltage drops in cells were the first anomaly encountered, and that the thermal event was hot enough to melt and weaken the aluminum module frames and cause material to be ejected from some of the cells. As is explained in Exponent's report:

- Exponent and LG Chem independently tested the deposits in question using two distinct methods and found that the deposits were non-conductive. Therefore the deposits could not have caused an internal short circuit. Moreover, the available data do not show the dramatic cell-performance degradation which would occur if lithium ions in the electrolyte were being reduced to lithium metal in the quantities required to create a short circuit capable of initiating thermal runaway.
- Voltage drops were not the first anomaly encountered. The insulation monitoring device showed intermittent isolation drops prior to the voltage excursions. This could only occur if the rack electrical isolation failed
- The extent of the damage and the fact that the damage is primarily noted on the edge of the cells is more consistent with an attack on the cells from an intense external heat source than from an internal short circuit

**Safety Standards**

LG Chem agrees that, today, there is an industry consensus that NOVEC 1230 clean agent cannot stop module to module propagation during a thermal runaway event. This was not known at the time the third parties responsible for the McMicken system design selected NOVEC 1230. Moreover, the relevant safety standards in place then did not require prevention of module to module propagation in the event of thermal runaway. Today, new standards are in place that require mitigation measures to control module to module spread, and LG Chem is a leader in the development of technologies that allow new BESS installations to meet or exceed these new standards.

The LG Chem cells and modules installed at the McMicken site were state of the art cells and designed to meet all relevant safety standards in place when the site was commissioned. LG Chem treats safety as a top priority and regularly participates in industry standard safety efforts, including the NFPA 855 Technical Committee and UL 1973 Technical Standards Panel. As

**LG Chem, Ltd.**

LG Twin Tower, 128 Yeoui-daero, Yeongdeungpo-gu, Seoul 07336, Korea  
T. +82-2-3773-1114 F. +82-2-3773-7935 [www.lgchem.com](http://www.lgchem.com)

discussed above, more recent standards developed after consultation with relevant industry stakeholders focus on mitigating the risk of module to module spread if thermal runaway occurs in BESS installations. As the industry continues to evolve and relevant stakeholders learn more about best practices for cells with higher energy density, new designs and monitoring systems are being developed to satisfy new consensus standards. In sum, LG Chem's module designs were fully compliant with standards in place when the McMicken system was commissioned, and its current designs are fully compliant with more recently adopted safety standards.

**Flammable off-gas venting**

LG Chem agrees that flammable off-gases associated with thermal runaway concentrated within the container because there was no venting mechanism. To be clear, the system design for the McMicken site was the responsibility of other parties, not LG Chem, as discussed in the DNV-GL report. That said, LG Chem does not agree that related risks were "unknown" to industry participants when the McMicken system was designed, built and commissioned. According to Exponent, "[a]s early as 2005, researchers were able to show that the products of incomplete combustion during thermal runaway were, themselves, flammable gases." Moreover, as discussed in the attached Exponent report, *"the risk of explosion from thermal runaway vent gases was known well in advance of the design and installation of the Surprise, AZ facility and methods existed to measure and understand the explosive behavior of lithium-ion battery vent gases in a way that makes engineering ventilation systems for stationary power storage facilities possible. A properly designed ventilation system could have prevented the atmosphere within the container from ever reaching explosive concentrations."*

Further underscoring the widespread knowledge of this risk, during a Workshop on Energy Systems and the Built Environment by the NFPA Fire Protection Research Foundation hosted by the Fire Department of New York held in November 2015, these hazards were clearly recognized and considered by the nearly 100 industry participants. As stated in written program materials prepared by the Foundation:

*Combustible and toxic gases produced pose a hazard and need to be ventilated safely. Some ESS (box) have ventilation designed to off-gas to the enclosure (room). The room would then need to be ventilated. Consideration needs to be given for the types of gases produced and separate ventilation from building HVAC systems as well as potential interaction with the activation*

**LG Chem, Ltd.**

LG Twin Tower, 128 Yeoui-daero, Yeongdeungpo-gu, Seoul 07336, Korea  
T. +82-2-3773-1114 F. +82-2-3773-7935 [www.lgchem.com](http://www.lgchem.com)

*and effectiveness of suppression systems within these operating ventilation systems.<sup>1</sup>*

It bears noting that the DNV-GL report states (at page 61) that “[f]or DNV GL, explosion risk of off-gases from individual battery cells became a ‘known-known’ in 2012 ....” Thus, these hazards were widely known in the fire safety industry and reasonably knowable to others with a responsibility for fire safety, including the APS team, before the McMicken site was commissioned.

**Emergency response plan**

LG Chem agrees that the emergency response plan and the overall incident site control protocol implemented by APS and Fluence were inadequate. LG Chem disagrees with DNV-GL’s comments that the plan’s shortcomings can be attributed in any way to “limited or incomplete” disclosure of information by LG Chem.

As discussed above, the risk of thermal runaway and recommended safety methods for addressing it were well known in the industry when the site was designed and constructed. APS’s failure analysis firm acknowledges the common sense proposition that the site owner (APS) and the parties designated to design the system and manage site operations (AES and Fluence) shared a collective duty to develop and implement an emergency response plan and an incident command and control plan. The site owner and designated day-to-day operations vendors are the subject matter experts relied upon by first responders for competent and safe technical advice during such incidents. The time to develop careful plans to protect first responders is during the design and commissioning and operation of these projects – not after an incident has started. Knowledgeable experts in the field have commented that if effective planning, training and documentation had been undertaken in accordance with accepted practices, APS and its agents would have followed a well-established protocol that directed first responders to refrain from opening the BESS enclosure door—until it could be opened safely. And that is the advice LG Chem provided when Fluence contacted LG Chem on April 19th during the incident, before the site owner and its agents subsequently allowed the first responders to open the door, triggering the deflagration event.

---

<sup>1</sup> “Workshop on Energy Storage Systems and the Built Environment.”, Proceedings, p. 5. Held: 19 November 2015 in New York, New York. Prepared by Daniel J. Gorham National Fire Protection Research Foundation, Quincy, Massachusetts, USA.

**LG Chem, Ltd.**

LG Twin Tower, 128 Yeoui-daero, Yeongdeungpo-gu, Seoul 07336, Korea  
T. +82-2-3773-1114 F. +82-2-3773-7935 [www.lgchem.com](http://www.lgchem.com)

Inexplicably, the DNV-GL report does not review the events that occurred at the site between 17:48 (fire department arrival) and 20:04 (explosion). There is no discussion at all about incident command-and-control, communications, decision-making, and information transfer necessary to allow first responders to prevent the final deflagration event – that is – not opening the door of the BESS container until that operation could be conducted safely. In contrast, on July 28, 2020, Underwriters Laboratories issued a comprehensive report about the management of the April 19, 2019 event, including specific recommendations (“Four Firefighters Injured in Lithium-Ion Battery Energy Storage System Explosion – Arizona”). The UL report carefully reviews the events that occurred during the response to the emergency event (in contrast to the APS report), and LG Chem fully supports the recommendations for improved management of emergency responses in the UL report.

The root cause of the initial thermal runaway event at McMicken has not been identified to a reasonable degree of scientific certainty, as the observed data and evidence suggest alternative possibilities. However, the theory advanced by DNV-GL can be ruled out based on the testing performed and data reviewed. Of course, the risk of thermal runaway (whatever the cause) was well-known during the design of this system, and LG Chem agrees with DNV-GL’s conclusion that the ultimate direct cause of the injuries was poor system design and lack of necessary safety planning for this well-known potential failure mode.

LG Chem’s lithium-ion battery technologies are safe and proven solutions that enhance the performance and reliability of electric power delivery systems throughout the United States, and LG Chem looks forward to helping all industry stakeholders safely accomplish their objectives as the industry evolves.

Respectfully,

/s/ Kyunghyun Nahm  
Deputy General Counsel  
LG Chem Ltd.

Exponent<sup>®</sup>

**APS McMicken Progress Report**





## APS McMicken Progress Report

Prepared by

Exponent  
23445 North 19<sup>th</sup> Avenue  
Phoenix, Arizona 85027

July 30, 2020

---

Jan Swart, Ph.D., C.F.E.I., C.V.F.I

---

Kevin White, Ph.D.

---

Michael Cundy, Ph.D., P.E., C.F.E.I.

© Exponent, Inc.

# Contents

---

	<u>Page</u>
<b>List of Figures</b>	<b>4</b>
<b>List of Tables</b>	<b>9</b>
<b>Acronyms and Abbreviations</b>	<b>10</b>
<b>Authors</b>	<b>11</b>
<b>Introduction</b>	<b>12</b>
<b>Executive Summary</b>	<b>13</b>
Analysis of Cell Deposits	14
Lithium Deposits and the LG Chem SRS Separator	16
Analysis of SEL Cell Cycling and CT Data	19
<b>Background</b>	<b>28</b>
<b>Incident Timeline</b>	<b>34</b>
<b>Site Inspection</b>	<b>36</b>
Fire Damage Observed	41
Liquid Intrusion Observations	45
Battery Module Connection Observations	45
Key Observations	46
<b>Data Analysis</b>	<b>47</b>
Key Observations	47
Captured and Stored System Data	47
Failure Data Limitations	50
Laboratory Parallel Cell Pair Voltage Profile Characterization	54
Module Level Test	54
Cell Pair Level Test	59
Comparison to Incident Voltage Profile	62
Failure Event Data Analysis	64
Rack Voltage and Current Data Analysis	64

Rack 15 Electrical Isolation Analysis	68
Key Observations:	69
<b>McMicken Module Performance Analysis</b>	<b>70</b>
Module Discharge and Inspection	70
Analysis of Module Discharge Data	75
Key Observations	78
<b>Inspection and Removal of Rack 15</b>	<b>80</b>
Key Observations	88
<b>Rack 15 Module Removal and Inspection</b>	<b>89</b>
Key Observations	93
<b>Cell Level Analysis</b>	<b>94</b>
Introduction	94
Lithium-ion Cell Operation and Failure Concepts	95
Short Circuit Characteristics	95
Lithium Plating in Lithium-ion Cells	97
External Heating as a Route to Thermal Runaway	99
Flammable Gas Production	100
Data Analysis	102
Analysis of Cell Deposits	102
<b>LGC SRS Separator Characteristics</b>	<b>107</b>
<b>Analysis of CT Data</b>	<b>110</b>
<b>Analysis of SEL Cell Cycling and CT Data</b>	<b>112</b>
<b>Environmental Data and System Analysis</b>	<b>117</b>
Key Observations	134
<b>Summary of Observations</b>	<b>136</b>
<b>Limitations</b>	<b>138</b>
<b>Appendix A – Resume for Jan Swart</b>	<b>139</b>
Professional Profile	139

Academic Credentials & Professional Honors	140
Licenses and Certifications	140
Professional Affiliations	140
Patents	140
Publications	140
Project Experience	144
<b>Appendix B – Resume for Kevin White</b>	<b>146</b>
Professional Profile	146
Academic Credentials & Professional Honors	147
Professional Affiliations	147
Patents	147
Publications	147
<b>Appendix C – Resume for Michael Cundy</b>	<b>150</b>
Professional Profile	150
Academic Credentials & Professional Honors	151
Licenses and Certifications	151
Professional Affiliations	151
Publications	151
<b>Appendix D</b>	<b>153</b>
<b>Appendix E</b>	<b>154</b>

# List of Figures

---

	<u>Page</u>
Figure 1 Non-conductive negative electrode deposits.	14
Figure 2 Cross-section of the SRS separator used in the LGC JP3 cells.	17
Figure 3 Representative 3D (left) and 2D (right) images of extensive cell damage in Rack 15.	18
Figure 4 (a, left) A histogram of the number of cycles that had various max charge voltages.	20
Figure 5 (a) Planar and (b) cross-sectional views of one representative feature tracked	21
Figure 6 Peak pressure rise vs. gas concentration in air for hydrogen, methane and simulated lithium-ion vent gas.	23
Figure 7 Aerial photograph of the BESS and adjacent substation taken prior to the first joint scene examination.	29
Figure 8 Aerial photograph of the BESS taken prior to the first joint scene examination.	29
Figure 9 Schematic Layout of the BESS.	30
Figure 10 Schematic of a rack assembly showing two banks of seven battery modules, the BPU, SDU, and PCS (inverter).	31
Figure 11 Exploded view of module EM048128P6B4.	33
Figure 12 Event data plot created by LG Chem.	35
Figure 13 Inspection sequence.	37
Figure 14 The hallway separating the odd numbered and even numbered module racks.	38
Figure 15 The hallway.	39
Figure 16 The ceiling above the hallway, showing the VESDA sampling tube, lighting, and HVAC ductwork.	40
Figure 17 Photograph showing the hallway and lower areas of racks. Rack 15 shows the most significant heat damage.	41
Figure 18 Photograph showing heat damage to the lower-middle section of Rack 15.	42
Figure 19 Photograph showing heat damage to the middle-upper section of Rack 15.	43
Figure 20 Photograph showing heat damage to the upper section of Rack 15.	44
Figure 21 The odd numbered racks which includes Rack 15.	45

Figure 22 Likely corrosion observed on module terminals.	46
Figure 23 Data acquisition sample rates.	48
Figure 24 The data captured for the minimum voltage in the system at the time of the incident.	50
Figure 25 Example of signal aliasing using the incident excursion data points.	51
Figure 26 A partial list of data points during the incident.	52
Figure 27 Photograph showing the installation of voltage taps and cell thermocouples.	55
Figure 28 Photograph showing the thermocouple attached to the outer surface of the Cell 7 pair.	55
Figure 29 Photograph showing thermocouples attached to the negative busbar fuse (left) and busbar (right).	56
Figure 30 Photographs showing three thermocouples attached to the bottom (left) and top (right) panels of the module along the centerline in the front, middle, and rear.	56
Figure 31 Photograph showing the heated pad installed on outer surface of the Cell 7 pair.	57
Figure 32 Photograph showing the front face of the module pre-test, with the communication cable and charging cables attached.	58
Figure 33 Voltage profile of Cell 7 pair during thermal runaway event inside the module.	59
Figure 34. Patch heater attached to the bottom cell with Kapton tape.	60
Figure 35. Cells held in-situ using the module plastic cassettes.	60
Figure 36. Top and bottom cells connected in parallel using copper bars.	61
Figure 37 The voltage profile for a parallel JP3 cell pair thermal runaway event.	62
Figure 38 The incident and the cell level test thermal runaway voltage profile comparison.	63
Figure 39 The normal end of charge current profile.	66
Figure 40 The abnormal end of charge current profile prior and during the failure event.	67
Figure 41 Discharge current excursions.	67
Figure 42 IMD data showing electrical isolation excursions.	68
Figure 43 Module discharge count.	70
Figure 44 Module 8, Rack 13.	71
Figure 45 Module 7 Rack 17.	72

Figure 46 Module 7 Rack 17 power terminals.	72
Figure 47 Module 8 Rack 17.	73
Figure 48 Module 8 Rack 17 power terminals.	73
Figure 49 Module power terminals.	74
Figure 50 Module power terminals.	74
Figure 51 BPU in the rack.	75
Figure 52 The modules at McMicken cell voltage difference after the incident and prior to discharge.	76
Figure 53 The modules at McMicken cell voltage difference after the incident and after discharge was complete.	77
Figure 54 The modules at McMicken showing the amount of discharge capacity left.	78
Figure 55 Floor in front of Rack 15.	80
Figure 56 Wall behind the racks.	81
Figure 57 PCS (Inverter) from Rack 15 with clogged fan vents.	81
Figure 58 Rack 15 door.	82
Figure 59 Rack 15 door.	83
Figure 60 Rack 15 door with debris attached to the screen of the door.	83
Figure 61 Rack 15, module 11.	84
Figure 62 Rack 15, Module 3 - the red arrow points to the arc damaged positive terminal and busbar.	85
Figure 63 Rear module covers of Rack 15. Module 1 is at the bottom and module 14 at the top below the BPU.	86
Figure 64 Rack 15 power cable ground conductor.	87
Figure 65 Rack 15 prior to disassembly.	89
Figure 66 Rack 15 with front cover removed.	90
Figure 67 The front and right view of Rack 15. The red marked areas show the arcing at the positive and negative terminals, internal busbars, cell tab interconnects as well as on the metal front cover plate of Module 2.	91
Figure 68 Rear and left side of Rack 15. The red marked areas show the arcing at module rear plates, internal busbars and cell tab interconnects.	92

Figure 69	A summary of short circuit location, type, power dissipating capability and probability of thermal runaway initiation. Copied from “Lithium-Ion Batteries: Advances and Applications”, G. Pistoia, editor, Elsevier Publishing, 2013, Page 450	96
Figure 70	A scanning electron micrograph of lithium dendrites. Journal of Power Sources, Volume 409, 1 January 2019, Pages 132-138.	98
Figure 71	Results of an accelerating-rate calorimetry test on a lithium-ion cell, showing the increasing rate of self-heating with increasing temperature.	99
Figure 72	Peak pressure rise vs. gas concentration in air for hydrogen, methane and simulated lithium-ion vent gas. Intercepts of the curves with the X-axis give the lower explosion limit and upper explosion limit for each gas composition. Excerpted from "Quantification of combustion hazards of thermal runaway failures in lithium-ion batteries." SAE International Journal of Alternative Powertrains 3.1 (2014): 98-104.	101
Figure 73	Non-conductive negative electrode deposits.	103
Figure 74	Schematic of the experimental setup for conductivity testing of negative electrode materials.	104
Figure 75	Voltage – Current relationship for three different samples during a Voltammetry test.	105
Figure 76	A deposit found during a multiparty inspection of a LGC JP3 cell showing behavior consistent with the reaction of lithium upon exposure to air. The white color and bubbly morphology are consistent with the exothermic reaction of lithium metal with water.	106
Figure 77	Cross-section of the SRS separator used in the LGC JP3 cells.	107
Figure 78	Mechanical rupture test of LG Chem's SRS. (Left) Schematic of experimental setup. (Right) Rupture force of SRS compared to traditional polyethylene (PE) separator.	108
Figure 79	Representative 3D (left) and 2D (right) images of extensive cell damage in Rack 15.	111
Figure 80	(a, left) A histogram of the number of cycles that had various max charge voltages. (b, right) Current and voltage profiles for the end of charge for a typical cycle exhibiting overvoltage on charge.	114
Figure 81	Various cycling performance metrics by cycle number: (a) charge and discharge capacities of complete cycles, (b) coulombic efficiency, (c) maximum charge current, and (d) maximum charge voltage.	115
Figure 82	(a) Planar and (b) cross-sectional views of one representative feature tracked throughout cycling.	116

Figure 83 Environmental temperature measurements and dew points at the five measurement locations approximately two days prior to the incident.	119
Figure 84 Schematic of the McMicken BESS illustrating HVAC locations and environmental temperature sensor locations.	120
Figure 85 Drain pan discharge port below the evaporator coils.	121
Figure 86 Economizers were found installed on HVAC units.	122
Figure 87 Enthalpy sensors were found installed and connected to the economizer control board in the HVACs.	122
Figure 88 Photographs of all eight HVAC economizer control boards showing they were configured to receive dry bulb temperature sensor signals.	123
Figure 89 Evidence of liquid marks observed on the inside face of the HVAC #3, which mates with the exterior BESS wall. This photograph was taken as viewed through the return air cutout in the wall, adjacent to Rack 15.	124
Figure 90 Liquid drip marks observed on the BESS inside wall, adjacent to Rack 15.	125
Figure 91 Dried liquid marks on the same inner wall of the BESS towards the corner.	125
Figure 92 Photograph showing the floor underneath Rack 15.	126
Figure 93 Photograph showing liquid marks and what appears to be residue of rust on the floor underneath Rack 15.	126
Figure 94 Photographs taken at the top of HVAC #3 where it mates with the BESS. Black residue is observed adjacent to the flange which is likely due to venting during the event, but there is also an unexplained residue dripping from underneath the corrugated roof.	127
Figure 95 Photograph showing HVAC #3, and the overhang of the corrugated steel metal roof.	128
Figure 96 Zoomed in view of the left photograph in Figure 94. There is an unexplained residue emanating from underneath the corrugated steel roofing material.	129
Figure 97 Psychrometric chart.	131
Figure 98 Plot showing that the temperature measured at the sensor three location is higher than the minimum module temperature at times.	132
Figure 99 Relative humidities measured at each of the five measurement locations between June 2018 and the incident. Note that relative humidities regularly reached to between 80-90%, including at locations near Rack 15.	133

## List of Tables

---

Table 1 Event log analysis.	34
Table 2 Selected set of event data (negative indicate a charge current)	64
Table 3 Experimental Parameters	105

## **Acronyms and Abbreviations**

---

A: Ampere

AC: Alternating Current

APS: Arizona Public Service

BESS: Battery Energy Storage System

BPU: Battery Protection Unit

DC: Direct Current

Exponent: Exponent, Inc.

HVAC: Heating, Ventilation, and Air Conditioning

IMD: Insulation Monitoring Device

LOC: Loss of Communication

LGC: LG Chem

MC: Main contactor

PCS: Power Conversion System (Inverter)

SDU: Fluence Control Unit

SOC: State of Charge

V: Volts

VESDA: Very Early Smoke Detection Apparatus

## **Authors**

---

Jan Swart, Kevin White and Michael Cundy authored this report. Jan Swart is a Principal in the Vehicle Engineering Practice; Kevin White is a Principal in the Polymers Science and Materials Chemistry Practice and Michael Cundy is a Manager in the Thermal Sciences Practice. The authors of this draft report resumes can be viewed in Appendix A, Appendix B and Appendix C.

## Introduction

---

At approximately 5:41 pm on April 19, 2019, the Surprise Fire Department received an alarm for a “check smoke” incident at the McMicken Battery Energy Storage System at or around 16981 West Deer Valley Road in Surprise, Arizona. Upon arriving at the scene at approximately 5:48 pm, they observed a steady stream of smoke exiting the building. Peoria Fire Department units arrived, including the Hazardous Materials HM193 unit, at approximately 6:28pm. A hazard mitigation plan was developed, led by HM193, and including consultation with APS representatives, the contractor Sturgeon, the Phoenix Fire Department, and information from an accessible computer database. Following the development of the plan, temperatures and gas concentrations were measured outside of the unit. The door to the unit was opened, and a few minutes later an explosion occurred.<sup>1</sup> Four first responders were injured during the incident. Exponent, Inc. (Exponent) was retained to conduct an investigation on behalf of LG Chem to investigate specific issues related to the incident.

This report summarizes the observations we have formed to-date based on our investigation to date and is intended to be used only as a progress report since the investigation is ongoing. We may subsequently review additional documents and testimony, perform additional inspections, and/or prepare additional analyses and testing, and, accordingly, reserve the right to amend or reach additional opinions.

---

<sup>1</sup> City of Surprise, Arizona, Fire Department Report, NFIRS-1S Supplemental, page 21

## Executive Summary

---

Exponent, Inc. (Exponent) was retained to investigate specific issues related to the incident at the McMicken Battery Energy Storage System (BESS) in Surprise, Arizona. During this analysis, Exponent followed National Fire Protection Association 921, Guide for Fire and Explosion Investigations, by exercising the scientific method and evaluating all the available evidence.

The investigation revealed that Rack 15, including LG Chem battery modules, an LG Chem battery protection unit, a Fluence-supplied power conversion system (PCS), and a Fluence Advancion Node Controller, was the only rack that was consumed by fire and which had cells that had vented. The remaining racks showed smoke and limited thermal damage but the modules and cells in the adjacent racks were still functional.

Exponent conducted system level analysis and analysis on exemplar and incident cells and assessed cell level data that was generated by other parties associated with this matter.

The overall goal of analyzing the exemplar and incident cells was to determine if the available data supported one of the two proposed routes to initiation of thermal runaway in the LG Chem JP3 cells installed in Rack 15. The two hypotheses for initiation of the thermal event were:

1. Internal Cell Short Circuit – An internal cell short circuit is a single point failure event that propagates to the full extent of the event. This hypothesis involves the formation of lithium plating in a cell which resulted in the establishment of a short circuit within the cell electrode stack that resistively heated, causing thermal runaway of the cell and propagation of thermal runaway to all the other cells in Rack 15.
2. External Cell Heating – There are various causes for external cell heating to occur, for example by external fire attack, resistive heating, or electrical arcing. Due to the observed rack DC current at the time of the incident and the correlating PCS heating, this hypothesis involves two (or more) electrical isolation failures present at the same

time, and which produces arc heating and cell thermal runaway in one or more cells that then propagated to all the remaining cells in Rack 15.

Other parties associated with this matter assert that an internal cell fault or short circuit, within the rearmost cell of parallel Cell 7 pair of Module 2 is responsible for initiating cell thermal runaway that then propagated to the other cells in Rack 15. However, the data acquired during the investigation do not support this hypothesis. Rather, the data collected and analyzed to date and the relevant literature tends to support initiation of cell thermal runaway through intense heating of the incident cells by an external heat source that is likely related to electrical arcing on Rack 15.

### **Analysis of Cell Deposits**

During various inspections associated with this matter, deposits were found on the negative electrode and adjacent separators of LGC JP3 cells from the McMicken and Festival Ranch BESS'. Figure 1 shows an example of one of these deposits.



Figure 1 Non-conductive negative electrode deposits.

At the time the deposits were discovered, in the absence of any analytical chemistry data to establish the composition of the deposits or electrical measurements to determine the

conductivity of the deposits, other parties associated with this matter concluded that the deposits were lithium metal and that a similar deposit initiated thermal runaway in one of the cells in Cell 7-2 of Module 2 in Rack 15.

Contrary to this pre-mature conclusion, Exponent and LG Chem independently measured the electrical conductivity of similar deposits extracted from cells not involved in the incident using two different methods and shared those results with all interested parties. The results of these measurements showed that deposits of this type are non-conductive and are unlikely to be pure lithium metal. It is impossible for a non-conductive deposit to establish an internal cell short circuit, carry current, resistively heat and cause thermal runaway.

### **Non-conductive Deposit Behavior in Air**

It is a fact that some of the observed non-conductive deposits were highly reactive in air. Most often deposits turned from a dull gray color to white with the coincident formation of gas bubbles. In a single example, a deposit that was adhered to the surface of a negative electrode and the adjacent separator showed pyrophoric behavior when the separator was peeled back from the surface of the electrode. Both behaviors are consistent with the reaction of lithium metal in air.

It is difficult to reconcile the facts that the deposits have been shown to be non-conductive and that they have reactivity in air that is similar to that of lithium metal. A likely explanation, that has been ignored by other parties associated with this matter, is that the deposits contain lithium metal in an otherwise non-conductive matrix.

According to the recently released report prepared by DNV GL, the consulting firm Safety Engineering Laboratories (SEL) conducted measurements on a deposit or deposits using inductively coupled plasma–optical emission spectroscopy (ICP-OES) in an effort to determine the composition of the deposits. To Exponent’s knowledge, these data have not been shared with the other parties associated with this matter and the information is not presented in the DNV GL report. The DNV GL report simply states:

*“Bulk Inductively Coupled Plasma – Optical Emission Spectroscopy detected elevated concentrations of Lithium metal within the deposits thereby proving that these deposits were indeed composed of Lithium”*

While ICP-OES is a sensitive technique capable of detecting individual elements in complex mixtures of compounds, it is not capable of providing information related to the physical environment in which those elements existed at the start of the measurement. The quote above indicates that *“elevated levels of Lithium metal”* were detected, presumably coincident with the detection of other elements that were not reported. Rather than *“proving that these deposits were indeed composed of lithium”*, the ICP-OES data alluded to in the DNV GL report supports the theory that the deposits contain lithium metal in an otherwise non-conductive matrix. However, in the absence of thorough characterization of the composition and morphology of the deposits, it is impossible to reach a conclusion from the ICP-OES data regarding the impact of the observed deposits on cell stability.

## **Lithium Deposits and the LG Chem SRS Separator**

Undesirable lithium metal deposits in lithium-ion cells occur when lithium ions in the electrolyte are reduced to lithium metal at the surface of the negative electrode. The deposited lithium metal can form a conductive pathway between the negative and positive electrodes, a short circuit. However, due to the morphology that lithium metal adopts when deposited in lithium-ion cells, it is difficult to establish a short circuit that can carry sufficient current to heat the cell to the point of thermal runaway<sup>2</sup>. The most common result of lithium deposition is a measurable decrease in cell performance due to the removal of lithium ions from the electrolyte.

In extreme cases of lithium plating, the generation of so called “dead lithium,” the electrode separator membrane can be torn, resulting in short circuit and thermal runaway. However, the generation of “dead lithium” consumes large quantities of lithium ions from the electrolyte and results in dramatic cell performance degradation. The available Rack 15 module and cell level

---

<sup>2</sup> Santhanagopalan, Shriram, Premanand Ramadass, and John Zhengming Zhang. "Analysis of internal short-circuit in a lithium ion cell." *Journal of Power Sources* 194.1 (2009): 550-557

diagnostic data do not support cell performance degradation, let alone cell performance degradation of the magnitude expected if “dead lithium” was being generated.

Further, the LG Chem SRS separator was specifically designed to be highly resistant to deposited lithium short circuiting. The SRS separator is a hybrid design comprised of a microporous polymeric membrane coated on both sides with relatively dense organic/inorganic (O/I) protective layers with very small pore sizes. A cross-sectional view of the SRS and its layers is shown in Figure 2.

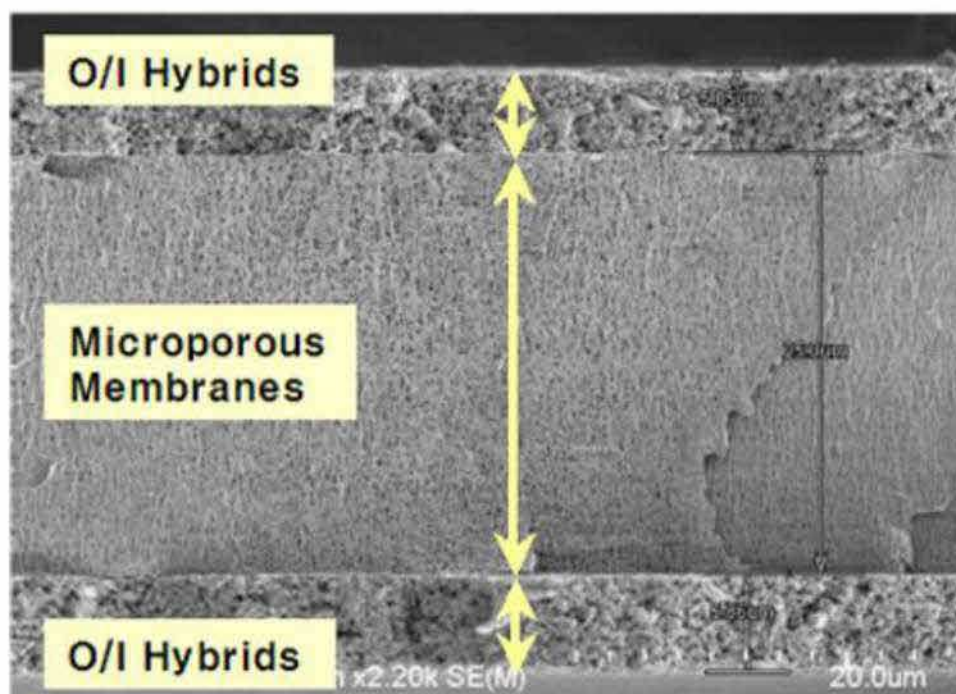


Figure 2 Cross-section of the SRS separator used in the LGC JP3 cells.

The SRS separator has two complementary features that address different risks associated with lithium plating. First, the pore diameters of the O/I layers are small enough to limit the size of any lithium growing through the separator effectively limiting the ability to carry current sufficient to heat the cell to thermal runaway. Second, the mechanical strength provided by the I/O layers has been shown to resist tearing at loads that are much higher than what can be produced between the unconstrained electrode layers of a lithium-ion pouch cell. The combined

physical properties of the SRS components and design of the cell make it highly unlikely for lithium plating in a JP3 cell to result in a short circuit leading to a thermal runaway.

## Analysis of CT Data

Exponent was provided with computed tomography (CT) X-ray data of twenty-one cell pairs from Modules 1 – 13 in Rack 15 for analysis. The analysis included Cell 7-2 which others have suggested suffered an internal short circuit, initiating thermal runaway. The data was analyzed with the intent of understanding any damage patterns that would help determine the root cause failure of Rack 15. The data is not consistent with an initiation from an internal short circuit but is consistent with an attack on the cells from an intense external heat source.

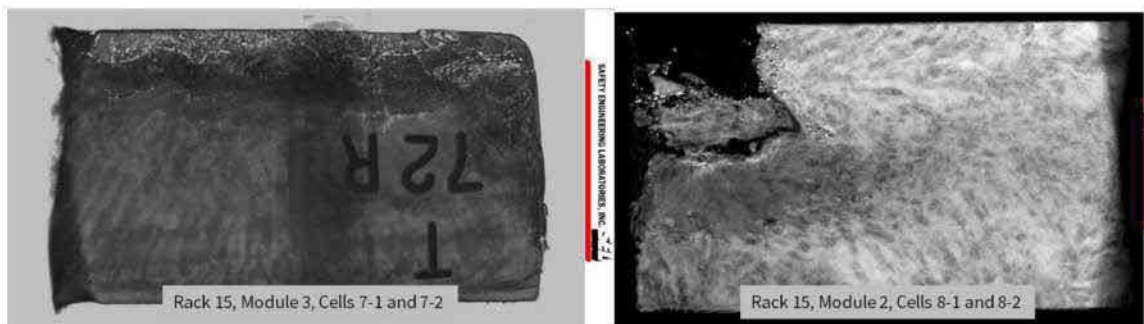


Figure 3 Representative 3D (left) and 2D (right) images of extensive cell damage in Rack 15.

Based on Exponent's experience, the electrode damage is significantly more extensive than would be expected for a thermal runaway initiated by an internal short circuit. A short circuit in a lithium-ion cell is an isolated, transient source of heat that causes localized damage to the adjacent electrodes and often locally exceeds melting point of copper ( $\approx 1085\text{ }^{\circ}\text{C}$ , a temperature not typically reached by the exothermic chemical reactions responsible for thermal runaway). However, it is not characteristic for a short circuit to remain a significant source of heat once thermal runaway has begun. An internal cell short circuit relies on resistive heating and the electrical energy stored in the cell to generate the intense heat required to melt copper. A cell undergoing thermal runaway is not a reliable source of electrical energy.

The damage patterns on the cells of Rack 15 are primarily located on the edges of the cells and often present as the absence of large portions of the electrode stack, including the copper of the

negative electrode current collector (see Figure 3). As a result of thermal runaway, it is common for the aluminum of the positive electrode current collector to melt and be redistributed. However, it is rare for large portions of the copper negative electrode current collector to melt, leaving large voids in the electrode stack. Because these large voids in electrode stacks are present in multiple cells from multiple modules in Rack 15 and the locations of the voids in the cells correspond with melting damage to the metal structures outside the cells, it is reasonable to consider a scenario where there was an attack on the cells from an intense external heat source, such as electrical arcing on the modules and rack. To ignore these data is contradictory to the scientific method.

### **Analysis of SEL Cell Cycling and CT Data**

Safety Engineering Labs (SEL) provided a data set purporting to show charge/discharge cycling and X-ray computed tomography (CT) of one JP3 cell taken from an unknown module with an unknown history. After analyzing the data, Exponent found evidence of the previously discussed non-conductive deposits in the cycled cell but no evidence that the deposits changed as a result of cycling. Furthermore, numerous experimental issues are apparent in the data which undermine the integrity of SEL's results.

Over the course of the cycling experiment the parameters used were changed multiple times, were unstable or simply beyond the specifications for the cell. In particular:

- The maximum charge current was varied between 8.2A and 16.5A and was unstable at any chosen current during the 463 cycles of the experiment.
- The files describing cycle 401 and after are labeled “constrained”. SEL has not provided any further explanation about the nature of the constraint (electrical or physical) or why it was applied after 400 cycles.
- The charge voltage consistently exceeded the maximum charge voltage specified by LG Chem<sup>3</sup>. Figure 4 (a) clearly shows that most cycles exceed the maximum charge

---

<sup>3</sup> 190708\_ESS\_cell\_JH3\_JP3\_JH4\_Cell\_data\_APS.df

voltage, in most cases by at least 18mV. Figure 80 (b) shows the charge voltage and current for a typical cycle exhibiting overvoltage behavior.

- The transition from the constant-current (CC) charge to constant-voltage (CV) charge was uncharacteristic of typical cell cycling equipment suggesting that the equipment SEL used for this cycling test was not designed for and was simply incapable of accurately performing an ordinary charge algorithm on this cell.
- The ratio of charge capacity to discharge capacity (coulombic efficiency) was extremely poor but the cycling data or the CT data does not indicate a problem with the cell. This further supports that the equipment SEL used to cycle this cell was either inaccurate, improperly configured, or incapable of performing this test.

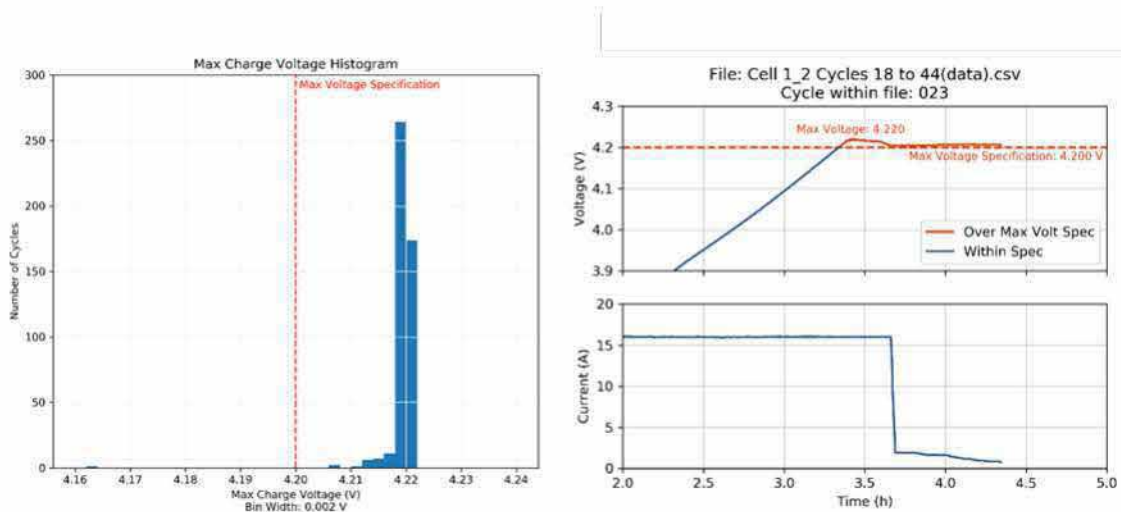


Figure 4 (a, left) A histogram of the number of cycles that had various max charge voltages. (b, right) Current and voltage profiles for the end of charge for a typical cycle exhibiting overvoltage on charge.

In addition to the cycling data, SEL provided ten sets of CT data consisting of scans of the cycled cell at five cycling intervals (0, 100, 209, 285 and 400 cycles). CT scans conducted prior to cycling showed the uncycled cell contained several features consistent with deposits on the negative electrode, similar to those found to be non-conductive (as discussed above). These features did not change in size or shape during the 400 cycles, see Figure 5. Additionally, despite the issues with the cycling protocol noted above, no measurable swelling of the pouch or localized swelling around the deposits were observed over the 400 cycles tracked.

In spite of the cycling data showing overcharge of the cell, a condition that would promote lithium plating, the CT data do not support the growth of the observed internal cell features as a function of cycle count and subsequently do not support the growth of lithium deposits capable of causing a short circuit that may result in thermal runaway. Discussion of these data is absent from the DNV GL report representing another instance where available information, contradictory to the assertion that an internal cell fault is responsible for thermal runaway of Rack 15, was ignored.

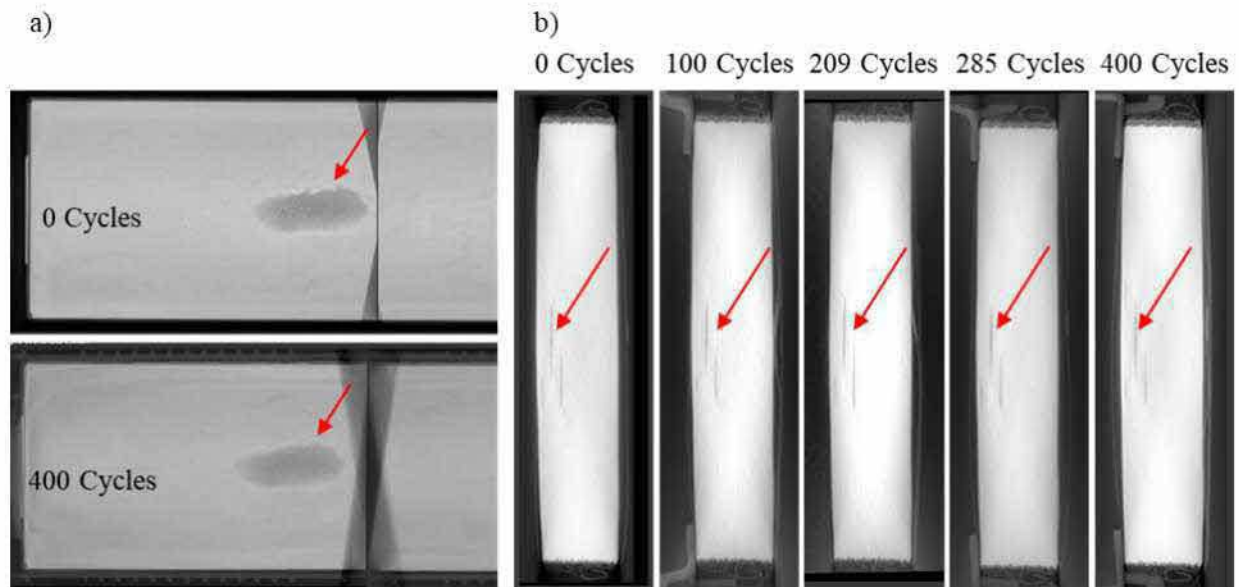


Figure 5 (a) Planar and (b) cross-sectional views of one representative feature tracked throughout cycling.

## Flammable Gas Generation During Lithium-ion Cell Thermal Runaway

Thermal runaway in lithium-ion cells is a highly exothermic process that generally results in the combustion of flammable materials within the cell. However, there is rarely enough oxygen present within the cell to facilitate complete combustion of the flammable materials. As early as 2005, researchers were able to show that the products of incomplete combustion during thermal runaway were, themselves, flammable gases.<sup>4</sup>

<sup>4</sup> "Effects of additives on thermal stability of Li ion cells." Journal of power sources 146.1-2 (2005): 116-120

Since this early work, substantial effort has focused on more clearly understanding the composition and quantity of the flammable gases produced during thermal runaway and the behavior of those gases in the presence of sufficient oxygen and a competent ignition source. Based on Golubkov et. al.<sup>5</sup>, and other similar documents, the primary composition of the vent gases from a thermal runaway event are hydrogen, carbon monoxide, carbon dioxide (non-flammable) and a mixture of light hydrocarbon gases. Under the correct conditions, flammable thermal runaway vent gases can combine with oxygen to form an explosive mixture.<sup>6</sup> The plot in Figure 6, excerpted from Somandepalli et. al.<sup>6</sup>, shows the peak pressure rise for hydrogen, methane and a simulated lithium-ion vent gas mixture after ignition in air.

The important outcome of this research is that the risk of explosion from thermal runaway vent gases was known well in advance of the design and installation of the Surprise, Arizona facility and methods existed to measure and understand the explosive behavior of lithium-ion battery vent gases in a way that makes engineering ventilation systems for stationary power storage facilities possible. A properly designed ventilation system could have prevented the atmosphere within the container from ever reaching explosive concentrations.

---

<sup>5</sup> "Thermal Runaway Experiments on Consumer Li-ion Batteries with Metal Oxide and Olivin-type Cathodes" RSC Advances., 2014, 4, 3633

<sup>6</sup> "Quantification of combustion hazards of thermal runaway failures in lithium-ion batteries." SAE International Journal of Alternative Powertrains 3.1 (2014): 98-104

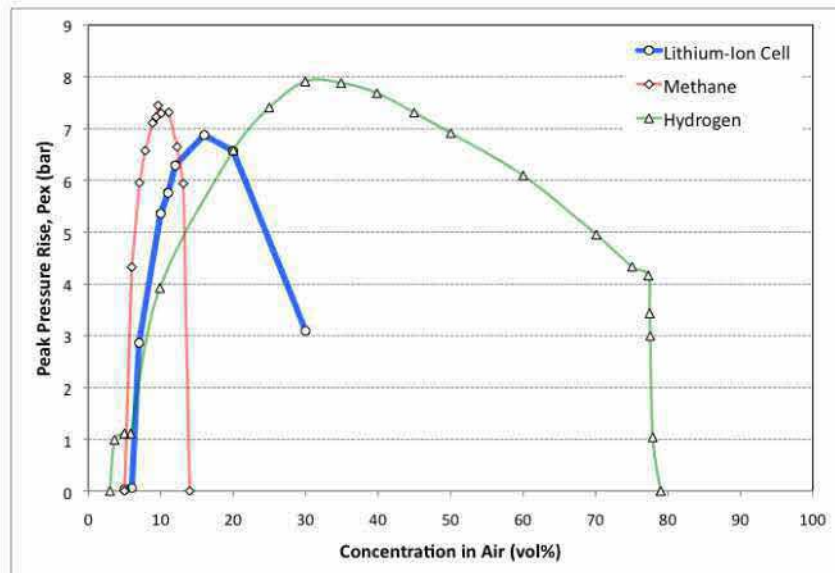


Figure 6 Peak pressure rise vs. gas concentration in air for hydrogen, methane and simulated lithium-ion vent gas.

## Analysis of BESS Data Logged During the Incident

An analysis of the BESS acquisition system data and a review of the DNV GL report authored by Dr. Hill identified the following:

- A single cell failure event was investigated and a single cell failure as the root cause of the fire was ruled out for the following reasons:
  - The McMicken BESS data acquisition rate was performed at one sample per 2 second intervals (0.5 Hz). This acquisition rate is too slow to capture high-frequency events such as an electrical arcing or short circuit event. Hence, a cell voltage profile with this limitation would not conclusively show whether a single cell failure event occurred or if a double point electrical isolation failure event was responsible for initiating thermal runaway.
  - Two tests using the same model cell used in the McMicken modules were performed by Exponent to evaluate this hypothesis, one with a cell pair outside of a module and the other with a cell pair inside of a module to characterize the voltage profile when a single cell failure was introduced. The two tests showed that the voltage profile of the failed cell pair does not match the incident parallel Cell 7 pair voltage excursion

- profile. The tests also show that the parallel cell voltage did not recover after thermal runaway occurred, which occurred in the incident data as is discussed later.
- The cell temperature and voltage plot in DNV-GLs report is not consistent with typical onset of thermal runaway (see Figure 12 -- top graph). It was not stated which cell cathode chemistry, cell model, cell form factor and test procedure were used to generate the data. Without a clear explanation of the above, the cell voltage results may not be relevant to this investigation and are likely misleading. The source of the voltage test data is unknown. The following deficiencies were noted in the graph:
    - The cell voltage at time = zero seconds is 2 V and not 4.1V. 4.1V is a representative SOC of the McMicken cells at the time of the failure event. Two volts represent a highly discharged lithium-ion cell.
    - Just prior to the indicated (red line) thermal runaway event, the cell temperature peaked at approximately 200°C, cooled to less than approximately 50°C and then thermal runaway occurred. This part of the temperature curve is not explained in the DNV-GL report and is not representative of typical pre-thermal runaway cell behavior.
  - The modules used at the McMicken site were configured as a 2 parallel, 14 series cell configuration and not a single cell configuration. DNV-GL's cell thermal runaway characterization of the cell voltage was likely for a single cell configuration and not a parallel cell configuration. The voltage behavior of a parallel cell configuration is significantly different as shown in this report (see Figure 38)
  - In the incident data, the Rack 15 DC voltage recovered following the voltage excursion, which is an additional indicator that the event is inconsistent with a single cell failure hypothesis.
  - DNV-GL selectively noted that the Rack 15 voltage dropped from 799.9 V to 796.1 V during the voltage excursion, but failed to note that the rack voltage lowered to 796.1 V over approximately 10 seconds, recovered to 798.9 V eight seconds later, and remained at this voltage for another 29 seconds before dropping again. The rate of the initial cell voltage excursion in the incident is not consistent with Exponent's testing, and the voltage recovery

is not consistent with Exponent's testing nor with DNV-GLs test with unspecified experimental conditions.

- The current hypothesis under evaluation by Exponent involves a double-point electrical isolation failure mechanism and this mechanism is supported by the following observations:
  - High-frequency events, such as intermittent electrical arcing, have not been ruled out as a root cause for the initial failure event. Electrical arcing damage was observed at several locations within Rack 15.
  - The Rack 15 DC charge current became unstable during the voltage excursion and became a discharge current after the cell voltage data stopped recording. Current flowing through Rack 15 could only occur if the rack electrical isolation failed in two different locations on Rack 15.
  - The insulation monitoring device (IMD) showed intermittent insulation fluctuations prior to the voltage excursion and was the first anomaly recorded in the available data. This suggests the Rack 15 electrical isolation was compromised prior to the Cell 7 pair of Module 2 voltage excursion.
    - DNV-GL's report ignored IMD insulation fluctuations and incorrectly noted that the voltage drop was the first anomaly recorded.
- The DNV-GL report did not address and explain the following key evidence, most of which is inconsistent with DNV-GL's short-circuit theory:
  - The rate at which the Module 2, Cell 7 pair voltage decayed,
  - Rack 15 DC voltage recovery following the initial voltage excursion,
  - Rack 15 DC discharge current during the incident,
  - The arcing at the edge of the two parallel cells at location 7 in Module 2,
  - Arcing at Module 2, parallel cell pair 14 to the enclosure,
  - The arcing at Module 3 positive power terminal,
  - IMD electrical isolation anomalies prior to the voltage excursion.

## **Environmental Conditions within the BESS, Container Integrity, and Heating, Ventilation, and Air Conditioner System Evaluation**

The environmental conditions within the BESS were investigated for their potential role in the cause of the initial failure event. A humidity excursion approximately three days prior to the

event was recorded and may have contributed to the failure event. However, the provided environmental data was found to be not representative of the temperature and humidity extremes experienced in the container, because the sensor locations generally did not spatially align with the cold air supply discharge ducts or the source of water vapor, the latter of which was discovered during the investigation. Lower temperatures than is represented in the data are likely to occur at the front face of Rack 15 when the heating, ventilation, and air conditioning (HVAC) system #3 is running. The water vapor concentration would be expected to be higher nearest the source, but additional evidence examinations and testing must be done to determine the source of the water vapor. There is evidence of liquid penetrating the roof panels and evidence of liquid marks within a BESS wall which is not readily explained by overpressure damage and rainfall after the incident. The water vapor source could have also been through the HVAC systems. The HVAC systems included economizers which were incorrectly configured, so it is not possible to determine how they are working without characterization testing.

Lower temperatures and higher water vapor concentrations could facilitate condensation and/or corrosion on electronic equipment and batteries. Condensation may result in electrical isolation failures, which may result in electrical arcing. Additionally, corrosion may lead to high resistance electrical connections and ignition of combustible materials if sufficient heat is generated at the connection.

## **Preliminary Conclusions**

Exponent followed NFPA 921, Guide for Fire and Explosion Investigation guidelines and evaluated all failure mechanisms known at the time of this report against the evidence and test data in Exponent's possession. It is our current preliminary opinion that the analysis and testing performed to-date does not support a single cell failure initiating the BESS failure event. All the evidence and testing data reviewed to date, more likely supports a double point electrical isolation failure mechanism. Understanding the root cause and sequence of events associated with a double point electrical isolation failure will require additional characterization, testing and analysis.

This report summarizes the observations we have formed to-date based on our investigation and is intended to be used only as a progress report since the investigation is not complete. We may subsequently review additional documents and testimony, perform additional inspections, and/or prepare additional analyses and testing, and, accordingly, reserve the right to amend or reach additional opinions.

## Background

---

Arizona Public Service (APS) purchased three battery energy storage systems (BESSs) from AES in 2017. In January 2018, Siemens and AES formed a joint venture called Fluence, which currently maintains the BESS product. Based on work order records, the subject unit was installed at the McMicken location in Surprise, Arizona, on or around September 2017. The system was reportedly initially used for frequency regulation and was utilized for peak shifting for the eight months preceding the event.<sup>7</sup> A second, reportedly identical unit was installed in the Festival Ranch location, and a third unit was installed in the Punkin Center location.

The APS McMicken BESS is a 2MW/2MW-h transportable lithium-ion BESS terminating into an APS 12.47kV feeder. The system has been designed to run automatically under modes selected by remote operators. The container contains 27 nodes or racks. Each rack consists of 14 modules. Each module contains two sub-modules. Each sub module consists of seven JP3 cell pairs in series (28 individual cells per module), and a Battery Management System (BMS). A rack of 14 modules will include a LG Chem Battery Protection Unit (BPU), a Fluence Advancion Node Controller (SDU), and a Parker GTR 80kW power conversion system (PCS) a direct current (DC) to alternating current (AC) inverter during discharge, and AC to DC converter during charging. Each node is connected into a 4kA low voltage collection panel, with a 4kA main circuit breaker.

The container is cooled by eight Marvair heating, ventilation, and air conditioning (HVAC) units, model AVPA72ACD060CU-A5-200-VAR.<sup>8</sup> According to Fluence, the HVAC system was reportedly not setup to utilize an economizer feature, which allows for cooler external air to be drawn in to the container to assist in maintaining the set point temperature while reducing HVAC energy consumption. The container did not have a purpose-built overpressure relief feature.

---

<sup>7</sup> 190524\_Arizona McMicken Log Analysis\_v4

<sup>8</sup> First Responder Training US01-5133 r01, January 5, 2017

Aerial photographs of the BESS taken after the incident and prior to a joint scene examination are shown in Figure 7 and Figure 8. The burn damage is confined to the BESS container.



Figure 7 Aerial photograph of the BESS and adjacent substation taken prior to the first joint scene examination<sup>9</sup>.



Figure 8 Aerial photograph of the BESS taken prior to the first joint scene examination<sup>10</sup>.

A schematic layout of the BESS can be seen in Figure 9. The schematic shows the location of two entry doors, one on the southeast (SE) side and one on the southwest (SW) side. The eight-side mounted unitary HVAC units are drawn as red rectangles on the outside of the container.

---

<sup>9</sup> Colwell Consulting

<sup>10</sup> Colwell Consulting

Inside the container, the red rectangles indicate racks, with the BN prefix indicating a battery rack. Some racks on the SW side were empty. Note the position of Rack 15 (also referred to as node 15), which sustained significant damage in the incident, along with the adjacent HVAC-X103 (hereafter referred to as HVAC #3).

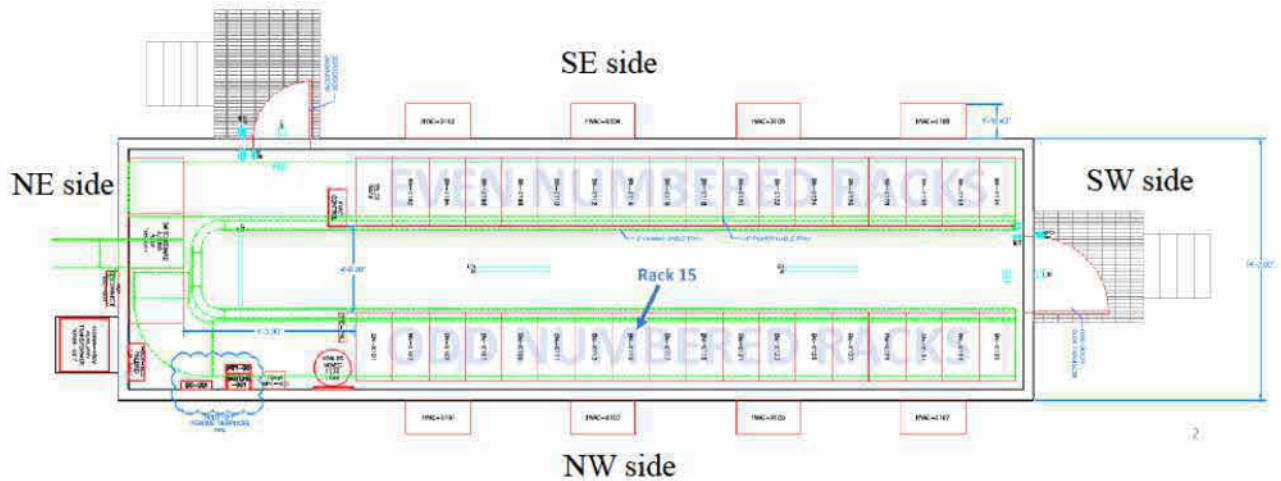


Figure 9 Schematic Layout of the BESS.<sup>11</sup>

A schematic of a rack (supplied by Fluence) showing the relative locations of the battery module banks (supplied by LGC), BPU (supplied by LGC), SDU (supplied by Fluence), and PCS (supplied by Fluence) is shown in Figure 10. An exploded view of a battery module can be seen in Figure 11.

<sup>11</sup> Fluence LLC Presentation to Arizona Public Service; Preliminary Data Analysis of Event

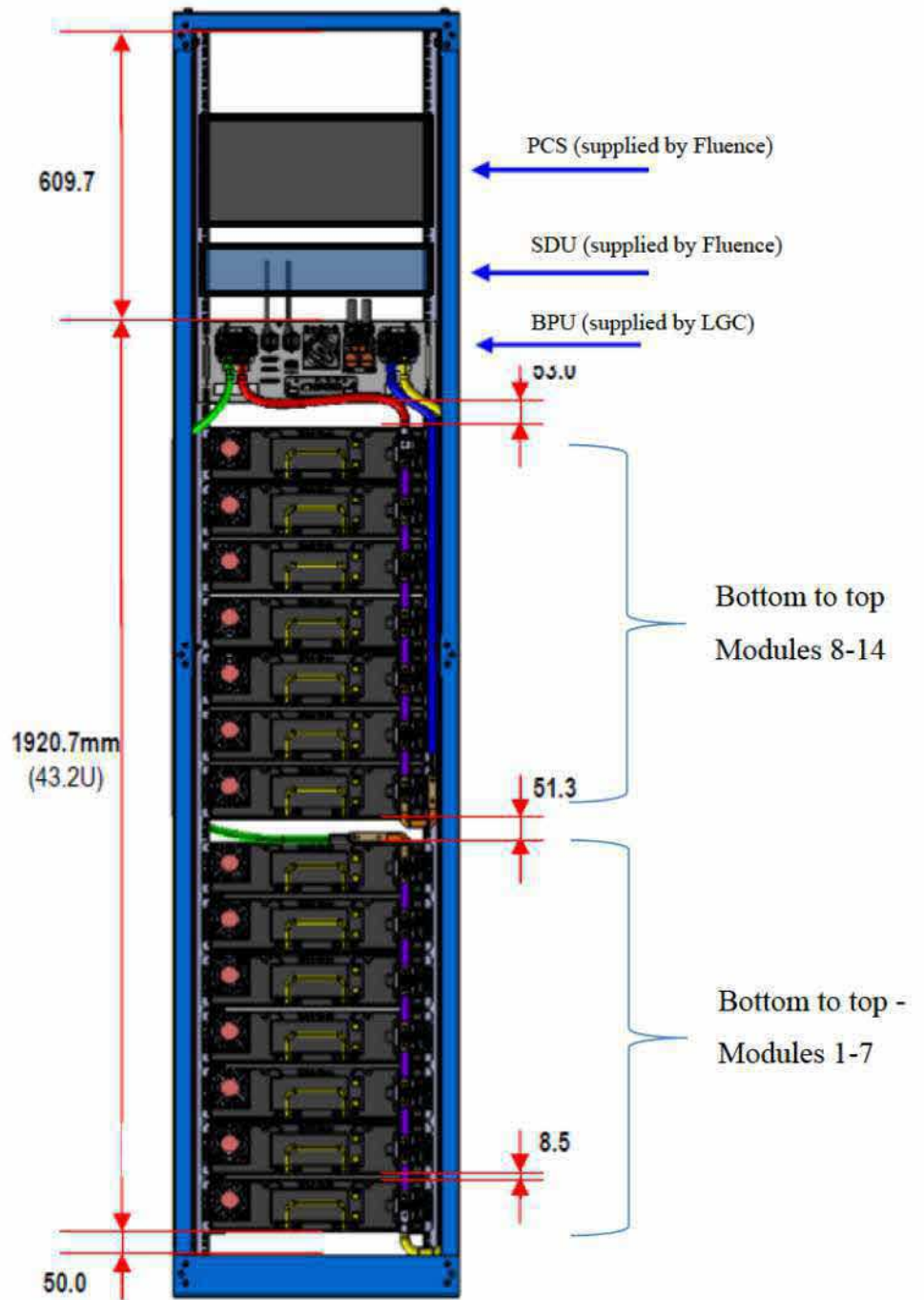
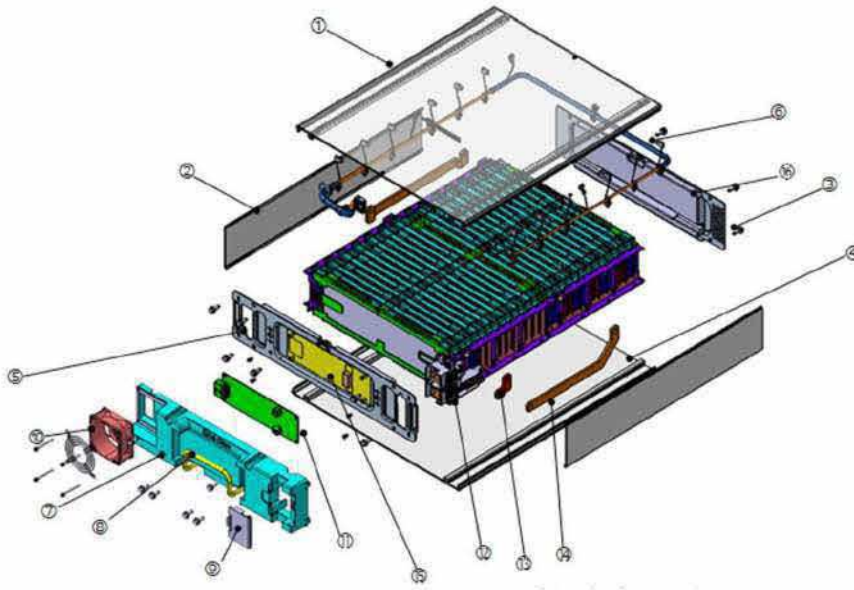


Figure 10 Schematic of a rack assembly showing two banks of seven battery modules, the BPU, SDU, and PCS (inverter)<sup>12</sup>.

<sup>12</sup> 190528\_Arizona McMicken Log Analysis\_v6.pptx

A current transducer measures the current that flows through the rack and is located in the BPU. The current transducer is electrically connected between modules 1-7 and modules 8-14. Hence a current that flows between modules 1-7 and modules 8-14 will be measured. The cells in the modules were electrically isolated from the grounded rack frame and hence the cells positive and negative terminals were floating and not referenced to the rack frame (chassis) or ground. This implies that if a single cell electrical isolation failure occurs, a second cell electrical isolation failure needs to occur for a current to flow through the rack frame. The insulation monitoring device (IMD) is reportedly connected by a 1 M $\Omega$  resistor between the PCS AC side and ground.

The BESS hallway is considered the cool space where the AC systems discharge cold air, and the area between the back of the modules and the BESS outside wall is considered the warm space where the AC systems extract the warm air for cooling. In Figure 11, the fan is mounted on the front of the module blowing cool air from the BESS cold side to the rear of the module into the BESS warm space. The Module Battery Management System (MBMS) is located in the front of the modules adjacent to cell pair 14 and the cool air space. Cell 7 pair is located at the rear of the module nearest the warm air space. From front to back, the cell pairs identifiers are cell pair 14 to cell pair 8 and then cell pair 1 follows towards Cell 7 pair. Each module has two temperature sensors which are located between foam cushions which separate the submodules, towards the edge of the adjacent cells.



No.	Part
1	Base Plate 2P
2	Pack Side Cover 2P
3	Rear cover Assy
4	Base Plate 2P
5	Front Cover Assy Blowing
6	Sensing Cable Assy 2P
7	BMS Cover
8	BMS Cover Handle
9	Terminal Cover
10	Fan
11	MBMS
12	Power Terminal Assy
13	Positive Busbar
14	Negative Busbar 2P
15	Insulation Sheet
16	Insulation Plate

Figure 11 Exploded view of module EM048128P6B4.<sup>13</sup>

<sup>13</sup> [Module specification]\_EM048128P6B4\_JP3\_2P\_Blowing\_Eng\_RevAD\_171228.docx

# Incident Timeline

A log analysis was performed. The event history is shown in Table 1, and a plot of selected data traces produced by LG Chem is reproduced in Figure 12.

Table 1 Event log analysis.

Local Time	Status	Ref	Remarks
16:22:36	Insulation resistance fluctuations begin	IMD	
16:54:30	Rack #15 min Cell V starts to drop from 4.06 V	BMS	Rack #15-Module#2-Cell#7 (Second module from the rack, most rear part of module)
16:54:38	Rack #15 Min Cell 3.81V (▼ 250 mV for 8 sec) Rack #15 DC voltage 799.9 V Module Data Missing (MR LOC Count starts)	BMS	No update on cell voltage and module temperature of Rack #15 while rack level voltage and current could be read
16:54:40	Rack #15 DC voltage reaches min of 796.1 V	BMS	
16:54:44	The air temperature measured inside PCS starts to increase from 40°C	EMS	The air temperature of rack #15 and #17 became 49.8°C at about 15:55:38
16:54:48	Rack #15 DC voltage recovers to 798.9 V		
16:55:16	All Rack#1~#27 AC Contractor Open	EMS	AC Contractor Open
16:55:18	All Rack#1~#27 E-Stop Fault, MC/CB Open	BMS	MC/CB Open
16:55:20	Fire Alarm Level 1&2	EMS	
	Core Main Breaker Open Alarm	EMS	Core main Breaker Open
16:55:45	IMD Fault	EMS	IMD Fault
16:55:50	Rack #15 M-R LOC Diagnosis	BMS	MR LOC Diagnosis
16:55:50	<u>Novec</u> 1230 Discharge	EMS	<u>Novec</u> is discharged after 30sec from Level 2 Alarm at 16:55:20
16:56:10	Rack #15, #17 air temperature measured in PCS starts decrease	EMS	Temperature decreased Rack #15 : 44.2°C, Rack # 17 : 45.7°C Probably due to the NOVEC 1230
17:44:08	Site Communication Loss	EMS	From this point, there is no data available.

The first cell voltage excursion that was noted in the data was at 16:54:30 April 19, 2019, when the Rack 15, Module 2 (second from the bottom) minimum cell voltage begins to drop from between approximately 4.097V and 4.061V to approximately 3.81V over approximately eight seconds. Approximately 10 seconds after the minimum cell voltage excursion, the air temperature inside the PCS in Rack 15 begins a gradual increase from approximately 43°C to 50°C over approximately 54 seconds. This is also the time when the positive current in Rack 15 was observed.

Twenty-two seconds before the peak temperatures of PCS 15 and PCS 17 are reached, the AC contactors open in all racks (1-27). Two seconds later, the E-stop fault occurs, and the Main

Contactor/Circuit Breaker (MC/CB) in the BPU opens. An additional two seconds later, the fire alarm level 1&2 occurs and the core main breaker opens. An IMD fault occurs 25 seconds later, followed by the Novec 1230 discharge.

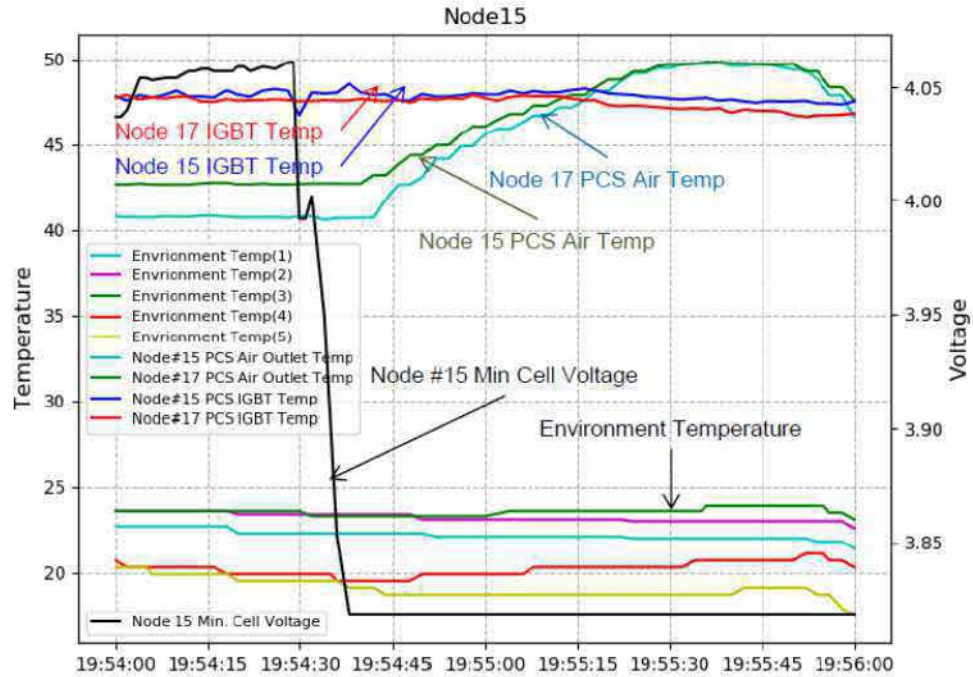


Figure 12 Event data plot created by LG Chem.<sup>14</sup>

The fire department received an alarm at 17:41, over 45 minutes after the McMicken BESS Fire Alarm Level 1 & 2. Smoke was observed in the area of Deer Valley Road and Grand Avenue (near the McMicken location), and the Surprise Fire Department was dispatched.

<sup>14</sup> Time zone changes cause the data to be offset by 3 hours.

## Site Inspection

---

After the incident, the McMicken site was electrically isolated from the grid by APS and there was no longer an electrical connection between the storage system and the electrical grid. The McMicken storage system contained in the container consisted of 378 modules contained in 27 racks. Each rack consisted of 14 modules connected in series. Each rack also consisted of a Power Conversion System (PCS; inverter and converter), Fluence Control Unit (SDU), Battery Protection Unit (BPU), Main Contactor (MC) and a Ground Fault detector (IMD).

The inspection of the container was complicated by the fact that the modules were charged to approximately 90% SOC and each rack in the system was energized with an output voltage of 794 V. The energized racks posed an electrical shock and arc flash hazard and the safety of the modules were unknown. Hence an initial inspection inside the container was not performed. It was decided by APS to follow the inspection process as shown in the flow chart of Figure 13.

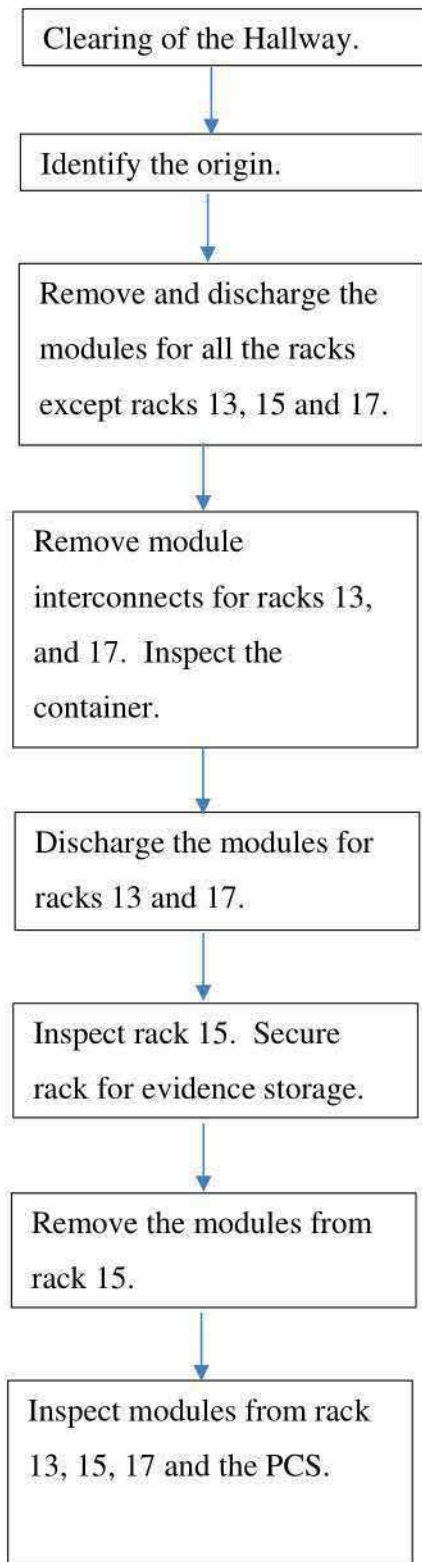


Figure 13 Inspection sequence.

The hallway in the container separating the two sets of module racks was filled with debris (see Figure 14 through Figure 16) after the incident and was not accessible. In Figure 16, the sampling tube for the very early smoke detection apparatus (VESDA) can be seen hanging down because of heat exposure. It was noted that artifacts stored in the vacant racks, close to the door were consumed by fire.



Figure 14 The hallway separating the odd numbered and even numbered module racks.



Figure 15 The hallway.



Figure 16 The ceiling above the hallway, showing the VESDA sampling tube, lighting, and HVAC ductwork.

The debris was removed, logged, and inspected. Once the hallway was cleared, the racks were inspected. The rack identified as the most likely origin was Rack 15 (see Figure 17). All the racks in the container sustained smoke damage. Racks 13 and 17 were adjacent to Rack 15 and sustained minor thermal damage in addition to smoke damage. Rack 15 showed fire damage extending from the bottom of the door to the top of the rack (see Figure 18 through Figure 20). The wiring conduit, wiring trays and general wiring above Rack 15 also sustained significant fire damage. Rack 15 was left intact.

## Fire Damage Observed

Exponent did not enter the container until most undamaged modules had been discharged. However, Exponent was provided with photographs prior to the removal of many components. The burn damage was concentrated near and around Rack 15.



Figure 17 Photograph showing the hallway and lower areas of racks. Rack 15 shows the most significant heat damage.



Figure 18 Photograph showing heat damage to the lower-middle section of Rack 15.



Figure 19 Photograph showing heat damage to the middle-upper section of Rack 15.



Figure 20 Photograph showing heat damage to the upper section of Rack 15.



Figure 21 The odd numbered racks which includes Rack 15.

## **Liquid Intrusion Observations**

During site-examinations, observations of liquid intrusion into the McMicken BESS were made. These are described in more detail in a subsequent section.

## **Battery Module Connection Observations**

While modules were being disconnected to be removed from the BESS for discharge, a few of the external jumper cables which connected the modules together were observed to be loose. On at least one module, there appeared to be a white residue and discoloration on the terminals (see Figure 22). Additional observations relating to this are described later in the report. Exponent was not permitted in the BESS to observe disassembly.



Figure 22 Likely corrosion observed on module terminals.

## **Key Observations**

Inspection of the McMicken container showed that the origin of the fire was Rack 15. The remaining 26 racks sustained external thermal and smoke damage.

## Data Analysis

---

LG Chem provided an analysis of the log data obtained during the incident<sup>15</sup>. The module data was limited and only captured eight seconds of data after the first cell voltage anomaly was reported. However, at the systems level, the “Core 01 Node 15 BMS Rack DC Voltage” and the “Core 01 Node 15 BMS Rack DC Current” continued to be recorded until the Rack 15 breaker opened at 16:55:18.

## Key Observations

Based on the data that was obtained, four significant observations can be made:

1. Cell 7 pair in Module 2 shows a drop in voltage from an unknown voltage above 4.06 V to 3.81 V in eight seconds.
2. The current transducer located between modules 1-7 and modules 8-14 indicates a reverse (discharge) current flowed during the failure event. This suggests current flowed from an unknown module located between module 1-7 and a second location electrically on the modules 8-14 side of the current transducer, which includes, the wiring, and modules 8-14, the BPU, SDU and PCS.
3. Rack 15 isolation resistance changes were recorded by the IMD prior to the failure event.
4. The humidity in the container increased significantly three days prior to the failure event, as will be discussed in more detail later.
5. The role of the PCS units in the incident, if any, has not been fully investigated at the time of this report.

## Captured and Stored System Data

Exponent reviewed the data file, and according to LG Chem and Fluence, Rack 15 cell average, minimum and maximum cell voltages, and modules temperatures for the modules in the racks were recorded and logged (see Figure 23).

---

<sup>15</sup> 190528\_Arizona McMicken Log Analysis\_v6.pptx

The DAS sampling intervals at McMicken were as follows: (19.4.30)

Data Source Name	Sampling Interval
BMS	2 seconds
PCS	2 seconds
Environment	2 seconds
RTAC	5 seconds
Bender	2 seconds

Figure 23 Data acquisition sample rates.<sup>16</sup>

Certain parameters were logged when the system was operational. The following subset of data captured in the “Core 01 Node 15 BMS\_2019-04-19.xlsx” file was reviewed in this analysis:

- **Core 01 Node 15 BMS Battery Modules per Rack** – Each module has 2 Battery Management System (BMS) control circuits on one circuit board, each BMS monitors a sub module of 7 series cell pairs in the battery module. The two BMS control circuits together form the modules BMS (MBMS). The MBMS in each battery module is monitored by the rack BMS (RBMS) through a Controller Area Network (CAN) bus.
- **Core 01 Node 15 BMS Heartbeat** – This is a counter that determines whether the BMS is active.
- **Core 01 Node 15 BMS Cell Balancing Status** – When true, it implies the cell balancing in the modules are active. However, this feature and the column “Core 01 Node 15 BMS Remaining Balancing Time” is not fully understood.
- **Core 01 Node 15 BMS Cell Sum Voltage** – This is the sum of the voltages of the 196 cells in the rack.
- **Core 01 Node 15 BMS Module 01 Max Module Temp to Core 01 Node 15 BMS Module 14 Max Module Temp** – The maximum temperatures reported by the modules.
- **Core 01 Node 15 BMS Rack Avg. Cell Voltage** – This is the average voltage of the 196 cell pairs in the rack. The data is not sensitive to single cell voltage excursions and due to the rack total of 14 modules, not sensitive to minor module voltage changes.

<sup>16</sup> 190528\_Arizona McMicken Log Analysis\_v6.pptx

- **Core 01 Node 15 BMS Rack DC Current** – The current going into the rack and out of the rack under normal operating conditions. The current is measured between modules 7 and 8.
- **Core 01 Node 15 BMS Rack DC Voltage** – The rack DC voltage is measured at the BPU. The rack voltage is a different measurement compared to the “Cell Sum Voltage” and there may be a small difference between these measurement values. The reason for this is the BMS Rack Voltage accounts for voltage drops in the rack, and the cell sum voltage is purely a sum of all 196 cells voltages in the rack. Compared to the BMS Rack DC Voltage, the Core 01 Node 15 BMS Cell Sum Voltage should be equal when the rack is at rest, higher when the rack is discharged and lower when the rack is charging.
- **Core 01 Node 15 BMS Rack Max. Cell Voltage** – The maximum cell pair (parallel) voltage in the rack which consists of a 196S 2P cell stack.
- **Core 01 Node 15 BMS Rack Max. Module Temperature** – The highest module temperature in the rack.
- **Core 01 Node 15 BMS Rack Max./Min. Cell Voltage Location** – The module with the highest and lowest cell voltage.
- **Core 01 Node 15 BMS Rack Max./Min. Cell Voltage Number** – The cell location in the identified module (spread across the 14 modules) that has the highest and lowest cell voltage.
- **Core 01 Node 15 BMS Rack Min. Cell Voltage** – The voltage of the lowest voltage cell in the rack.
- **Core 01 Node 15 BMS Rack SOC** – The state of charge of the rack.
- **Core 01 Node 15 BMS RBMS S/W Version** – The rack BMS software version.
- **Core 01 Node 15 BMS Remaining Balancing Time** – How long it will take to balance the cells in the rack.
- **Core 01 Node 15 BMS Fan Operation Fault** – Alarm showing whether a fan is operational or not.
- **Core 01 Node 15 BMS Fan Status** – Whether a fan is running or not.
- **Core 01 Node 15 BMS MBMS Communication Loss** – Indication of whether communication to a module BMS is lost.
- **Core 01 Node 15 BMS MBMS Loss of Communication Events Count** – Count of lost communication events.

## Failure Data Limitations

The BESS data logging system implemented at the McMicken site was found to have data logging limitations which limited the information and hence made a detailed failure investigation at module and cell level challenging. It seems the system was designed to capture data for normal operations at systems level and hence individual cell voltages were not recorded. At the rack cell level, cell voltage data capturing was limited to the minimum (min), maximum (max), cell sum and average rack-cell voltages. This means that the cell voltages of the remaining cells were not available, for example, if the lowest cell in the module racks voltage was recorded, there was no voltage recording of the adjacent cells in the module, nor the state of the other modules cells in the module rack. The same applies to the high voltage recording. The method of recording data had additional limitations, for example:

- The sample rate of data that was logged was slow at 1 sample for every two seconds (see Figure 23 and Figure 24). The data logger takes a snapshot of the minimum cell voltage data every two seconds, similar to a photo that is taken – this means that the data does not indicate a rising, falling or static value.

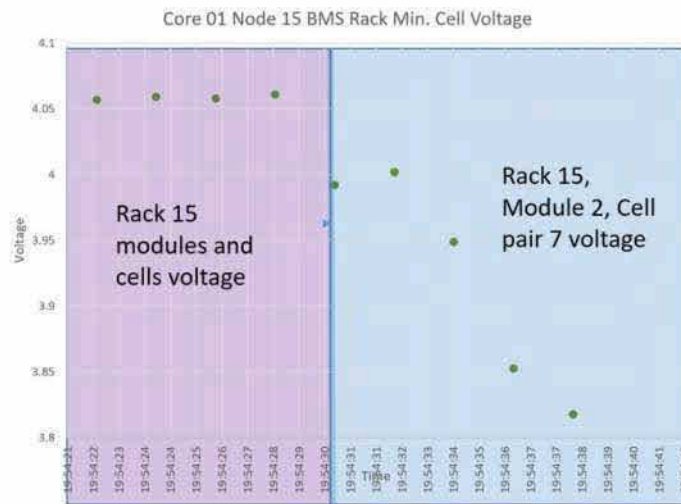


Figure 24 The data captured for the minimum voltage in the system at the time of the incident.

- It is just a voltage level that the data logger captured at that point in time. Hence, the shape and slope of the voltage data cannot be determined. Limiting the data acquisition to only minimum, maximum, average values and cell sum voltage created another challenge. The

first challenge is that measurements need to be sensitive and accurate in the millivolt range, depending on rounding, and single cell voltage excursions or multi cell voltage excursions may be diluted within the 196 cells in the rack cell stack data. The data acquisition system response to high-frequency events or fast voltage transients at the multi-cell level may produce data that appears to be similar to low frequency single cell pair voltage excursion.

- In the case where a cell becomes the minimum voltage in the rack and it is therefore being recorded, the data does not capture its initial cell voltage state prior to becoming the low cell voltage measurement.
- The data does not show what happens to the cell voltage in between the two second data points. For example, if the cell voltage has higher frequency fluctuations than the data logger sample rate, then the true voltage signal is not reproducible with the recorded data and is therefore unknowable.

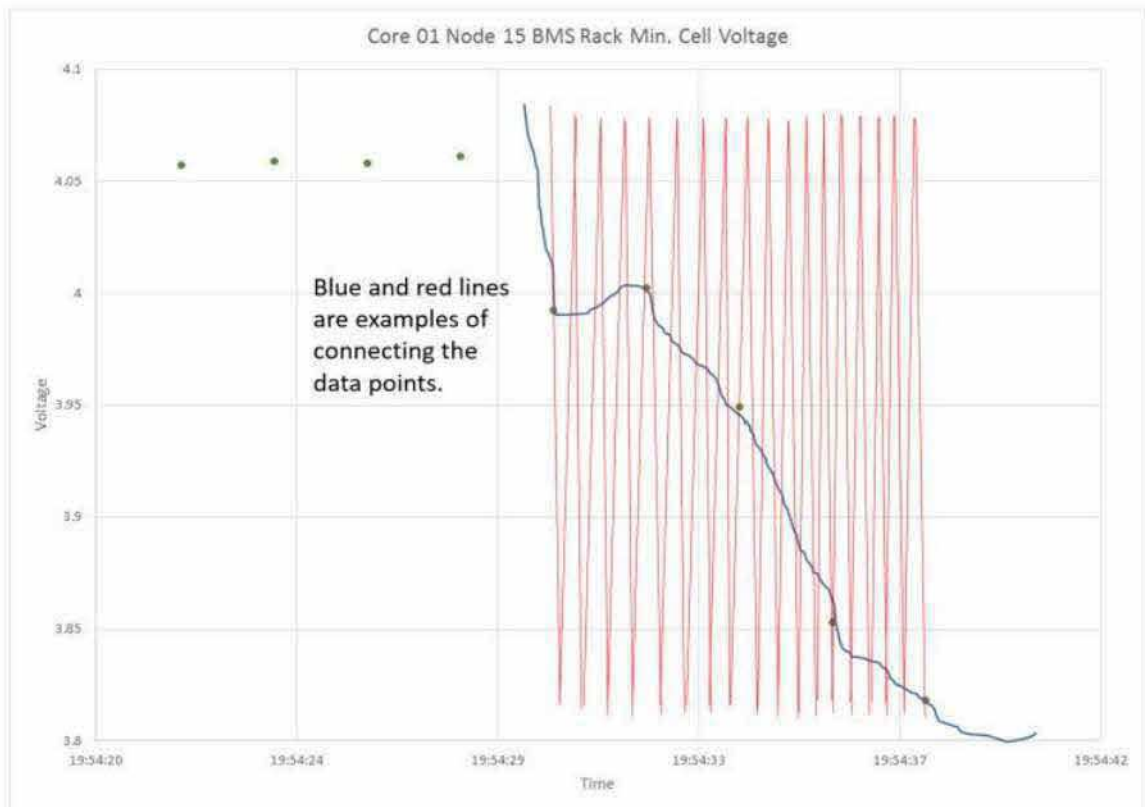


Figure 25 Example of signal aliasing using the incident excursion data points.

An example of signal aliasing is shown in Figure 25. The sample rate is 0.5Hz which is too slow to accurately recreate a higher frequency signal. Excel tends to connect the data points based on the type of graph template that was selected. This can result in an undue confidence in understanding the true signal characteristics. The blue profile was artificially created using the data points. The red profile was also artificially created from the data points. Hence, the data points do not provide information on the frequency of the signal and hence by signal association, a specific failure mode cannot be identified. The data of the minimum voltage during the incident is shown in Figure 25 and Figure 26 .

Timestamp	Core 01 Node 15 BMS Rack Max./Min. Cell Voltage Location	Core 01 Node 15 BMS Rack Max./Min. Cell Voltage Number	Module cell recording for Min Voltage in the Rack	Module cell recording for Max Voltage in the Rack	Core 01 Node 15 BMS Rack Min. Cell Voltage
19:54:22	1283	16419	Module5, cell 8	Module 3 cell7	4.057
19:54:22					
19:54:24	1284	16439	Module 5 cell 8	Module 4 cell 13	4.059
19:54:26		16433	Cell 8	Cell 7	4.058
19:54:26					
19:54:26					
19:54:28	260	1073	Module 1 cell 4	Module 4 cell 7	4.061
19:54:29					
19:54:29					
19:54:30	518	5460	Module2 cell 7	Module 6 cell 14	3.992
19:54:31					
19:54:32					4.002
19:54:32					
19:54:32					
19:54:32					
19:54:34	515	5411	Module 2 cell 7	Module 3 cell 7	3.949
19:54:34					
19:54:36	518	5447	Module 2 cell 7	Module 6 cell 5	3.853
19:54:38	515	5411	Module 2 cell 7	Module 3 cell 7	3.818
19:54:38					

Figure 26 A partial list of data points during the incident.

From the log entries, at 19:54:28, module 1 cell 4 had the lowest cell voltage recorded at 4.061V. At 19:54:30, the data logger recorded Module 2 Cell 7 pair voltage at 3.992V. At each subsequent two second intervals, the data logger recorded Module 2, Cell 7 pair voltages. The data points were plotted and are shown in Figure 24. It is not known what Module 2 Cell 7 pair voltages behavior was in between the two second recording intervals – this is due to signal aliasing. Hence, it is not known whether the voltage signal was a low frequency signal or a high frequency signal as illustrated in Figure 25. Additionally, it is not known if other cells became the lowest voltages in the rack within these 2 second intervals.

- The data for minimum cell voltage and maximum cell voltage is not individually recorded for each module. Again, data recording was setup at systems level assuming 196 cells in series and not separated into module data sets.
- Not all the cells in a module or submodule are exactly the same. There will be a weakest cell pair and a strongest cell pair. In the cell racks there will be a weakest module and a strongest module. The weakest cell pair will charge and discharge the fastest and hence, when a module is loaded, the weakest cell pair with the lowest voltage will be recorded. Therefore, depending on the cells in the rack’s state of charge, during the end of discharge or at the end of charge:
  - The modules with the weakest cell pairs will, typically during charge, show the highest cell voltage and during discharge the lowest cell pair voltage.
  - The modules with the heathiest cell pairs will show the lowest voltage during charge and the highest voltage during discharge.

Therefore, in any operating state, of the 196 cells, there will be a cell pair that registers the highest cell voltage and a cell pair that registers the lowest cell voltage.

- The cell level data was available for eight seconds until the CAN BUS failed at approximately 19:54:38. However, at systems level, the “Core 01 Node 15 BMS Rack DC Voltage” and the “Core 01 Node 15 BMS Rack DC Current” continued to be recorded until the rack breaker opened at 19:55:18.
- There is evidence of what appears to be cell voltage fluctuations in the lowest cell voltage measurement (see Figure 26). For example, during the charge cycle, the low cell voltage data for module 5, cell 8, changed in the time period 19:54:22 to 19:54:26, from 4.057V, to 4.059V to 4.058V. This change in voltage is considered abnormal and the reason for this

observation is not known and should be further investigated. It is not known why the voltage fluctuation occurred.

## **Laboratory Parallel Cell Pair Voltage Profile Characterization**

The slow data acquisition rate and the effects of aliasing limited the information of the voltage data of Module 2 Cell 7 pair. It is therefore not known (and unknowable) whether the voltage profile was a high frequency or a low frequency voltage event (see Figure 25) and hence it is unknown whether the profile was associated with arcing and rapid changes in the module cell voltages as a result of external arcing.

### **Module Level Test**

A test was designed to evaluate the hypothesis that the thermal event in the McMicken BESS initiated in cell number 7 in the module. The objective was to force a thermal event to begin at this particular cell in an exemplar module and observe heat generation, heat transfer indicators, and analyze the failure damage sequence and patterns.

#### **Test Setup**

A Model EM048128P6B4BMA ESS battery module (similar to the McMicken modules) was instrumented and utilized for the test. All 14 cell-pair temperatures were recorded by sliding a thermocouple between the cells (see Figure 27). High-temperature, fiberglass insulated thermocouples were used for the testing. An additional thermocouple was attached to the outer part of Cell 7 (see Figure 28). Thermocouples were attached to the negative busbar at the front-facing side of the fuse, and towards the middle of the module (see Figure 29). Thermocouples were also attached to the exterior of the module casing on the bottom plate and the upper plate at the front, middle, and rear locations (see Figure 30).



Figure 27 Photograph showing the installation of voltage taps and cell thermocouples.



Figure 28 Photograph showing the thermocouple attached to the outer surface of the Cell 7 pair.



Figure 29 Photograph showing thermocouples attached to the negative busbar fuse (left) and busbar (right).



Figure 30 Photographs showing three thermocouples attached to the bottom (left) and top (right) panels of the module along the centerline in the front, middle, and rear.

Cell voltage sensing conductors were spliced in with the module voltage sensing conductors (high-temperature, fiberglass thermocouple wire was used to withstand the temperature; also see Figure 27). Wires were routed out of the enclosure through small holes drilled into the side panels and were run through fiberglass sheathing for protection.

An approximately 350 W self-adhesive heat pad was attached to the outer surface of the Cell 7 pair (see Figure 31) and used to initiate the thermal runaway.



Figure 31 Photograph showing the heated pad installed on outer surface of the Cell 7 pair.

Since the earliest evidence to date indicates that the McMicken incident occurred during the charging state, a DC power supply (TDK-Lambda) was used to charge the module in constant current – constant voltage mode with approximately 30 A during the initiation of the thermal runaway event. When the charger was turned on immediately prior to the test, the constant voltage setting was 56.5 V.

A communication cable was connected to the module and the RBMS measurements were recorded via an attached computer with the LGC BenchLink Data Logger (see Figure 32). Additionally, a Bender Iso685 insulation monitoring device was connected to measure the insulation resistance. The case of the module was connected to building ground via a wire on the rear of the case.



Figure 32 Photograph showing the front face of the module pre-test, with the communication cable and charging cables attached.

### **Test Procedure**

The test began when the Cell 7 pair heating pad was turned ON (using 110V AC). The DC power supply was turned on to supply approximately 30A of current to charge the module. At approximately 8 minutes, the charge current and heater were turned OFF to evaluate if thermal runaway was taking place. At approximately 10 minutes into the test, the charge current was turned back ON, and at approximately 14 minutes, the heater was turned back ON. When thermal runaway was confirmed audibly and visually, the heater was turned OFF.

### **Test Result**

The test result (see Figure 34) shows that when one cell in the parallel cell pair goes into thermal runaway, the second cell will compensate for the parallel pair voltage and attempt to keep the cell pair voltage close to the original state of charge cell pair voltage. In the test the initial voltage after approximately eight seconds dropped from approximately 4.09V to 4.05V and took approximately 85 seconds to reach 3.8V. The intermittent voltage drops are likely to be instrumentation related and not to the cells themselves. To validate this voltage profile, the

test was repeated using only one parallel cell pair and causing one cell to go into thermal runaway – similar to the module test.

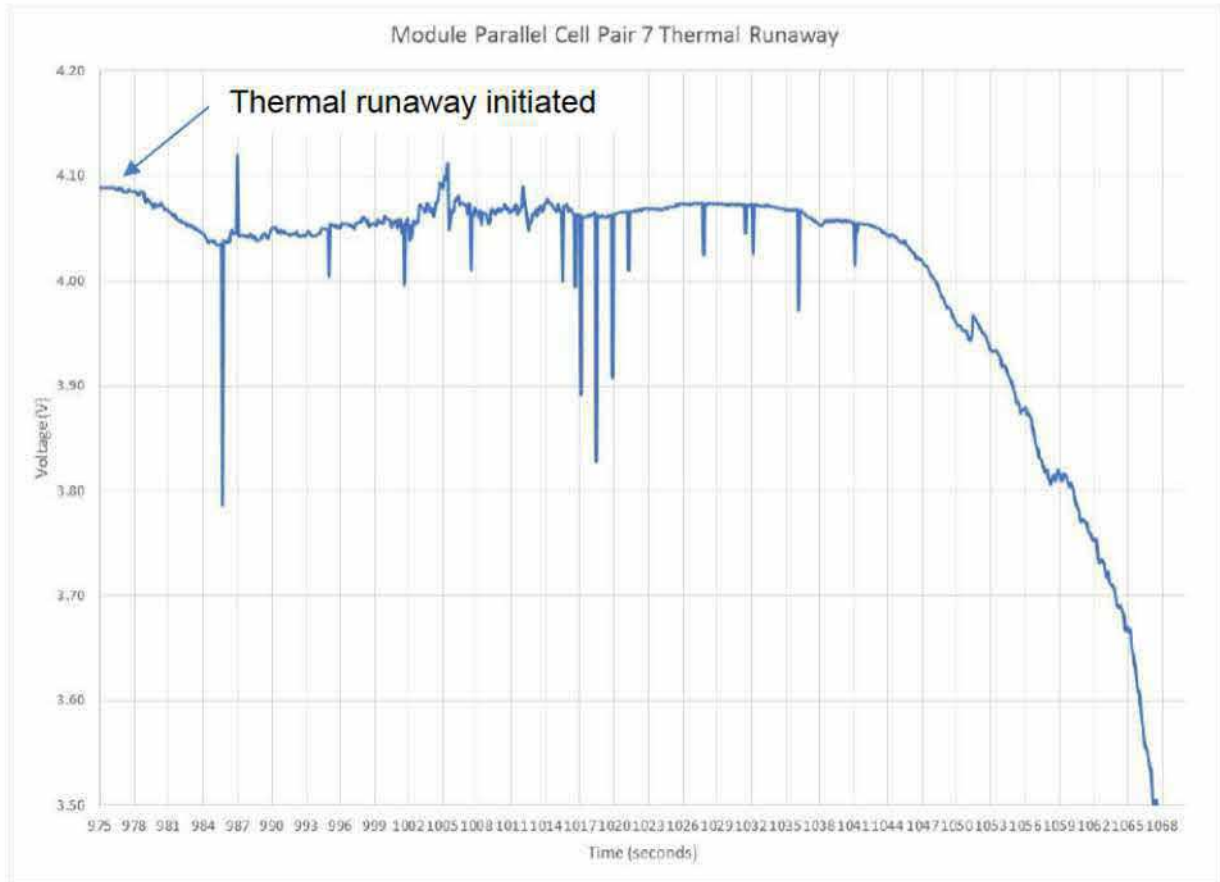


Figure 33 Voltage profile of Cell 7 pair during thermal runaway event inside the module.

### Cell Pair Level Test

Two parallel JP3 cells, similar to the McMicken module cells were used for the test. The cells were pre-charged to 4.08V (a cell voltage similar to the McMicken cells prior to the incident) using a constant current (CC, 32A) – constant voltage (CV, 4.08V) charge profile with a charge cutoff at 3.2A. A patch heater rated at ~ 350W was attached to the bottom cell to initiate thermal runaway as shown in Figure 34. The top and bottom cells were held in-situ using plastic enclosures which keeps them physically separated as shown in Figure 35. The cells were connected in parallel using copper bus-bars (as shown in Figure 36) and charged using an external power supply set at 4.2V, 30A while the bottom cell was initiated to failure. The heater

was disconnected when the cell went into thermal runaway. The thermocouple locations are identified by the red arrows in Figure 34 and Figure 35.

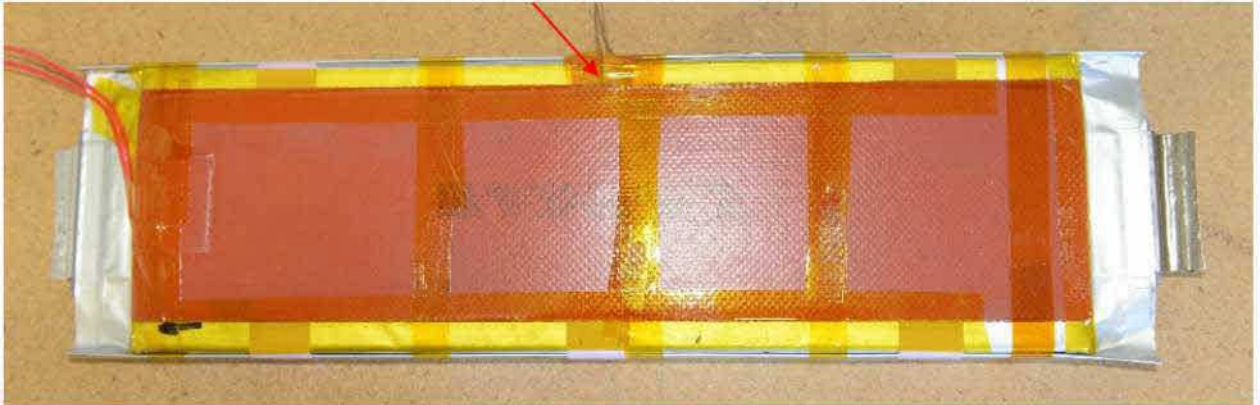


Figure 34. Patch heater attached to the bottom cell with Kapton tape.

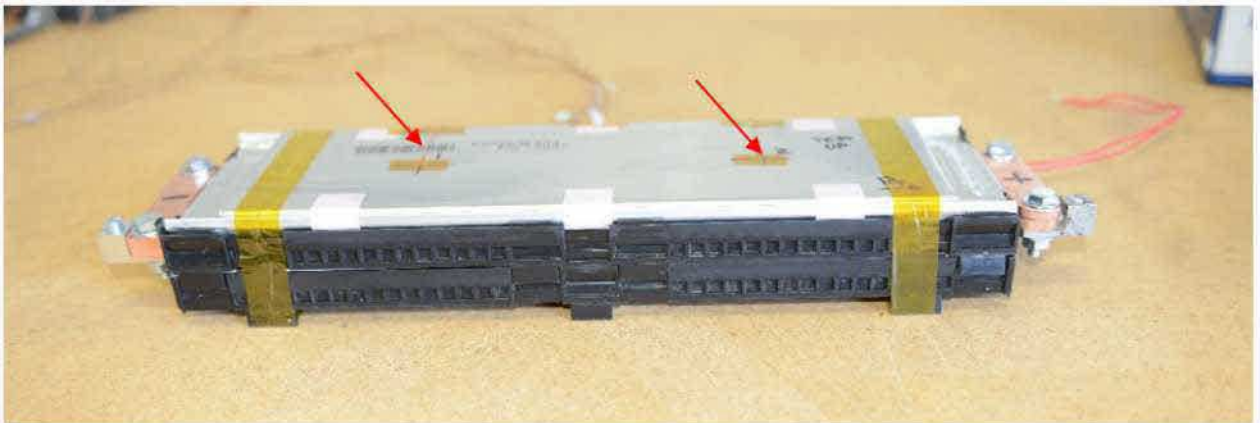


Figure 35. Cells held in-situ using the module plastic cassettes.

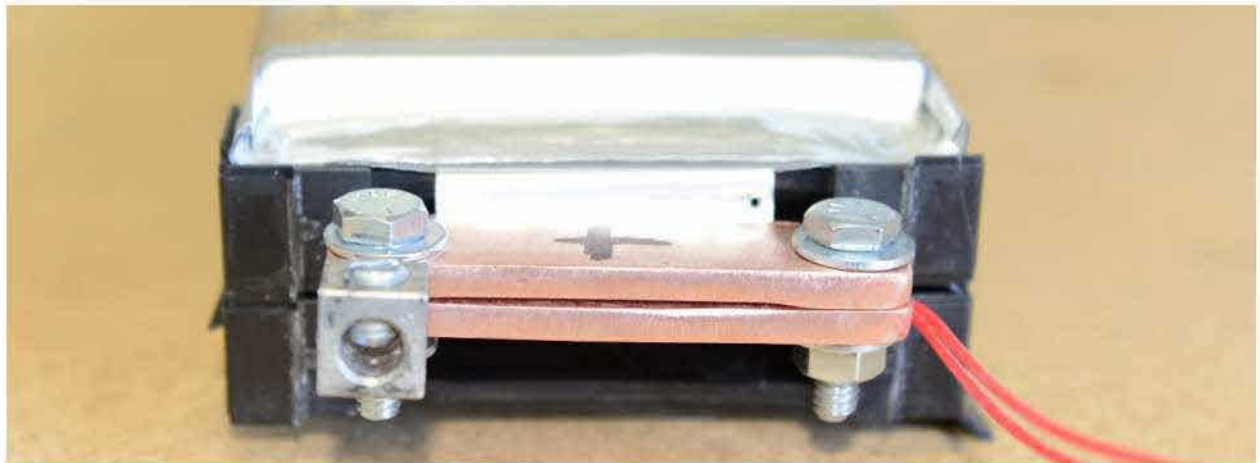


Figure 36. Top and bottom cells connected in parallel using copper bars.

### **Test Result**

The test result (see Figure 37) shows that when one cell in the parallel cell pair goes into thermal runaway, the second cell will compensate for the parallel pair voltage and attempt to keep the cell pair voltage close to the original state of charge cell pair voltage. In the test, the initial voltage, after approximately eight seconds, dropped from approximately 4.09V to 4.05V and took approximately 83 seconds to reach 3.8V. This voltage profile is very similar to the module test voltage profile.



Figure 37 The voltage profile for a parallel JP3 cell pair thermal runaway event.

### Comparison to Incident Voltage Profile

The test results of a single cell failure in a parallel cell configuration were compared to the incident voltage profile as shown in Figure 38.

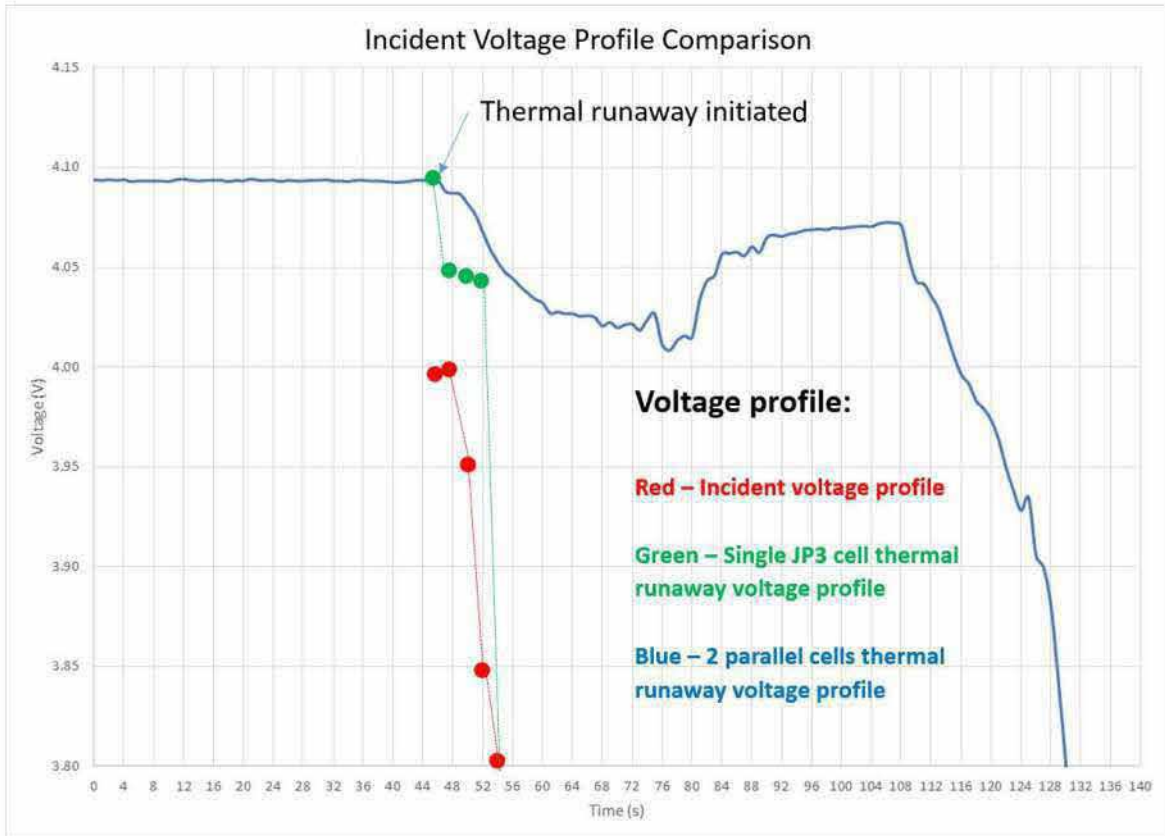


Figure 38 The incident and the cell level test thermal runaway voltage profile comparison.

In Figure 38 the red line is the incident voltage excursion. The blue line is the tested parallel cell with single cell thermal runaway event. Three tests, a single cell thermal runaway event (green data in Figure 38), a module level test and a parallel cell level test (blue data in Figure 38) show that the incident profile is not representative of the cell failure in a parallel cell pair configuration. Testing shows that the voltage profile for a single cell thermal runaway in a parallel configuration is closely reproducible, however this observation is based on limited sample testing. The same test should be conducted in a fully functional rack for further verification.

Based on the parallel cell test results, which matches the configuration in the incident, the incident voltage profile does not match the test result profile and hence it is unlikely that a single cell failure caused the observed voltage excursion. The single cell test, where a single cell was removed from a parallel cell pair in a module for testing, appears to have a somewhat

similar voltage profile to the incident voltage profile, but this configuration is fundamentally different than what was installed in the BESS and hence the single cell voltage profile is fundamentally different compared to a parallel cell voltage profile.

## Failure Event Data Analysis

Data analysis was performed using the recorded data from three independent sources, the BMS DC rack voltage measurement, the rack DC current transducer and the CAN BUS data from the modules.

### Rack Voltage and Current Data Analysis

The module data was limited and only captured eight seconds of data after the first cell voltage excursion was reported. However, at systems level, the “Core 01 Node 15 BMS Rack DC Voltage” and the “Core 01 Node 15 BMS Rack DC Current” continued to be recorded until the rack breaker opened at 19:55:18. A selected set of data is show in Table 2.

Table 2 Selected set of event data (negative indicate a charge current)

Time	Rack DC Voltage	DC Rack Current	Sum of Cell Voltages	Difference in Voltage	Vmaximum	Vmimumum	Vaverage
19:53:52	795.7	0	797	-1.3	4.079	4.039	4.066
19:54:02	795.3	0	797.2	-1.9	4.079	4.040	4.067
19:54:04	797.9	-30	799.1	-1.3	4.089	4.054	4.077
19:54:20	799.2	-30	800.1	-0.9	4.095	4.059	4.082
19:54:28	799.2	-30	800.4		4.097	4.061	4.083
19:54:30	798.9	-30	800.4		4.098	3.992	4.083
19:54:32	799.6	-29.8	800.2		4.097	4.002	4.083
19:54:36	799.5	-30	800.4	-0.9	4.097	3.853	4.083
19:54:38	799.9	-27.9	800.5	-0.6	4.097	3.818	4.084
19:54:40	796.1	-1.6	Data lost		Data lost	Data lost	Data lost
19:54:42	Approximately at this time, the PCS intel air temperature start to rise						
19:54:44	797	1	Data lost		Data lost	Data lost	Data lost
19:54:48	798.9	3.6					
19:55:17	796	4.9					
19:55:18	Rack Breaker opens						

When the data was analyzed the following was noted:

- When the cells in the rack charge, the cumulative internal resistance of the cells and the wiring voltage drop cause a difference between the Rack 15 DC voltage and the sum of the

rack cell voltages. It is not understood why the rack voltage is lower than the accumulative cell voltage during the charge cycle.

- A single cell voltage excursion cannot positively be identified or accounted for (see Appendix D):
- Evidence in the Rack 15 voltage data suggest multi-cell pair voltage excursions and not exclusively a single cell pair voltage excursion (see Appendix E).

The first negative voltage excursion cannot be accounted for in the voltage parameters stored in the logged data. The data logging algorithm is not clearly understood and it is therefore possible that the voltage data captured, could be an artifact of fast intermitted arc discharges. A sequential cell voltage measuring algorithm starting at cell 1 and ending at cell 196, may for example only capture certain cells voltage excursions if the module or rack voltage is disturbed in a fast-negative voltage transient, typically associated with intermittent arcing. This might have diluted the transient effect in the data and may explain the fact that the average voltage calculation was not affected. An understanding of system measurement accuracy, noise and characterization testing are required for further investigation.

The uncertainty of the voltage data analysis may support multi-cell fast negative voltage transient events. This observation is supported by the test data showing that a single cell failure voltage profile is not consistent with the incident Module 2 Cell 7 voltage profile. Testing is recommended to understand the effects of fast negative voltage transient events, and how the data acquisition system capture this data, so that a better understanding of the logged data can be obtained.

A current was observed at the time of the first parallel cell pair voltage excursion. An example of a normal charge current is shown in Figure 39. The DC current return to zero ampere after a small positive peak. It is not understood why this positive (discharge) current peak is present in the data. According to LG Chem, the 10 AC current is normal.

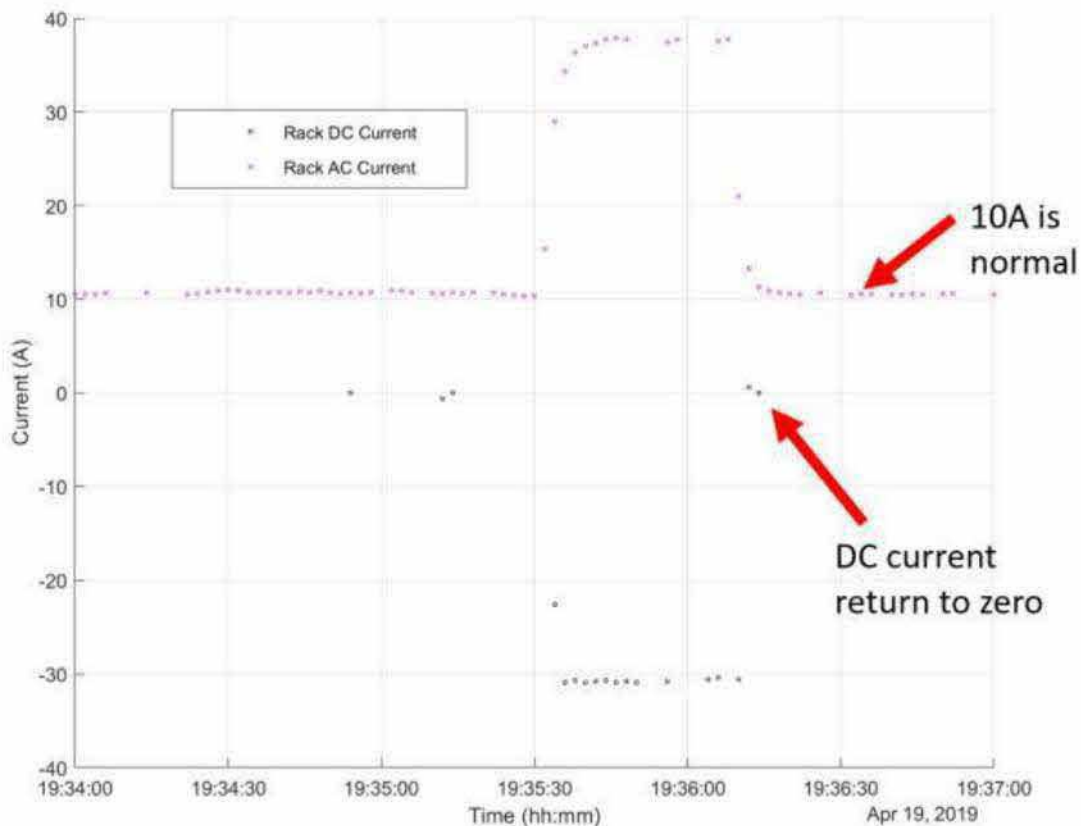


Figure 39 The normal end of charge current profile.

The incident current profile is shown in Figure 40 and is different. The Rack 15 current transitions from a charge (negative current) current to a discharge (positive current) current and continue to be present until Rack 15's breaker opens. When compared to the normal charge profile, this discharge current is abnormal. Again, signal aliasing likely does not show the actual current profile and hence current peaks could have been significantly higher between data points. When it is considered that the cells in Rack 15 are floating with respect to the rack (isolated from the rack), the only plausible way this current can be present is when there are two simultaneous electrical isolation faults in rack 15. This evidence supports a double electrical isolation failure due to the current measured by the current transducer located between modules 1-7 and modules 8-14.

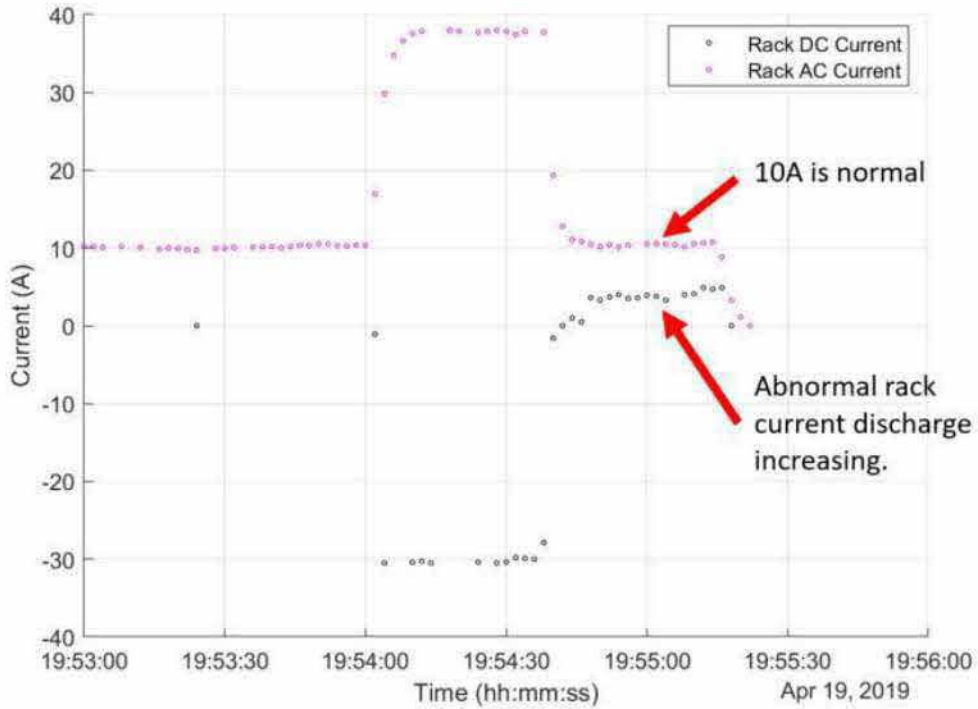


Figure 40 The abnormal end of charge current profile prior and during the failure event.

The charge current and unknown positive discharge current excursions were noted (see Figure 41) prior to the incident and should be further investigated.

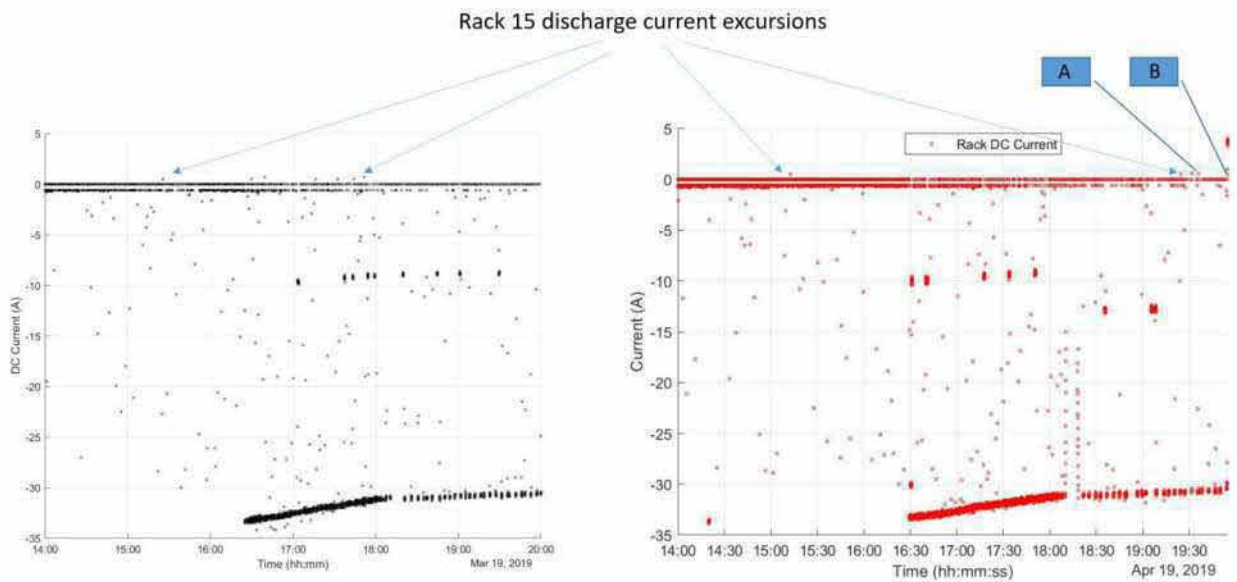


Figure 41 Discharge current excursions.

## Rack 15 Electrical Isolation Analysis

It was noted that electrical isolation excursions were reported by the IMD before and during the failure event as shown in Figure 42.<sup>17</sup>

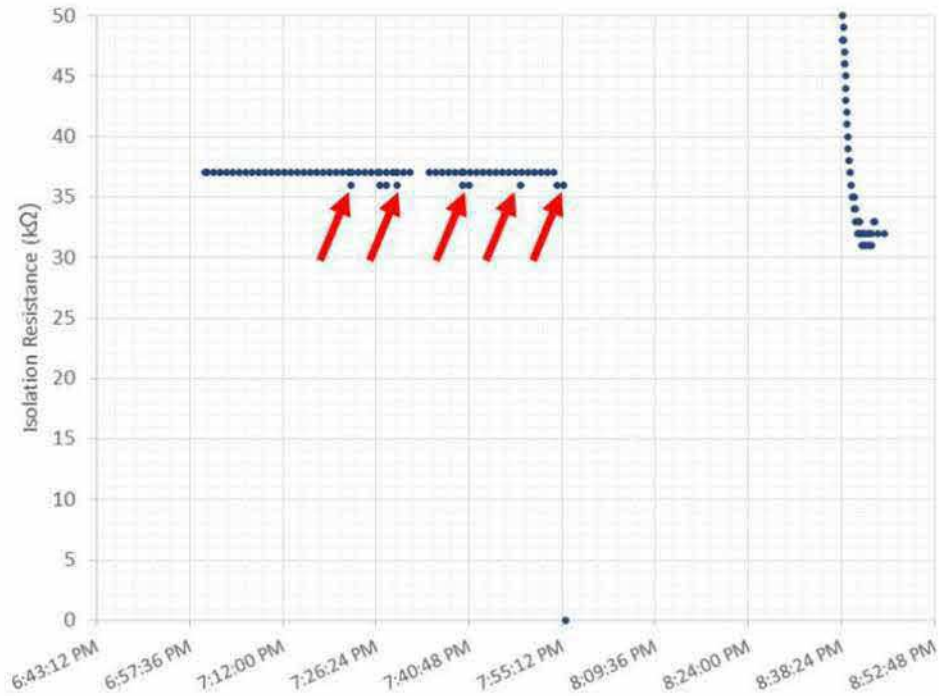


Figure 42 IMD data showing electrical isolation excursions.

The IMD resistance excursion indicates a single point electrical isolation failure or a double point electrical isolation failure. The data does not have sufficient information to distinguish between a single or a double point electrical isolation failure event. This suggests that the cell stack was not floating freely and electrical isolation between the cells and Rack 15 frame was momentarily compromised before and during the failure event. This evidence further supports an electrical isolation failure between modules 1-7 and modules 8-14. Exponent is aware of prior IMD electrical insulation resistance excursions, and these need to be further investigated.

<sup>17</sup> This data set is the full IMD data set provided to Exponent leading up to the voltage excursion.

## Key Observations:

The following key observations were noted:

- The module level event data was only recorded for eight seconds following the parallel Cell 7 pair voltage excursion. The DC Rack 15 voltage and current were recorded and available until Rack 15's breaker opened, for approximately 48 seconds following the parallel Cell 7 pair voltage excursion. The sequence of the logged Module 2 parallel Cell 7 pair voltage data, Rack 15's DC voltage data, Rack 15's DC current data are three independent measurements that were recorded.
- Testing performed by Exponent at the module and parallel cell pair level has shown that the Module 2 parallel Cell 7 pair voltage profile is not representative of a single cell failure event in a parallel cell pair configuration.
- The parallel Cell 7 pair excursion voltage could not be accounted for in all the stored voltage parameters. The characteristics of the data logger may mask fast negative voltage transient events.
- Rack 15's DC discharge current suggests a double point electrical isolation failure mechanism that was caused by fault current flow between modules 1-7 and modules 8-14. The DC rack discharge current coincides with the corresponding heating detected in the PCS. The rack DC current could have been associated with arcing and subsequent fire, causing the observed PCS heating.

## McMicken Module Performance Analysis

---

In order to inspect Rack 15, the site had to be cleared of any risk of electrical shock. The energized modules had to be discharged to 0% SOC so that they could be safely stored.

With the exception of Racks 13, 15 and 17, the modules from the remaining racks were sequentially discharged, starting at Rack 1 and module 14.

### Module Discharge and Inspection

Exponent personnel participated in the development of the disassembly protocol and witnessed the disassembly. Prior to the discharge task, the modules were first removed from the container in a deliberate, methodical, one-by-one process.

The modules were then discharged, inspected, photo documented and then stored. Once identified modules were discharged, the modules from Racks 13 and 15 were removed and discharged. A total of 361 modules were discharged as found (see Figure 43).

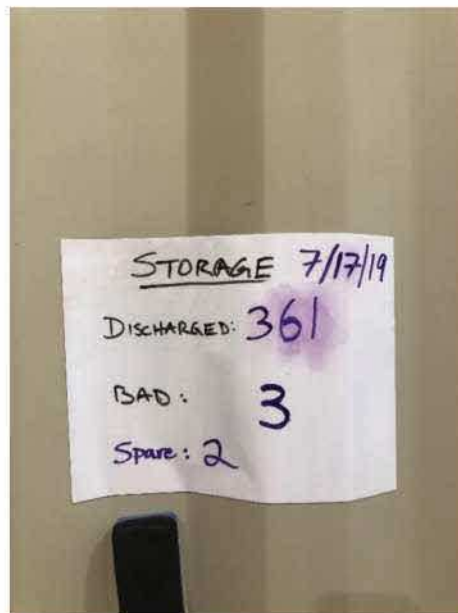


Figure 43 Module discharge count.

It was noted that the modules were smoke damaged and some modules showed thermal damage to the front cover. In three modules, Rack 20, module 14, Rack 24, module 14 and Rack 5, module 6, the MBMS seemed to be damaged as a result of the incident. These modules were discharged by replacing the MBMS and the modules discharged normally.

During discharge it was noted that the Rack 13, module 8 (see Figure 44) positive terminal heated during discharge. The module discharge current was reduced from 64A to 20A to maintain a terminal temperature at or below 50°C. The module was inspected but the terminals could not be inspected as they were covered. It was also noted that the Rack 17, module 7 positive power terminal heated to 40°C during discharge of the module. The cause of the terminal heating was not investigated.



Figure 44 Module 8, Rack 13.



Figure 45 Module 7 Rack 17.

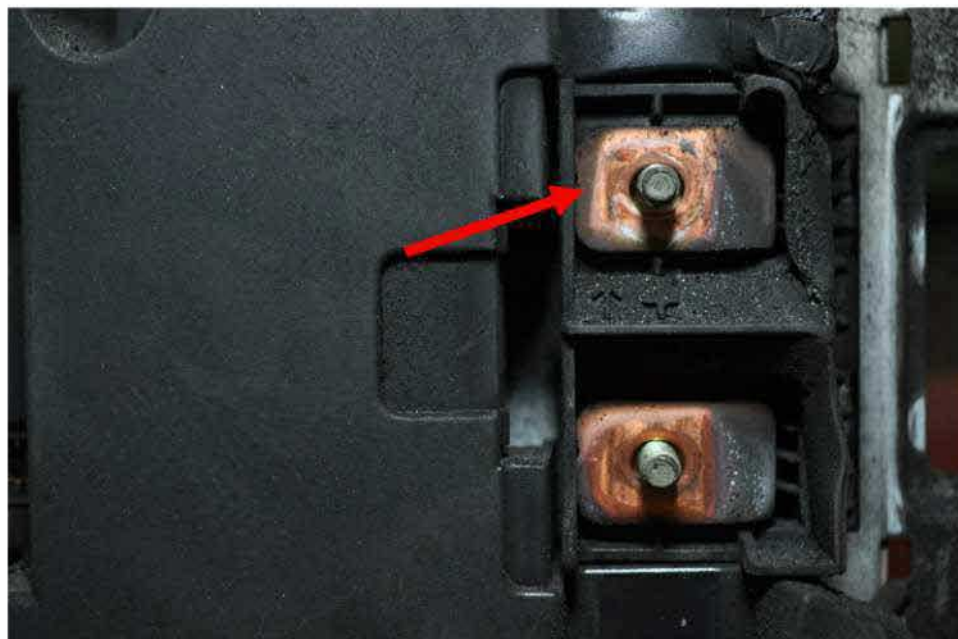


Figure 46 Module 7 Rack 17 power terminals.



Figure 47 Module 8 Rack 17.

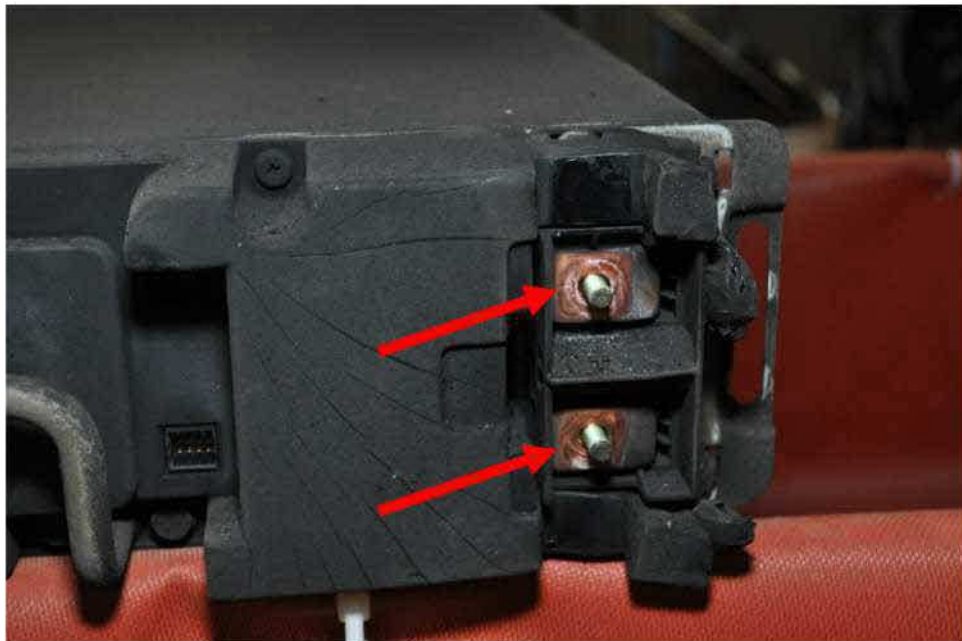


Figure 48 Module 8 Rack 17 power terminals.

White residue was observed on several modules including Rack 17, modules 7 and 8 (see Figure 45 and Figure 48). Module terminals in Rack 17, for example modules 7, 8 and 9 showed

evidence of a white residue at the contact area of the positive terminal. This observation was not consistent across all the module terminals. Rack 13 could not be inspected because the terminals were covered.



Figure 49 Module power terminals.



Figure 50 Module power terminals.



Figure 51 BPU in the rack.

## Analysis of Module Discharge Data

The discharge data was analyzed to identify abnormal module discharge behavior or modules with cells that are behaving abnormally. A total of 366 battery modules were discharged at the McMicken site and the data for 360 were evaluated as part of the current analysis (2 were spare modules). Rack 15 and modules with a submodule cell imbalance or showing a communication error likely due to a damaged MBMS circuit board were not evaluated. These modules are:

- 3 Modules could not initially be discharged
  - Rack 5, module 6 (Red/Green)
  - Rack 20, module 14 (Red)
  - Rack 24, module 14 (Red/Green)
- 1 Module had a submodule cell imbalance prior to discharge
  - Rack 2, module 13
- The modules in Rack 15 could not electrically be discharged due to the extensive thermal damage and were not considered in this analysis.

The cell imbalance in the modules were evaluated prior to and after the module was discharged. Cell pairs that are damaged or defective likely will have less capacity, discharge faster than the neighboring cells and show a large cell imbalance in the module. The data in Figure 52 to Figure 54 shows the rack on the Y-axis. Rack X101 is Rack 1. The X-axis show the module and 01 will be module 1 which is located at the bottom of the module rack.

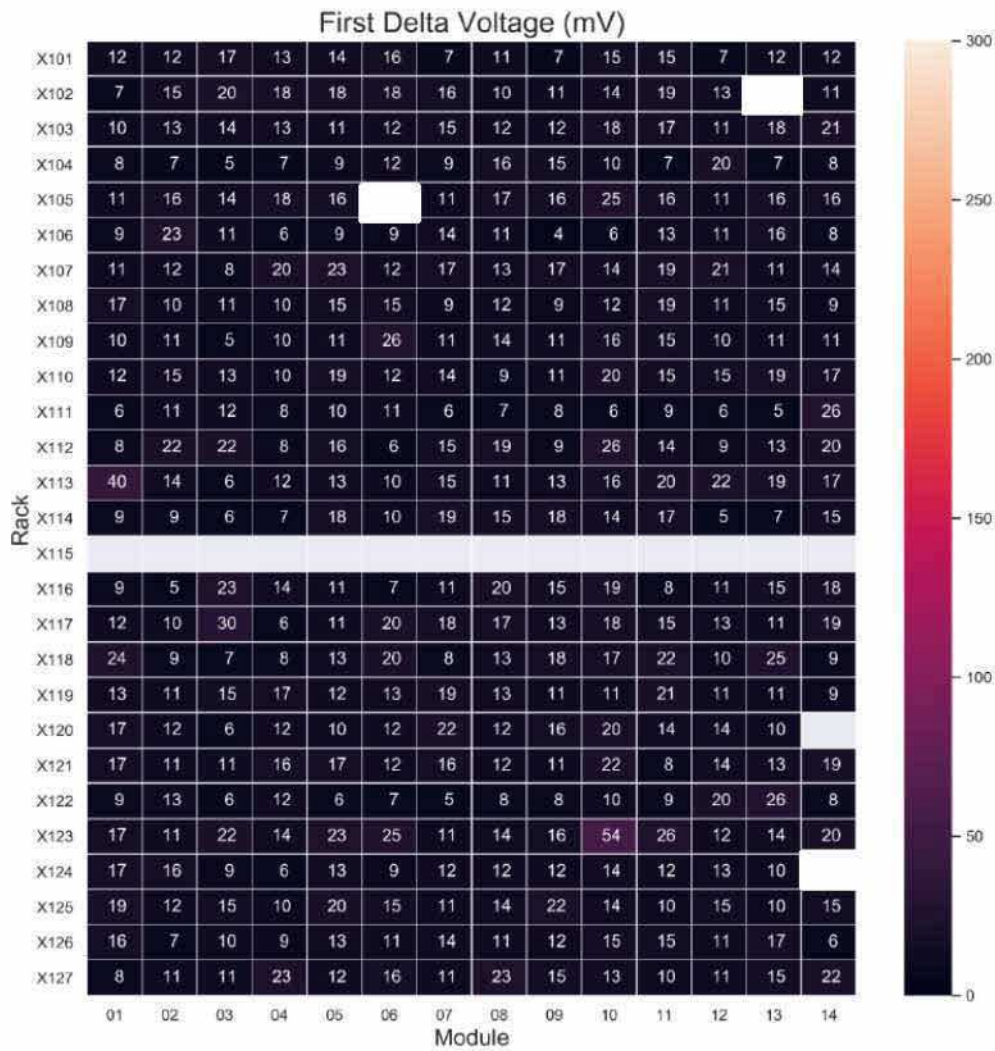


Figure 52 The modules at McMicken cell voltage difference after the incident and prior to discharge.

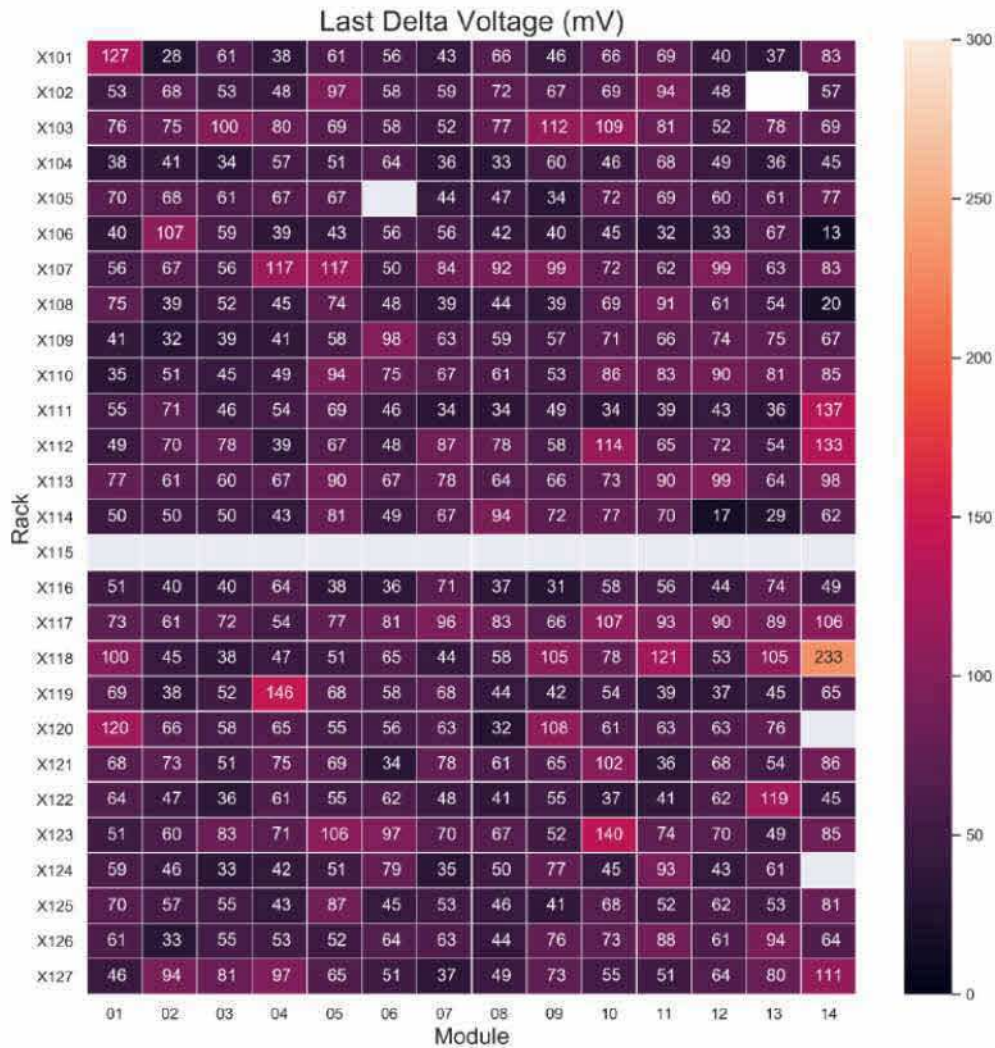


Figure 53 The modules at McMicken cell voltage difference after the incident and after discharge was complete.

The cell voltage imbalance analysis did not show any outlier cell pairs. The higher voltage deviation after discharge is a characteristic of the cells.

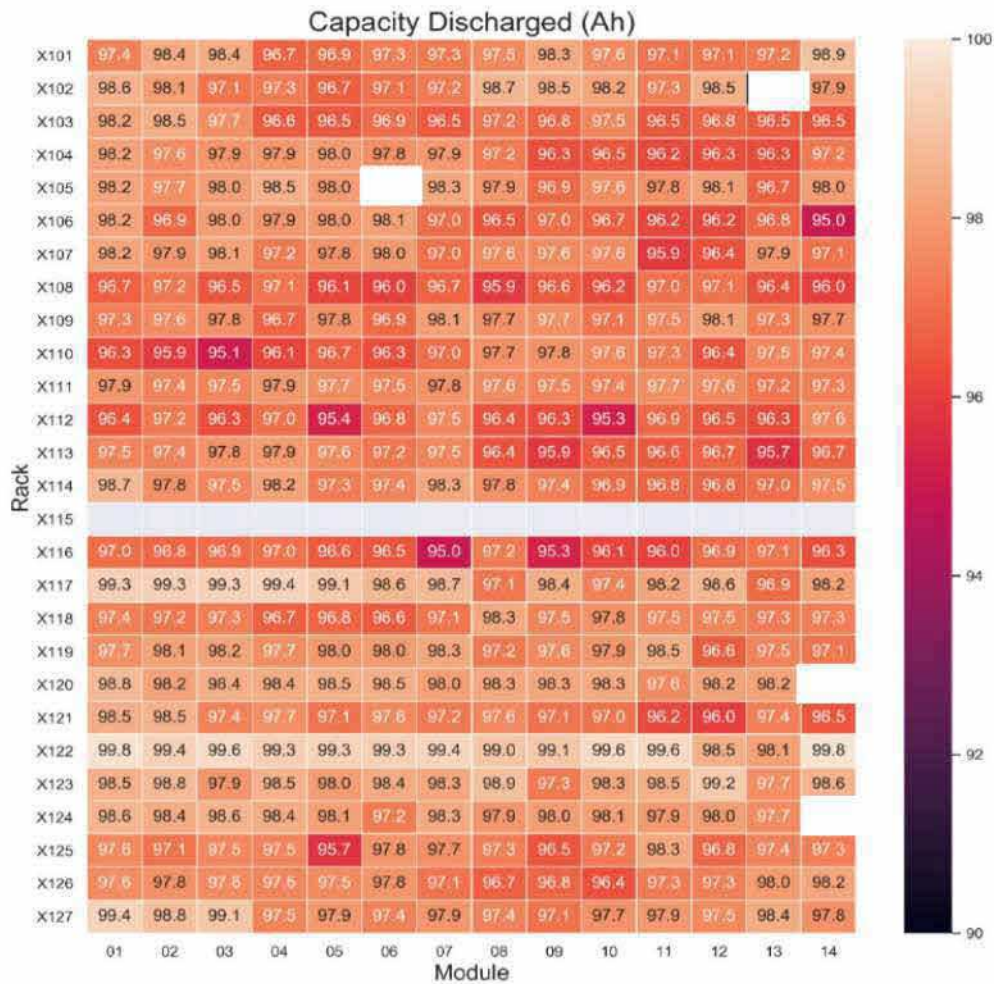


Figure 54 The modules at McMicken showing the amount of discharge capacity left.

The discharge capacity left in the modules after the incident was calculated and is shown in Figure 54. The discharge of the modules was not automated and hence variation may have occurred. However, the data supports the cell imbalance analysis and the cells in the tested modules behaved in a very similar manner and were well matched.

## Key Observations

The following key observations were noted:

- Three modules experienced MBMS failures likely because these modules were at the top of the racks and hence exposed to the highest temperatures. However, the MBMS failed safe and upon replacement of the MBMS, the modules discharged safely. A fourth module had a submodule imbalance – this module also discharged safely. Rack 15 modules all went into thermal runaway and were not functional to test.
- Two modules showed an elevated positive terminal temperature during discharge. It was noted that a white residue was present on the positive terminals on three of the modules, including a module that showed elevated positive terminal temperature. The cause of the terminal heating and white residue were not further investigated.
- The remaining modules all functioned as intended and discharged safely.
- Even after the modules were exposed to extreme temperatures, the discharged cells in the analyzed modules performed very similarly. There were no module and cell outliers when the cell imbalance voltage and module discharge capacity were reviewed.

## Inspection and Removal of Rack 15

---

Rack 15 was the last rack to be inspected. Rack 15 was inspected and it was observed that the rack was completely consumed by the fire.

The inspection showed that the center area of the module enclosure melted away to form a circular feature. Molten aluminum could be observed dripping from rack module to rack module and puddles of aluminum could be observed on the floor. The floor was covered with black soot.

Inspecting the face of the rack showed an interesting feature on the floor. There was an oval section of the floor right in front of the rack, exposing the original floor paint (see Figure 55). This suggests that debris covered the floor prior to soot coloring the floor.



Figure 55 Floor in front of Rack 15.

Spatter could be observed on the wall. The spatter coincided with the location of the inverter fans. Inspection of the inverter fans showed the fans were clogged with debris (see Figure 56 and Figure 57).



Figure 56 Wall behind the racks.



Figure 57 PCS (Inverter) from Rack 15 with clogged fan vents.

The door was removed and inspected (see Figure 58 to Figure 60). Debris of an unknown source was observed to be attached to the screen of the door in the general location of module 3's fan and power terminals.



Figure 58 Rack 15 door.

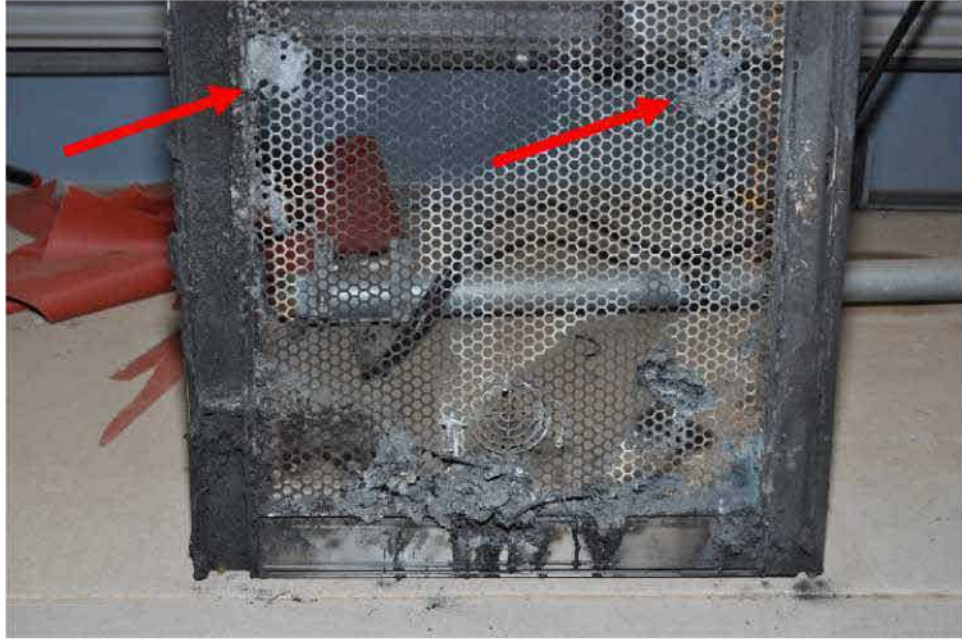


Figure 59 Rack 15 door.

Once the door was removed the front panels of the modules in Rack 15 could be inspected. It was noted that debris could be observed on the screen of the door, including in the general area of module 3's fan and power terminals.

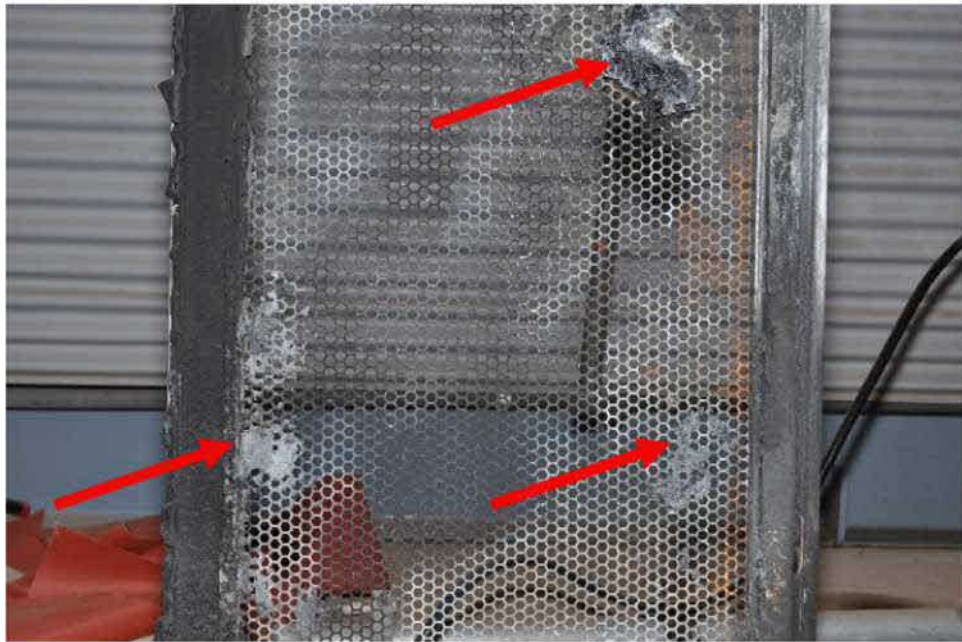


Figure 60 Rack 15 door with debris attached to the screen of the door.

The front plastic covers of the modules were completely consumed in the fire. The PCS, BPU and SDU were also completely consumed in the fire.



Figure 61 Rack 15, module 11.

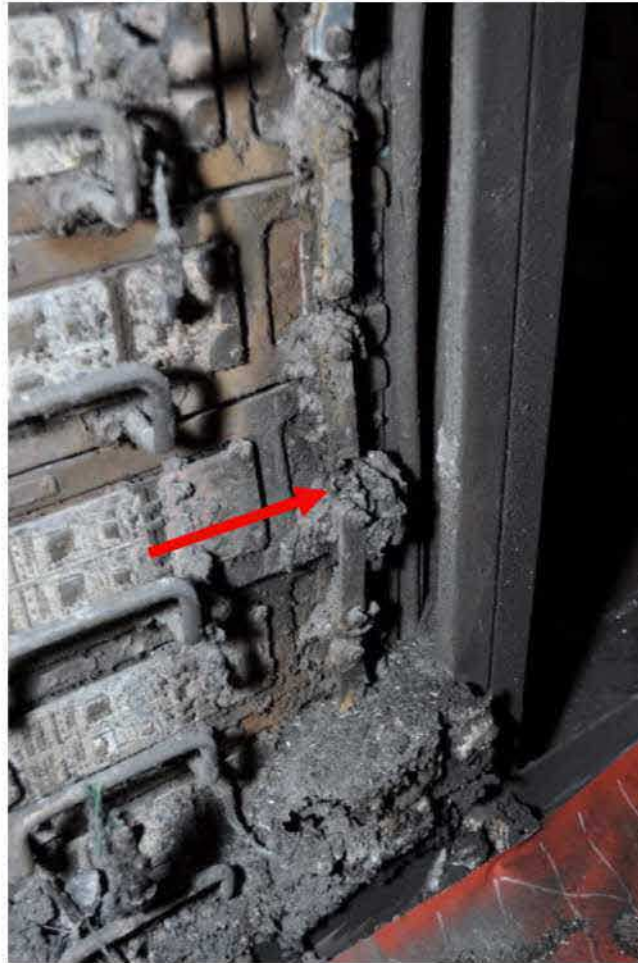


Figure 62 Rack 15, Module 3 - the red arrow points to the arc damaged positive terminal and busbar.

Inspecting the exposed sides of the modules showed evidence of melting, perhaps associated with arcing on the right side of module 11 (See Figure 61). The reason for the melting of the case is not known. The left sides of the modules were intact. It was noted that the external busbar of module 3 at the positive power terminal was electrically open and appears to be arc damaged (see Figure 62).

On rear covers of the modules there were interesting artifacts (see Figure 63). Modules 2, 3, 7, 8, 11, 13 and 14 show circular artifacts on their rear covers. All the artifacts seem to be independent to the specific module, except in the case of Module 3 and Module 2, which seem to share the same artifact. Black plastic drippings were observed.



Figure 63 Rear module covers of Rack 15. Module 1 is at the bottom and module 14 at the top below the BPU.

Modules 12, 13 and 14 show significantly more soot damage compared to the remaining modules.

Individual components of each module were tagged and bagged. The cells were grouped in the same order and containerized in a wooden box for shipping.

The wiring from Rack 15 to the panel was inspected. The power cable was a shielded power cable. It was noted that the rack power cable ground shield was connected to ground at the rack frame but at the panel the rack power cable shield did not seem to be electrically connected (see Figure 64). It is not known what effect this will have on the system common mode noise.

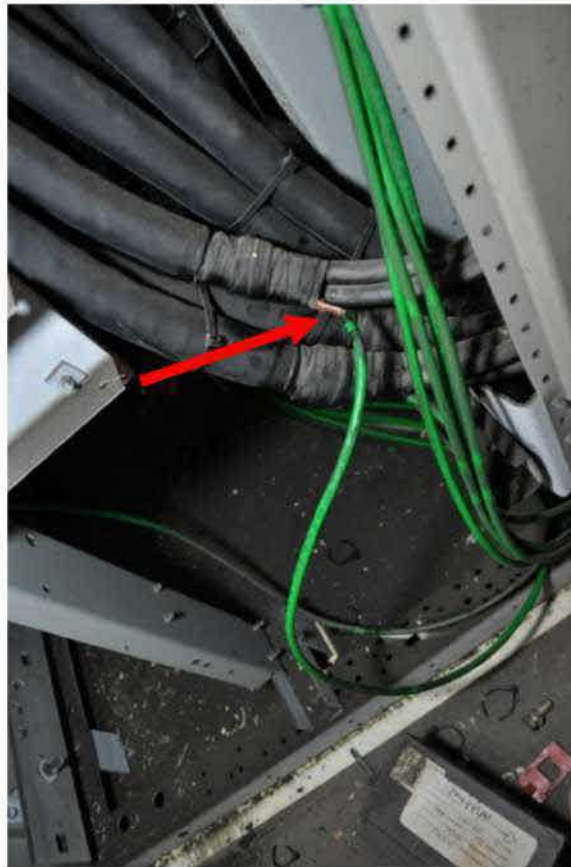


Figure 64 Rack 15 power cable ground conductor.

## Key Observations

Our key observations are as follows:

- Module 11 showed melting damage on the right side of its enclosure, likely due to arcing between the internal negative busbar and the aluminum enclosure.
- Module 3 positive terminal and external busbar shows thermal damage likely due to arcing from the positive terminal to module 4's interconnecting busbar.
- The ground shield of the power cable from Rack 15 to the panel was disconnected from ground. Although the shield was grounded at the rack, it is not known what effect this observation had on the common mode noise for Rack 15 – if any.
- The cause of the artifacts observed on the back covers of the modules, are likely due to the expansion of the cell stack and the resulting cell and or sense conductors touching the grounded enclosure. This observation indicates that the cells in Rack 15 were not electrically floating (electrically isolated from the rack frame) at the time the arcing occurred. This is likely more evidence that the electrical isolation was breached prior to the arcing to the module enclosures and rack frame events.

## **Rack 15 Module Removal and Inspection**

The disassembly of Rack 15 occurred at a Colwell Consulting facility in North Scottsdale. This rack was delivered intact as shown in Figure 65.



Figure 65 Rack 15 prior to disassembly.

The rack was then disassembled by removing the front cover as shown in Figure 66 with the modules tagged.



Figure 66 Rack 15 with front cover removed.

The modules were then disassembled individually. The disassembly was done by removing the module cover, front and rear plates, and then removing cells (where possible); in some cases, the individual cells could not be removed separately and multiple cells were removed.

The modules were inspected at Safety Engineering Laboratories located in Warren, Michigan. All 14 modules in Rack 15 were opened and inspected. The electrical arcing in the modules were noted as shown in Figure 67 and Figure 68.

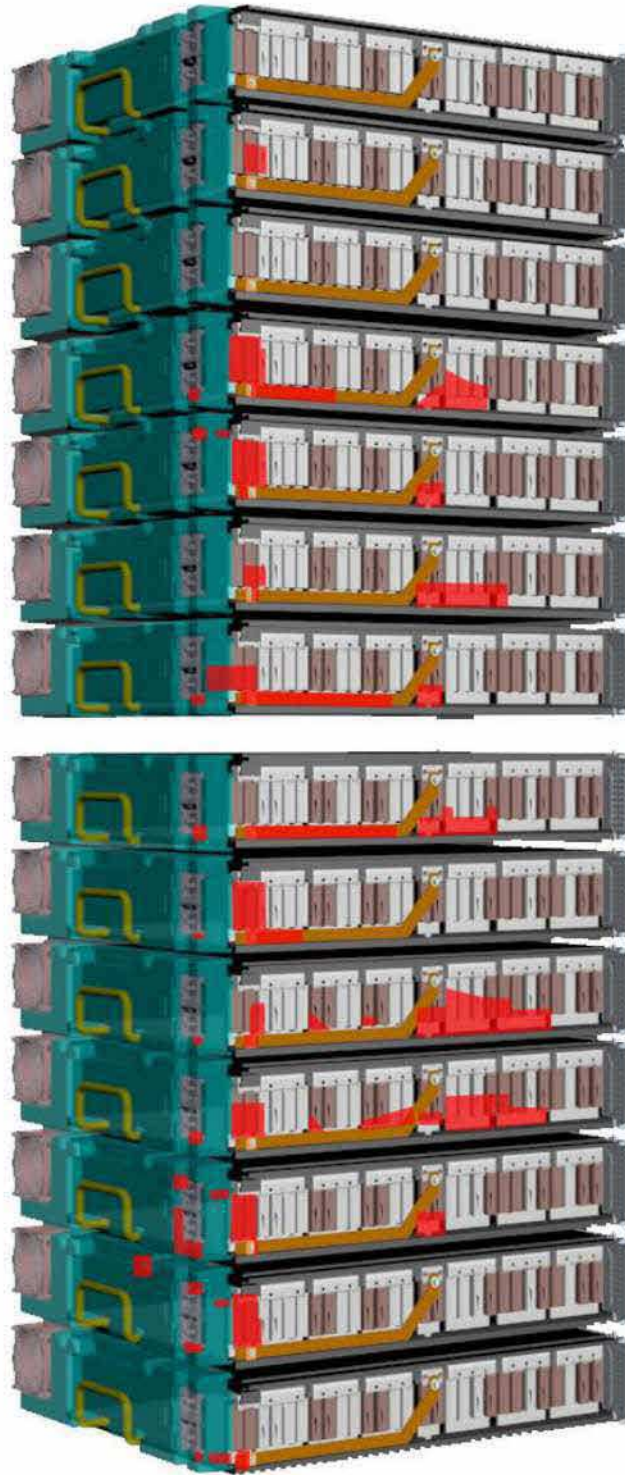


Figure 67 The front and right view of Rack 15. The red marked areas show the arcing at the positive and negative terminals, internal busbars, cell tab interconnects as well as on the metal front cover plate of Module 2.

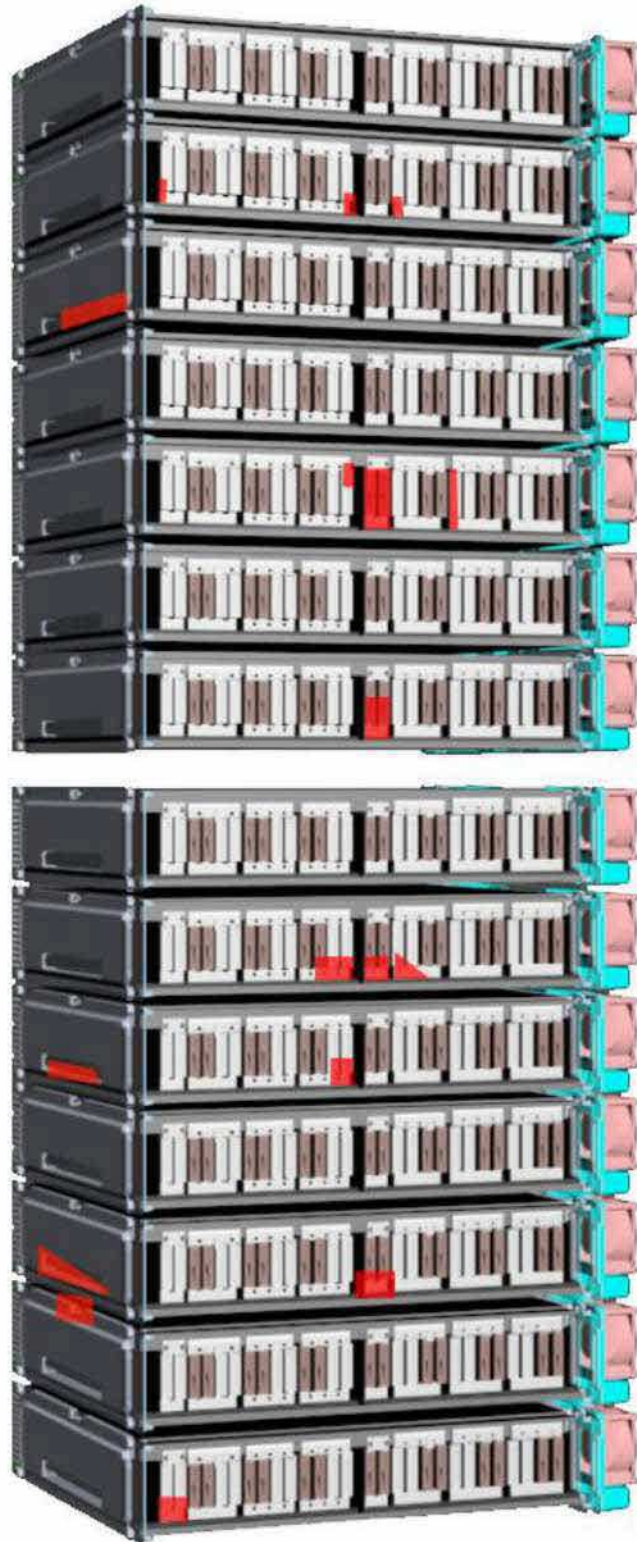


Figure 68 Rear and left side of Rack 15. The red marked areas show the arcing at module rear plates, internal busbars and cell tab interconnects.

Arcing to the module enclosure shows evidence that the rack was not floating or isolated at the time the arcing occurred. The arcing was mapped as shown in Figure 67 and Figure 68 using red blocks indicating the location and extent of the arcing.

## **Key Observations**

The following observations were made based on the arcing observed in the modules:

- The arcing did not show the origin of the event.
- The arcing patterns in the modules and rack do not provide sufficient evidence to support a single cell failure event as the root cause of the rack fire.
- The arcing to the rack frame and the module enclosures indicates that the cells were not electrically isolated from the rack at the time the arcing occurred.
- The arcing is predominant in the front right side of the modules.
- Module 3 positive terminal sustained severe arcing damage.
- In Module 2, Cell 14 arced to the front metal cover plate and Cell 7 in Module 2 arced to the rear lid securing tab.

Rack level failure testing needs to be performed to understand arcing behavior and patterns.

# Cell Level Analysis

---

## Introduction

In addition to the system level analysis, Exponent conducted analysis on exemplar and incident cells and assessed cell level data that was generated by other parties associated with this matter. The overall goal of this portion of the effort was to determine if the available data supported one of the two proposed routes to initiation of thermal runaway in the LGC JP3 cells installed in Rack 15. The two hypotheses for initiation of the thermal event were:

1. Internal Cell Short Circuit – An internal cell short circuit is a single point failure event that propagates to the full extent of the event. This hypothesis involves the formation of lithium plating in a cell which resulted in the establishment of a short circuit within the cell electrode stack that resistively heated, causing thermal runaway of the cell and propagation of thermal runaway to all the other cells in Rack 15.
2. External Cell Heating – There are various causes for external cell heating to occur, for example by external fire attack, resistive heating, or electrical arcing.

Other parties associated with this Matter assert that an internal cell fault, a short circuit, within one of the cells in Cell 7 pair of Module 2 is responsible for initiating cell thermal runaway that then propagated to the other cells in Rack 15. However, the data collected and analyzed to this point of the investigation does not support initiation of the Rack 15 thermal event by an internal cell fault. Rather, the data collected and analyzed to date tends to support initiation of cell thermal runaway through intense heating of the incident cells by an external heat source that is likely related to electrical arcing on Rack 15.

First, several concepts regarding lithium-ion cell operation and failure will be discussed and supported by literature references where appropriate. These concepts, and Exponent's experience with the science and engineering of lithium-ion batteries provide a basis for analysis of the available data related to the thermal event in Rack 15. The literature and available data

support Exponent’s opinion that sufficient evidence to implicate internal cell short circuit as the initiator of the thermal event in Rack 15 does not currently exist.

## **Lithium-ion Cell Operation and Failure Concepts**

### **Short Circuit Characteristics**

Thermal runaway failure of a lithium-ion cell is not the inevitable outcome of an internal short circuit between positive and negative electrodes in the lithium-ion cell. As was shown by researchers from Celgard, a prominent lithium-ion cell separator manufacturer, the location of the short circuit within the cell and the resistance to current flow of the short circuit strongly influence the probability that thermal runaway will occur<sup>18</sup>. As described in the table below (excerpted from Reference 18), a low resistance short circuit capable of carrying sufficient current, deep within the electrode stack has a higher probability of causing thermal runaway than a high resistance short circuit located near the edge of the cell. This proven concept can be better understood by considering how a short circuit within a lithium-ion cell initiates thermal runaway and how the location of that short circuit determines how easily the heat that it generates can escape the cell.

---

<sup>18</sup> “Lithium-Ion Batteries: Advances and Applications”, G. Pistoia, editor, Elsevier Publishing, 2013, Page 450

Case	Hard Short (Location)	Power	Chemical Reactant	Thermal Runaway Possibility from a Hard Short
1	Al—completely lithiated anode (inside)	High	Involved	Very high
2	Al—partially lithiated anode (edge)	High	Depends on Li amount	Low when Li content is small
3	Al—Cu (inside)	High	Involved	Could be high depending on cell size and design
4	Al—Cu (edge)	High	Not involved	Very low
5	Cu-cathode (inside)	Low	Involved	Very low
6	Cu-cathode (edge)	Low	Depends on cathode material	Very low
7	Anode—cathode (inside)	Low	Involved	Could be very low depending on cell size and design

Figure 69 A summary of short circuit location, type, power dissipating capability and probability of thermal runaway initiation. Copied from “Lithium-Ion Batteries: Advances and Applications”, G. Pistoia, editor, Elsevier Publishing, 2013, Page 450

A short circuit within a lithium-ion cell can be compared to a small resistance heater. The power dissipated by a resistance heater or a short circuit within a lithium-ion cell can be described by a simple relationship:

$$P = I^2R$$

Where  $P$  is equal to power dissipated as heat,  $I$  is equal to the current flowing through the short circuit, and  $R$  is equal to the resistance of the short circuit. Because the current term,  $I$ , is squared, the best way to maximize  $P$  is to maximize the current flowing through the short circuit. This necessitates that  $R$ , the resistance to current flow, is minimized. Because the cell chemistry and design dictate the maximum amount of current that can be produced, the value of  $R$  determines how much of the maximum current can flow through the short circuit. In simple terms, in order for  $P$  (and thus  $I$ ) to approach its maximum,  $R$  must be at its minimum. A low resistance short circuit is the most capable of producing heat.

The location of the short circuit also plays a critical role in determining if the short circuit will result in a thermal runaway event. If we think of the materials that make up the cell as a type of thermal insulation, it becomes easy to understand why a short circuit near the center of the cell

has a much higher probability of causing a thermal runaway event than a short circuit near the edge of the cell.

A short circuit that is dissipating heat near the center of a cell is surrounded by cell materials that tend to insulate the heat source. The ability for the heat to escape the cell is hindered by this insulating effect. As a result, the heat generated by the short circuit is trapped and increases the temperature of the materials around it rather than escaping to the surroundings. A short circuit that is dissipating heat near the edge of a cell is in a different environment in that it is more likely to have less “insulating material” around it. As a result, the heat generated by a short circuit near the edge of a cell has a much better chance of escaping to the surroundings and this lowers the probability that heat will build within the cell and initiate a thermal runaway event.

## **Lithium Plating in Lithium-ion Cells**

In some instances, the lithium ions that exist in the electrolyte of a lithium-ion cell can be electrochemically reduced to form lithium metal. This undesirable phenomenon causes performance issues and, in extreme cases, safety issues.

Performance issues arise because converting lithium ions to lithium metal is a largely irreversible process that can permanently remove lithium ions from the system. Removing lithium ions from the electrolyte has two performance related consequences. First, the relationship between the number of lithium ions participating in the cell reactions and the number of electrons that can be generated is 1:1. One lithium ion is required to produce one electron. Therefore, if lithium ions are removed from the system the capacity of the cell decreases. Second, lithium ions are responsible for carrying charge between the electrodes of the cell and the concentration of lithium ions in the electrolyte is directly proportional to the conductivity of the electrolyte. As the concentration of lithium ions goes down, the internal impedance of the cell goes up. The result is a loss in power capabilities for the cell. The overall result of these two consequences is a measurable decrease in cell performance.

Lithium metal is an electrical conductor and has the capability to establish short circuits in a lithium-ion cell as it deposits on the negative electrode and grows through the separator to the

positive electrode. However, the preferential morphology of a plated lithium deposit in a lithium-ion cell is a rod-like structure referred to as a dendrite. As can be seen in Figure 70, lithium dendrites are extremely thin whisker-like structures. Although dendrites are electrically conductive, their ability to carry current is limited by their size. In general, as the conducted current increases, the cross-sectional area of the conductor must increase to avoid the conductor resistively heating to its own melting point causing it to break the current path and “fuse open”. Because lithium dendrites have a small cross-sectional area and lithium metal has a relatively low melting point, lithium dendrites tend to fuse open before generating enough heat to cause thermal runaway.<sup>19</sup>

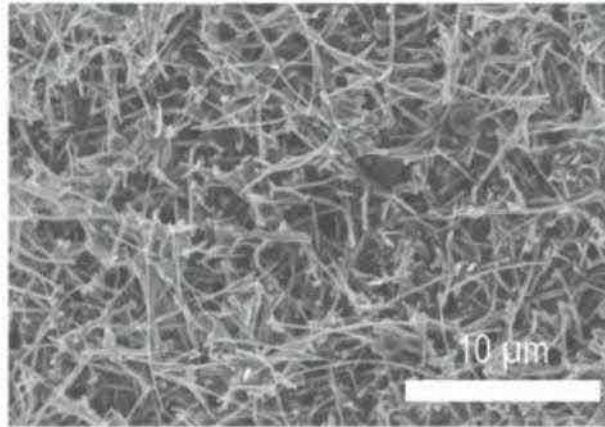


Figure 70 A scanning electron micrograph of lithium dendrites. *Journal of Power Sources*, Volume 409, 1 January 2019, Pages 132-138.

In extreme cases of lithium plating in lithium-ion cells, relatively thick, dense mats of lithium dendrites can form structures referred to as “dead lithium”. Dead lithium can have a cross-sectional area that is sufficient to carry enough short circuit current to result in the initiation of thermal runaway. The initiation of thermal runaway by dead lithium typically occurs when force concentrated by the physical size of the dead lithium causes rupture of the separator and establishment of a short circuit. Cells exhibiting dead lithium deposits are typically much lower

---

<sup>19</sup> Santhanagopalan, Shriram, Premanand Ramadass, and John Zhengming Zhang. "Analysis of internal short-circuit in a lithium ion cell." *Journal of Power Sources* 194.1 (2009): 550-557

in capacity and much higher in impedance because the formation of dead lithium consumes a large quantity of lithium ions.

## External Heating as a Route to Thermal Runaway

Once the interior of a lithium-ion cell has been heated to a sufficient temperature (usually about 180 °C; see Figure 71 below), exothermic decomposition of the positive electrode will cause rapid heating of the cell, ultimately leading to thermal runaway.<sup>20</sup> As explained above, internal short circuits can only reach this temperature under specific conditions and with specific defects in the cell. In contrast, external heating is a reliable way to drive any lithium-ion cell into thermal runaway. Given enough external heat, every lithium-ion cell will reach this threshold and enter thermal runaway. The only criteria to consider is whether the external heat source (such as an electrical arc) has the energy and power needed to heat the cell to this critical temperature.

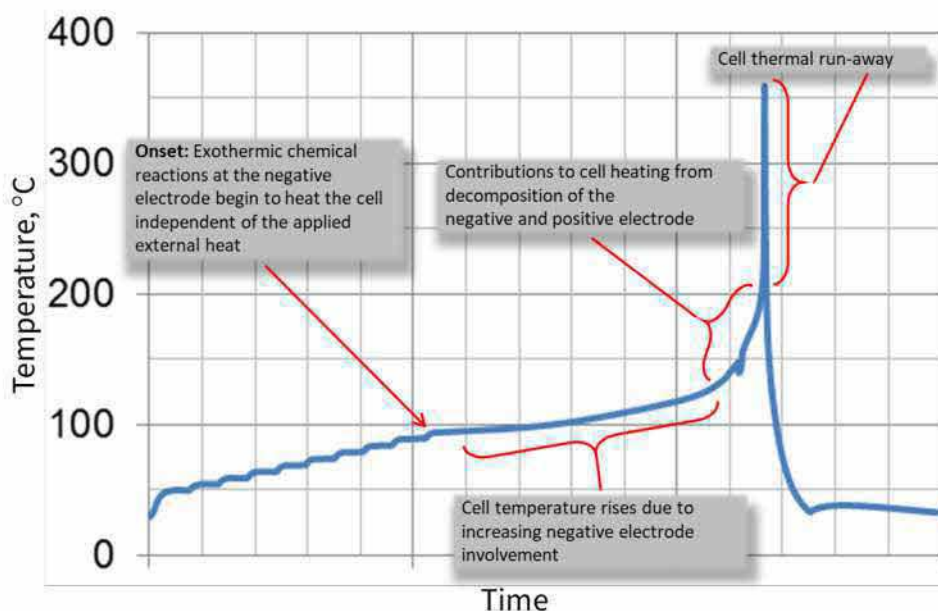


Figure 71 Results of an accelerating-rate calorimetry test on a lithium-ion cell, showing the increasing rate of self-heating with increasing temperature.

<sup>20</sup> Lisbona, Diego, and Timothy Snee. "A Review of Hazards Associated with Primary Lithium and Lithium-Ion Batteries." *Process Safety and Environmental Protection*, Special Issue: Centenary of the Health and Safety Issue, 89.6 (2011): 434–42

Despite the reliance on an external heat source, cells exposed to external heating may still propagate a fire or arcing incident farther and faster than it otherwise would have, leaving behind signatures that are similar to that of an ignition source. Cells that have entered thermal runaway due to external heating are thus sometimes mistakenly identified as the source of a fire. Every root cause analysis of a thermal runaway event must consider potential sources of external heating (such as electrical arcs from malfunctioning equipment) before attempting to claim that a defect in the cell must have been the cause of the failure.

## **Flammable Gas Production**

Thermal runaway in lithium-ion cells is a highly exothermic process that generally results in the combustion of flammable materials within the cell. However, there is rarely enough oxygen present within the cell to facilitate complete combustion of the flammable materials. As early as 2005, researchers were able to show that the products of incomplete combustion during thermal runaway were, themselves, flammable gases.<sup>21</sup>

Since this early work, substantial effort has focused on more clearly understanding the composition and quantity of the flammable gases produced during thermal runaway and the behavior of those gases in the presence of sufficient oxygen and a competent ignition source<sup>22</sup>. Based on Golubkov et. al.<sup>22</sup>, and other similar documents, the primary composition of the vent gases from a thermal runaway event are hydrogen, carbon monoxide, carbon dioxide (non-flammable) and a mixture of light hydrocarbon gases.

Under the correct conditions, flammable thermal runaway vent gases can combine with oxygen to form an explosive mixture.<sup>23</sup> The plot in Figure 72, excerpted from Somandepalli et. al.<sup>23</sup>, shows the peak pressure rise for hydrogen, methane and a simulated lithium-ion vent gas mixture after ignition in air. The left most intercept of each curve with the x-axis represents the

---

<sup>21</sup> "Effects of additives on thermal stability of Li ion cells." *Journal of power sources* 146.1-2 (2005): 116-120

<sup>22</sup> "Thermal Runaway Experiments on Consumer Li-ion Batteries with Metal Oxide and Olivin-type Cathodes" *RSC Advances.*, 2014, 4, 3633

<sup>23</sup> "Quantification of combustion hazards of thermal runaway failures in lithium-ion batteries." *SAE International Journal of Alternative Powertrains* 3.1 (2014): 98-104

lower explosive limit (LEL) and the right most intercept of each curve with the x-axis corresponds to the upper explosive limit (UEL). The explosivity window for lithium-ion vent gases is approximately mid-way between pure methane and pure hydrogen, consistent with the composition of actual and the simulated vent gas mixture.

The important outcome of this research is that methods exist to measure and understand the explosive behavior of lithium-ion battery vent gases in a way that makes engineering ventilation systems for stationary power storage facilities possible. A properly designed ventilation system could be capable of preventing the atmosphere within a container from ever reaching the LEL during a lithium-ion thermal runaway event.

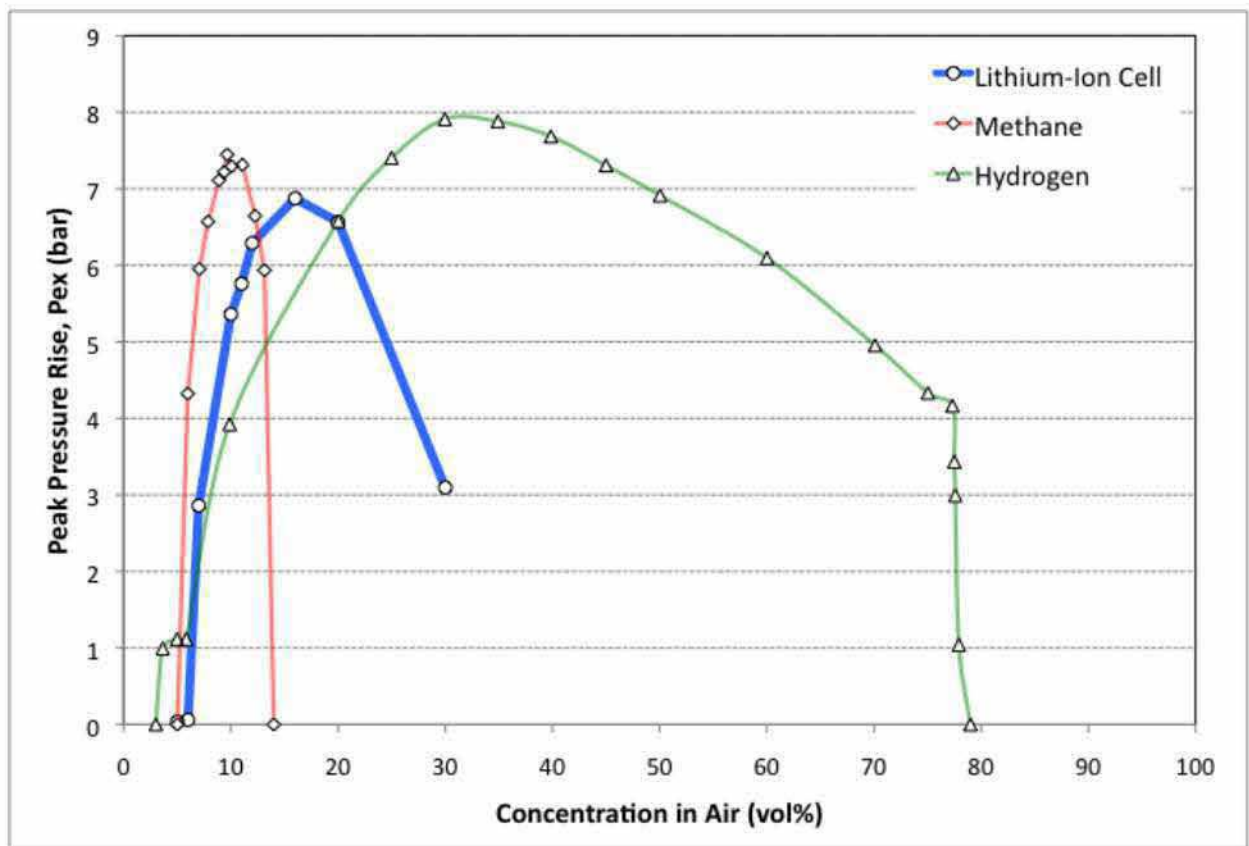


Figure 72 Peak pressure rise vs. gas concentration in air for hydrogen, methane and simulated lithium-ion vent gas. Intercepts of the curves with the X-axis give the lower explosion limit and upper explosion limit for each gas composition. Excerpted from "Quantification of combustion hazards of thermal runaway failures in lithium-ion batteries." SAE International Journal of Alternative Powertrains 3.1 (2014): 98-104.

## **Data Analysis**

In support of root cause determination, Exponent participated in several multi-party inspections of incident and non-incident cells and modules, generated and analyzed data, and undertook an analysis of data generated by other parties associated with this matter. Key aspects of this work are presented below. As was stated above, the information currently available is insufficient to conclusively establish root cause for the thermal incident.

### **Analysis of Cell Deposits**

Deposits have been found on the negative electrode and adjacent separators of LGC JP3 cells installed in stationary energy storage systems. Figure 73 shows an example of one of these deposits that was discovered during an inspection related to this matter. Prior to Exponent's involvement with this matter, one such deposit was inspected by LG Chem. Through a sophisticated approach involving monitoring the tip current of an atomic force microscope while the tip was over a deposit compared to the native electrode surface, it was determined that the deposit was non-conductive. The results of this analysis showed that that deposits of this type have a high impedance, are non-conductive, and are unlikely to be pure lithium metal. It is

impossible for a non-conductive deposit to carry current, resistively heat and cause thermal runaway.



Figure 73 Non-conductive negative electrode deposits.

As a compliment to work done by LG Chem that determined the observed deposits were non-conductive, Exponent designed an experiment to characterize and establish a quantitative comparison of the conductivity of different collected negative electrode materials. Three coin cells were assembled as depicted in Figure 74. Coin Cell 1 did not have a sample in the “Sample” location. This cell is representative of a short circuit condition for this experimental set-up. Coin Cell 2 contained an exemplar negative electrode in the “Sample” location. This cell served as a baseline for the conductivity of the negative electrode assembly in the absence of a deposit. Coin Cell 3 contained a section of a negative electrode exhibiting a deposit.



Figure 74 Schematic of the experimental setup for conductivity testing of negative electrode materials.

Linear voltammetry is a common technique used to identify parameters of an electrochemical system. This technique involves a varying potential that increases linearly with time starting at some initial value at a sweep rate  $v$  (in  $V s^{-1}$ ). As a result of the applied potential, the current rises from an initial value as the scan starts and attains a steady state value at each potential.<sup>24</sup> The resulting relationship between potential and current can be used to estimate the parameters of an electrochemical cell including the Ohmic resistance.

### Experimental Parameters

This experimental study was conducted on a Gamry Potentiostat Ref 600-05122 capable of handling a maximum current of 600 mA and a minimum current resolution of 20 aA. Table 3 Experimental Parameters provides a summary of the parameters used for the voltammetry testing of negative electrode materials.

<sup>24</sup> Bard, Allen and Faulkner Larry, “*Electrochemical Methods – Fundamental and Applications*”, Second Edition, John Wiley and Sons, Inc., pp. 15-18.

Table 3 Experimental Parameters

Parameter	Value	Units
Initial Potential	0.0	V
Potential Limit	2.0	V
Scan Rate	9.99	mV/s
Step Size	2	mV

### Experimental Results

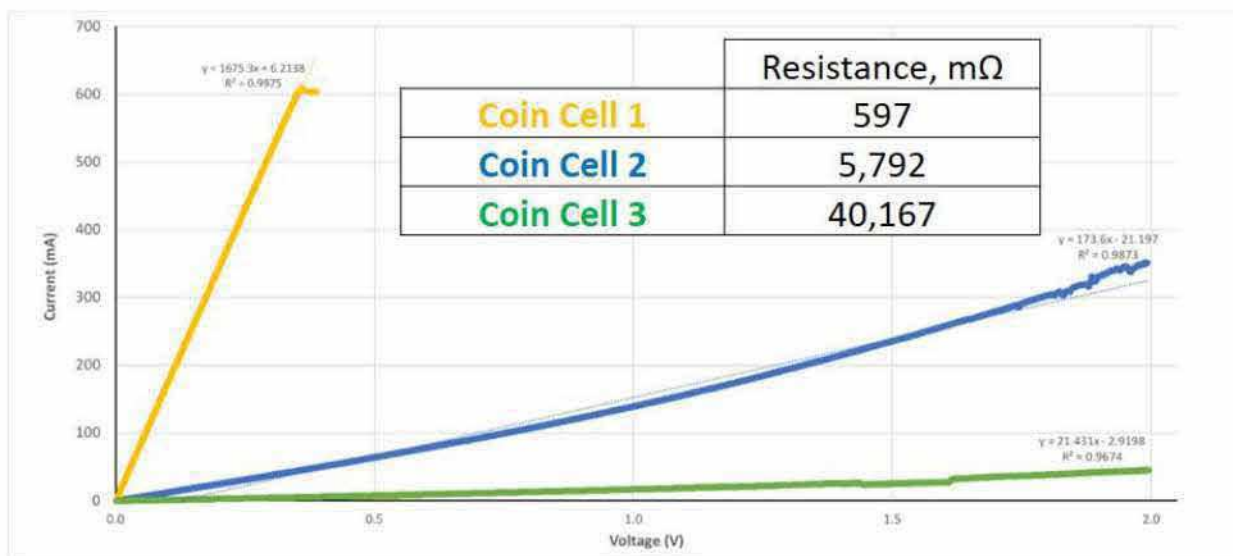


Figure 75 Voltage – Current relationship for three different samples during a Voltammetry test.

Figure 75 shows the measured current as a function of the applied potential for each coin cell. These results were used to fit the internal resistance of each coin cell using Ohm’s Law. The internal resistance of each coin cell is the inverse of the slope of the Voltage – Current relationship. The substantially increased impedance does not support characterization of the deposit material as pure lithium metal. As was stated before, it is impossible for a non-conductive deposit to carry current, resistively heat and cause thermal runaway

### Non-conductive Deposit Behavior in Air

It is a fact that some of the observed non-conductive deposits were highly reactive in air. For deposit samples that showed reactivity, the most common behavior that shown in Figure 76. In

this instance the deposit turned from a dull gray color to white with the coincident formation of gas bubbles. The white color and bubbly morphology are consistent with the exothermic reaction of lithium metal with water in air to form lithium hydroxide and hydrogen gas.

In another example, a deposit that was adhered to the surface of a negative electrode and the adjacent separator showed pyrophoric behavior when the separator was peeled back from the surface of the electrode. This behavior is also consistent with the reaction of lithium metal in air.

It is difficult to reconcile the facts that the deposits have been shown to be non-conductive and that they have reactivity in air that is similar to that of conductive lithium metal. One likely explanation is that the deposits contain lithium metal in an otherwise non-conductive matrix. However, in the absence of thorough characterization of the composition and morphology of the deposits, it is impossible to reach a conclusion regarding their impact on cell stability.



Figure 76 A deposit found during a multiparty inspection of a LGC JP3 cell showing behavior consistent with the reaction of lithium upon exposure to air. The white color and bubbly morphology are consistent with the exothermic reaction of lithium metal with water.

## LGC SRS Separator Characteristics

---

LG Chem has included their safety-reinforced separator (SRS) in these cells in order to minimize the ability for lithium plating to result in a short circuit leading to thermal runaway. This separator has been specifically engineered to eliminate this risk.

The SRS is a hybrid design comprised of a microporous polymeric membrane coated on both sides with relatively dense organic/inorganic (O/I) protective layers with very small pore sizes. A cross-sectional view of the SRS and its layers is shown in Figure 77.

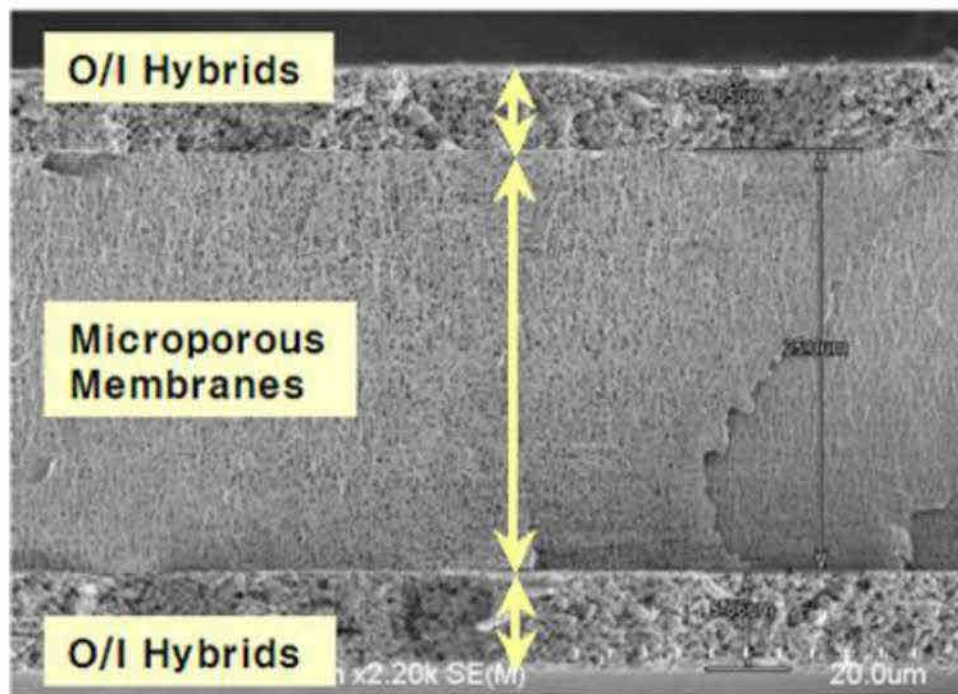


Figure 77 Cross-section of the SRS separator used in the LGC JP3 cells.

The SRS has two complementary features that address different risks associated with lithium plating. The first feature is the pore diameter of the O/I layer. The pore diameters are designed to be small enough to limit the size of any lithium dendrites growing through the separator. As discussed above, the power dissipated as heat ( $P$ ) in a short circuit is dependent on the amount of current flowing through the short circuit. By constraining the pore diameters in the O/I layer,

and thus limiting the diameter of any lithium dendrites growing through it, the amount of current capable of flowing through the lithium dendrites is constrained.

The second feature is the mechanical strength provided by the inorganic layers. These layers prevent “dead lithium” from rupturing the separator. One path to a short circuit event from the presence of dead lithium is through physical damage to the separator due to the pressure exerted from this lithium plating.

Results from LG Chem mechanical tests performed on their SRS suggest it is extremely unlikely that any pressure exerted from dead lithium could cause a rupture and establish a short circuit. In the LGC testing, iron particles were forced into the SRS materials at approximately 300 kg<sub>F</sub> (≈3000 N), an unrealistically high load for the interior of a pouch cell, before they were able to penetrate the organic/inorganic protective layer (see Figure 78).

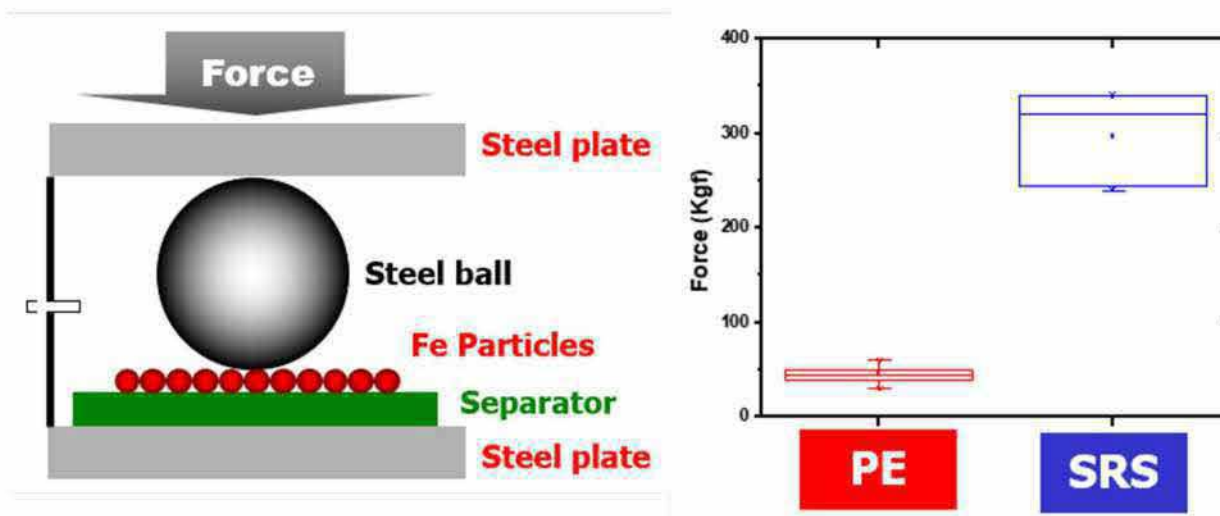


Figure 78 Mechanical rupture test of LG Chem's SRS. (Left) Schematic of experimental setup. (Right) Rupture force of SRS compared to traditional polyethylene (PE) separator.

Importantly, this experiment is very conservative when applied to dead lithium causing separator rupture in JP3 cells. First, lithium is substantially softer than iron. Second, the SRS in the JP3 cells is not constrained because these pouch cells are not rigidly fixed, providing ample space for the electrode and separator to move rather than cause rupture of the separator.

The combined physical properties of the SRS components and design of the cell make it highly unlikely for lithium plating in a JP3 cell to result in a short circuit leading to a thermal runaway.

## Analysis of CT Data

---

Exponent was provided with computed tomography (CT) X-ray data of twenty-one cell pairs from modules 1 – 13 in Rack 15. Exponent analyzed this data with the intent of understanding any damage patterns that would help determine the root cause failure of Rack 15. The data is not consistent with an initiation from an internal short circuit but is consistent with an attack on the cells from an external heat source.

CT data sets were provided for between one and three cell pairs in each of the modules. The cell pairs scanned were only a certain selection of external cell pairs in the modules (cell pairs 7, 8 and 14). Markings were placed on the cells to note the installed orientation of the cell pair in the module (front/back, top/bottom). Due to their size, each cell pair was scanned in two separate CT data sets, split lengthwise along the cell pair (marked as left and right). The scans were performed at a voxel size of  $\sim 82\mu\text{m}$ , with the exception of cell pairs 7-1 and 7-2 from Module 2 and module 3 (voxel size of  $42\mu\text{m}$ ).

Exponent systematically reviewed the data to assess the damage from the thermal event. Thermal damage to the cells was observed, beyond what is typical for a thermal runaway. The damage was present either as large regions of bright features in the electrodes or as large sections of electrode missing. The industry viewing convention of CT data is denser materials correspond to brighter voxels. In this case, localized bright spots like those shown in Figure 79 are indicative of extreme heat or electrical activity (i.e. arcing) resulting in melted and re-solidified metal.

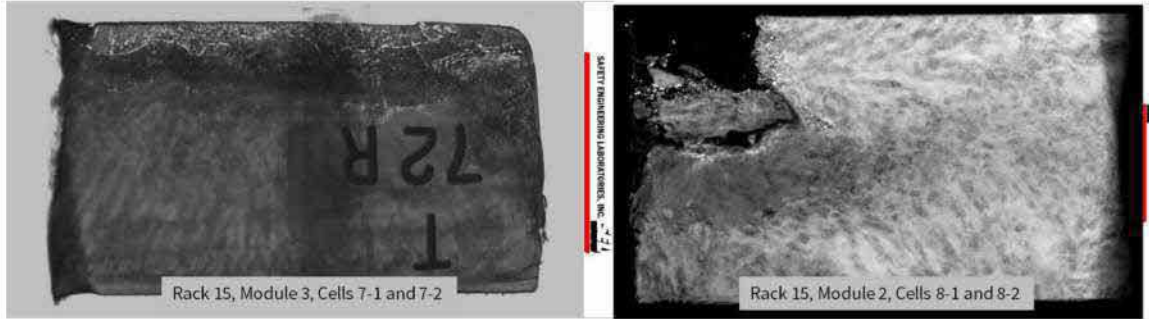


Figure 79 Representative 3D (left) and 2D (right) images of extensive cell damage in Rack 15. Almost all the cell pairs exhibited extensive damage to the electrodes. The damage to the cell pairs was observed to be in various combinations of large regions containing bright spots and missing electrodes as a result of the damage. The vast majority of the damage was concentrated on the cell edges. In some cases, the exterior damage spanned both cells in the pair.

The extent and location of the damage is not consistent with a thermal event due to an internal short circuit. Based on Exponent's experience, the electrode damage is significantly more extensive than would be expected for a thermal runaway that only included the cells in the rack. Additionally, no damage patterns were observed that would clearly indicate an initiation from an internal short circuit. Conversely, the damage supports a scenario where there was an attack on the cells from an intense external heat source, such as electrical arcing on the modules and rack, capable of exceeding the melting point of copper ( $\approx 1085^{\circ}\text{C}$ , a temperature not typically reached during thermal runaway).

## **Analysis of SEL Cell Cycling and CT Data**

---

Safety Engineering Labs (SEL) provided a data set purporting to show charge/discharge cycling and X-ray computed tomography (CT) of one JP3 format cell taken from an unknown module with an unknown history. After analyzing the data, Exponent found nothing in the cycling and CT data produced by SEL that demonstrates a possible fault or defect within the cell.

Furthermore, numerous experimental issues are apparent in the data which undermine the integrity of SEL's results and any conclusions that may be drawn from them.

The cycling data consists of 31 separate files that appear to document approximately 463 charge-discharge cycles on the test cell, providing only test time, applied current, voltage, and an unlabeled column that periodically reported metadata about the test conditions. A significant number of entries did not report either a voltage or a current (24% were missing voltage readings and 0.6% were missing current readings). Based on this limited data, Exponent identified the individual charge and discharge steps that make up the 463 reported charge-discharge cycles in order to perform a complete analysis of the test results.

Over the course of cycling, the parameters used were changed multiple times. In particular, the maximum charge current was 8.2A to 8.6A for the first 11 cycles, 16.6A for cycle 12A, to 12.4A for cycles 14 to 17, and approximately 16.5A thereafter. In two instances, the cycles were stopped mid-charge and the conditions changed. For example, cycle 13 was charged to 4.06V at 16.6A in file "Cell 1\_2 Cycle 12(data).csv", but charging resumed at 4.15V and 4.0A in file "Cell 1\_2 Cycle 13(data).csv" (a similar gap occurs in cycle 18). SEL does not provide any data to show how the cell was charged from 4.06A to 4.15A in cycle 13. Additionally, the files describing cycle 401 and after are labeled "constrained". SEL has not provided any further explanation about the nature of the constraint (electrical or physical) or why it was applied after 400 cycles. Exponent did not detect a meaningful change in the cell's cycling performance during these cycles.

SEL also did not provide any information about the equipment used to perform the cycling tests, nor did they provide any information about the calibration, accuracy, or specified capabilities of

their equipment (or even the date and time their tests were performed). Accordingly, Exponent cannot verify that the data provided by SEL accurately reflects the test performed or that the equipment SEL used was even capable of performing the test. This is reflected by several unusual behaviors found on nearly every cycle.

First, the charge voltage consistently exceeded the maximum charge voltage specified by LG Chem<sup>25</sup>. Figure 80 (a) clearly shows that many cycles exceed the maximum charge voltage, in most cases by at least 18mV. Figure 80 (b) shows the charge voltage and current for a typical cycle exhibiting overvoltage behavior. During a properly functioning charge test, the charger should transition from a constant-current (CC) charge to a constant-voltage (CV) charge as soon as the cell's voltage reaches the voltage upper limit. This should result in the voltage holding at the upper voltage limit throughout the CV charge, during which time the current should smoothly decay until reaching the end of charge. SEL's data do not follow this behavior; instead, the data indicate that the charger continued to apply a constant current voltage while the cell was above the upper voltage limit. This continues for approximately 20 minutes in most cycles. At the end of this period, the current rapidly falls to a small fraction of the constant current value and the voltage declines slightly, approaching (but remaining above) the upper voltage limit. These results suggest that the equipment SEL used for this cycling test was not designed for and was simply incapable of accurately performing an ordinary charge algorithm on this cell.

---

<sup>25</sup> 190708\_ESS\_cell\_JH3\_JP3\_JH4\_Cell\_data\_APS.df

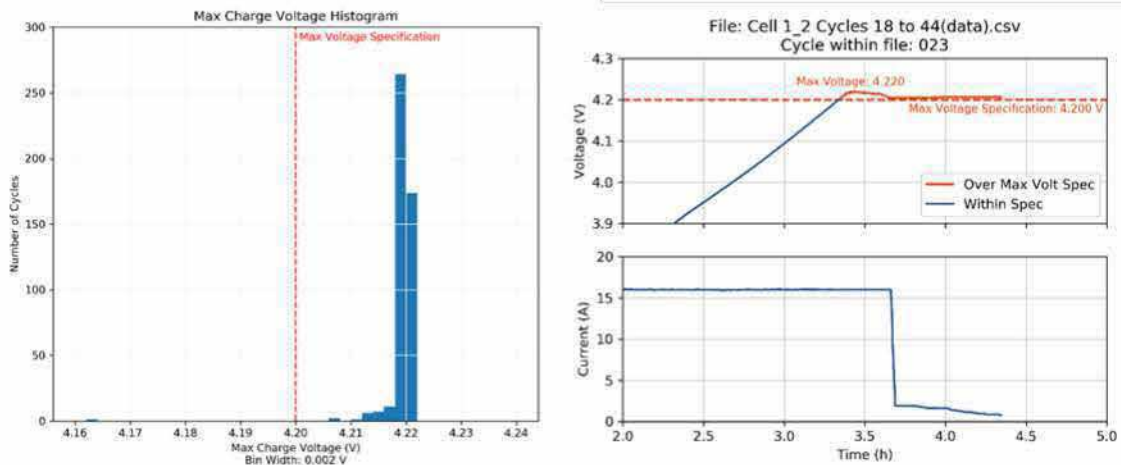


Figure 80 (a, left) A histogram of the number of cycles that had various max charge voltages. (b, right) Current and voltage profiles for the end of charge for a typical cycle exhibiting overvoltage on charge.

The coulombic efficiency (discharge capacity divided by the previous charge capacity) also undermines the test results. Lithium-ion batteries cycled under consistent conditions maintain a coulombic efficiency very close to 100% (often greater than 99.9%). Figure 81 (b) shows that the coulombic efficiency changes with the changes in the charge conditions; early cycles (with charge currents of 8.2 to 8.6 A) have coulombic efficiencies of 99% to 100%, consistent with cells operating normally. After the charge current was increased to 16.5 A, the coulombic efficiency dropped to 96% for the remaining cycles. Figure 81(a) shows that the change is entirely due to the changes in the measured charge capacity on each cycle. This indicates that the equipment SEL used to cycle this cell was either inaccurate, improperly configured, or incapable of performing this test.

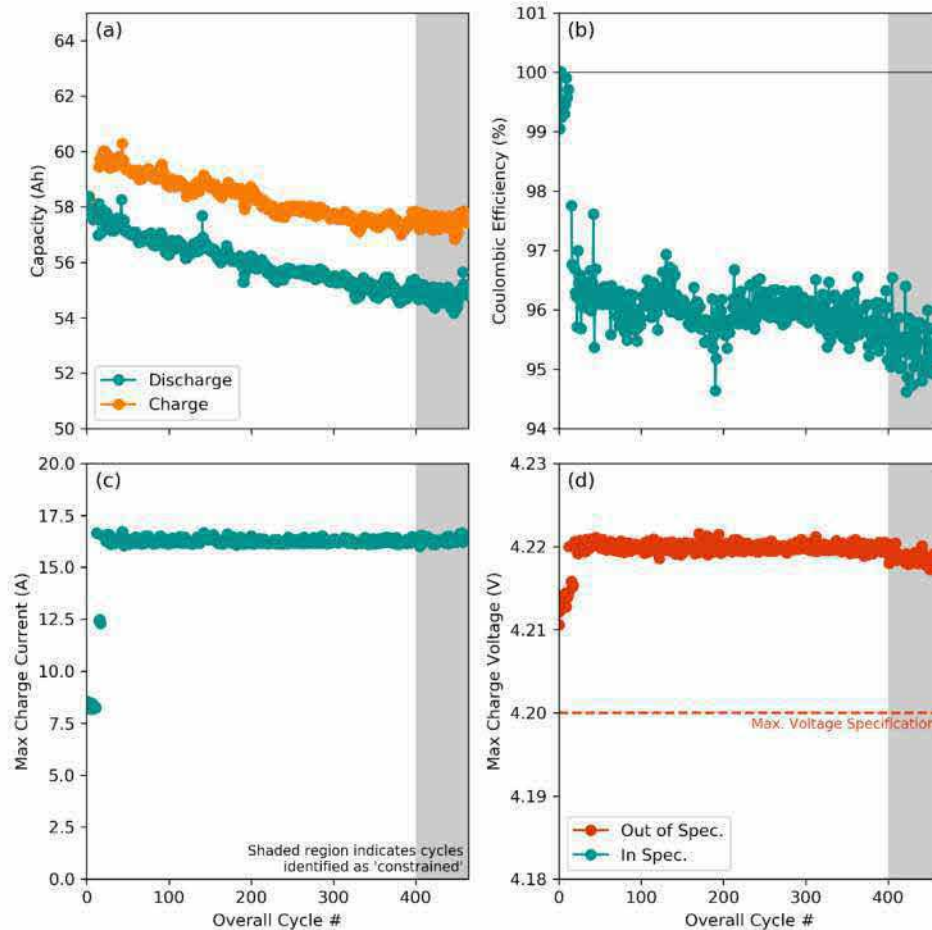


Figure 81 Various cycling performance metrics by cycle number: (a) charge and discharge capacities of complete cycles, (b) coulombic efficiency, (c) maximum charge current, and (d) maximum charge voltage.

In addition to the cycling data, SEL provided ten sets of CT data were included as part of the received data. The CT data consists of scans of the cycled cell at five cycling intervals (0, 100, 209, 285 and 400 cycles). Due to its size, the cell was scanned in two sections, split lengthwise along the cell pair (marked as left and right). The cell was CT scanned at a voxel size of ~85  $\mu\text{m}$ , except for the 400-cycle data (41  $\mu\text{m}$ ). Exponent reprocessed the data sets by first virtually stitching the left and right sides of the cell together. The 400-cycle data was also re-exported at half the resolution to match that of the other data sets.

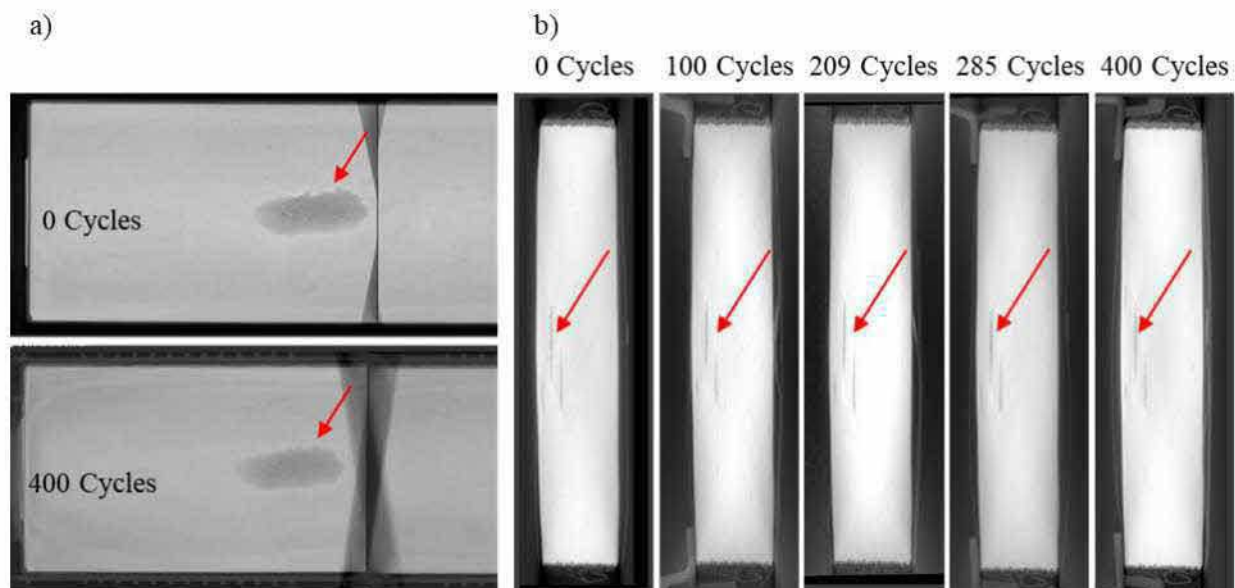


Figure 82 (a) Planar and (b) cross-sectional views of one representative feature tracked throughout cycling.

The uncycled cell contained several features consistent with deposits on the negative electrode, similar to those found to be non-conductive (as discussed above). These features did not change in size or shape during the 400 cycles, see Figure 82. Additionally, despite the issues with the cycling protocol noted above, no measurable swelling of the pouch or localized swelling around the deposits were observed over the 400 cycles tracked. This data does not support the growth of the internal cell features as a function of cycle count.

## **Environmental Data and System Analysis**

An analysis was performed to assess whether environmental factors contributed to the initial failure event. As part of the assessment, the provided data was critically analyzed and the HVAC units were inspected and analyzed. The analysis revealed that the BESS temperature and humidity data does not include the extremes of the temperature and humidity within the BESS because the sensor locations do not coincide with locations where the coldest air enters the BESS or where moisture enters the BESS. The analysis also revealed that, in addition to water intrusion patterns that are likely associated with rain after the incident, there were water intrusion patterns that are not readily explained by the damage sustained during the incident. Investigating the latter requires an additional inspection and destructive examination of the evidence.

The following observations were made from the data analysis and the inspection:

- The five environmental sensor locations are not located at locations where the coldest air enters the BESS or where the moisture source is, and therefore the extremes of the temperature and humidity are not captured in the data set (poor spatial resolution).
  - As a result, the temperature and relative humidity extremes are unknown.
  - The cold air supply from HVAC #3 was directly above the front face of Racks 13 and 15, but the nearest environmental sensors were affixed to Rack 19 and 16 (the latter is across the aisle).<sup>26</sup> As a result, the spatial resolution is inadequate and the data set has limitations.
  - At times, the environmental temperature at the measurement location nearest Rack 15 was higher than the Rack 15 minimum module temperature. These conditions would facilitate condensation of water vapor within the modules.
- Despite the poor spatial resolution, large temperature differences were still measured at the same point in time.
  - The air conditioning units did not all run simultaneously.

---

<sup>26</sup> This is based on the diagram provided to Exponent shown in Figure 84. Exponent was not permitted to inspect the BESS until most of the racks had been removed.

- The dew point temperature repeatedly increased following cooling cycles prior to the incident, indicating that the system was not a closed system and that there was a source of water vapor.
  - The source of water vapor has not been identified to-date.
- The HVAC systems were not configured per the manufacturer's specifications, and it is currently not known if the economizer doors were open at any time during the BESS operation.
- The data that is available showed that, over the history of operation of the BESS, the relative humidity consistently reached 80% or higher.
- The role of high relative humidity and/or condensation on electronics in the BESS cannot be ruled out as a contributor to the root cause of the initial failure.
  - Localized, adverse environmental conditions may affect all modules, electronics, or components within that zone. Therefore, adverse environmental conditions are not inconsistent with a single-point initial failure or a two-point failure.

Figure 83 shows the environmental temperature sensor data and dew point temperature sensor data at the five discrete measurement locations approximately two days prior to the event. The data window includes only one hour of measurements to illustrate features in individual air conditioning cycles.

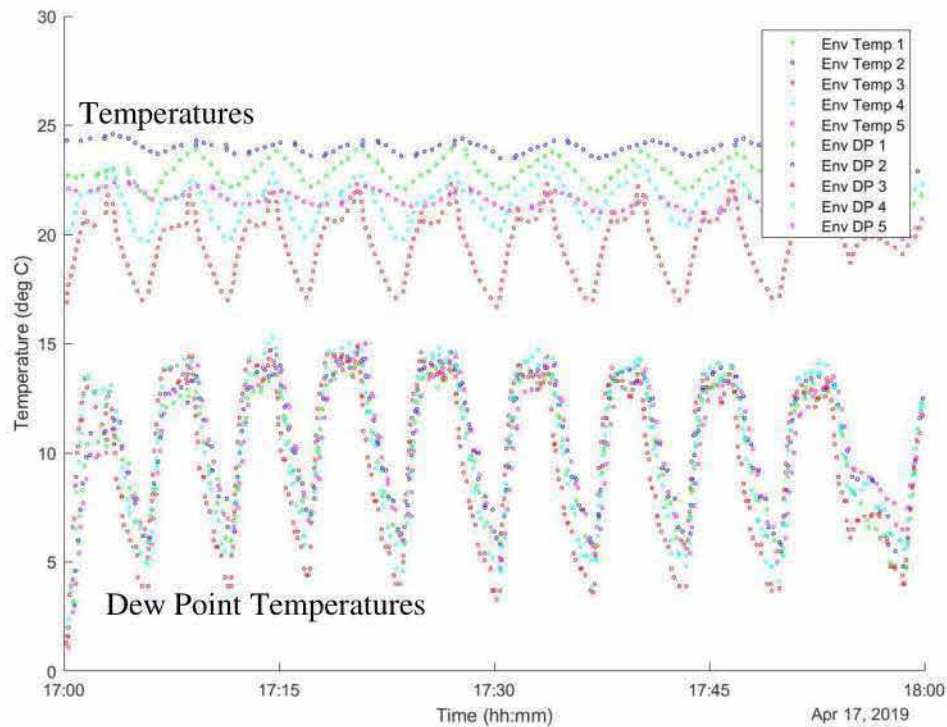


Figure 83 Environmental temperature measurements and dew points at the five measurement locations approximately two days prior to the incident.

The upper five traces correspond to environmental temperature measurements. The environmental temperature sensor three, which is closest to Rack 15 (see Figure 84, NetBotz: Container Temperature), is the coldest of the five measurement locations during the measurement window. The range of measured temperatures at specific times is up to approximately 7°C (12.6°F difference). Given that the sensor locations are not aligned with the HVAC cold air supply ducts, the spatial resolution is insufficient to understand the full range of temperatures experienced by the modules. To illustrate the presence of large temperature gradients, the sensor across the aisle at nearly the same location is measuring approximately 4°C (7.2°F difference) warmer at times. Temperature differences on the order of 1-2°C were also observed between the PLC sensor #4 and the environmental temperature sensor #3, and they are in the same or similar location.

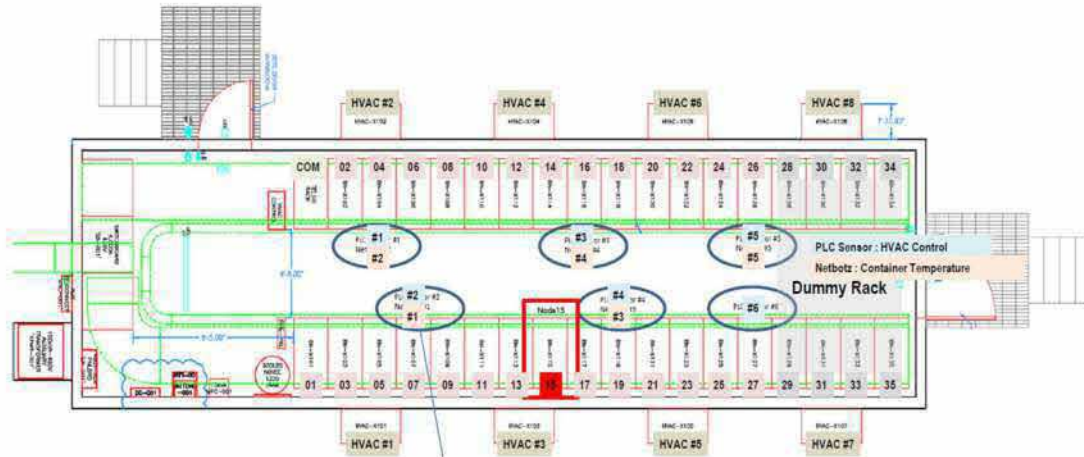


Figure 84 Schematic of the McMicken BESS illustrating HVAC locations and environmental temperature sensor locations.

The data also indicates that not all the HVAC units are running simultaneously. For example, environmental sensor two is near the exit for HVAC #2, but the variations are quite low compared to those, e.g. at sensor three.

The lower five traces in Figure 83 are the dew point measurements at each of the locations. The dew point is the temperature at which water vapor begins to condense into liquid water. The higher the dew point, the more water vapor molecules are in the air. The dew point at all five locations tends to decrease during cooling phases, which indicates drying of the air at the evaporator coils. The Marvair Model AVPA72ACD060CU A5-200-VAR HVAC units have a drain pan below the evaporator coils to collect condensation, and a discharge port to the right side of the drain pan (as viewed from the outside front of the unit) to route the condensation outside of the HVAC and BESS (see Figure 85). The dew point rises after each cooling phase, suggesting that there is a source of moisture either inside the BESS, or outside of the BESS which is entering the BESS. The available data indicates that the BESS is not a closed system with regards to moisture infiltration as it was reported to be. The source of the moisture has not been determined to-date.



Figure 85 Drain pan discharge port below the evaporator coils.

Possible sources of moisture prior to the incident include a liquid water leak from rainwater or condensation from HVAC #3, or the entrance of water vapor through the HVAC economizer dampers which may have allowed humid outside air to enter the BESS. Economizers, if configured properly, utilize outside air under specific circumstances to condition air in the BESS instead of running the compressor in order to lower energy consumption.

The HVACs were inspected to evaluate the possibility of a liquid water leak; to confirm that economizers were installed (since units are available without economizers); and if they were installed, how they were configured. Economizers were found installed in the HVAC units (see Figure 86). The economizer doors can be configured to actuate using a dry bulb temperature sensor or an enthalpy sensor. Enthalpy sensors were found installed (see Figure 87).

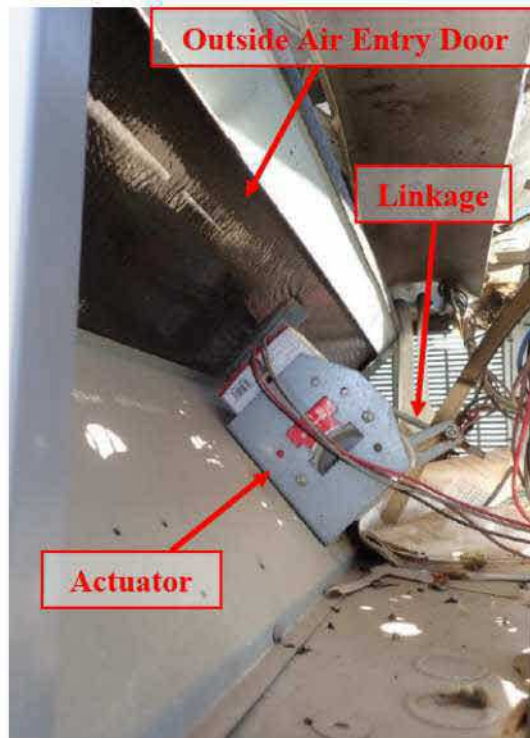


Figure 86 Economizers were found installed on HVAC units.



Figure 87 Enthalpy sensors were found installed and connected to the economizer control board in the HVACs.

Inspection of the economizer control boards revealed that they were improperly configured for use with dry bulb temperature sensors, when enthalpy sensors were installed. The economizer control board has three pins and one two pin jumper which control how it processes the sensor signal. Pins 1&2 are jumpered for enthalpy sensors, hence the “ENT” above the pins. Pins 2&3 are jumpered for dry bulb temperature sensors, hence the “DRY” above the pins. Figure 88 shows photographs of all eight control boards showing that pins 2&3 are jumpered together, which is the configuration for dry bulb temperature sensors. It is currently not known how the economizer controllers will operate and the durability of the system with enthalpy sensors connected and control boards configured to receive dry bulb sensor signals. A request was made for an inspection to collect economizer systems as evidence and possible testing, but that inspection has not taken place at the time of this report.

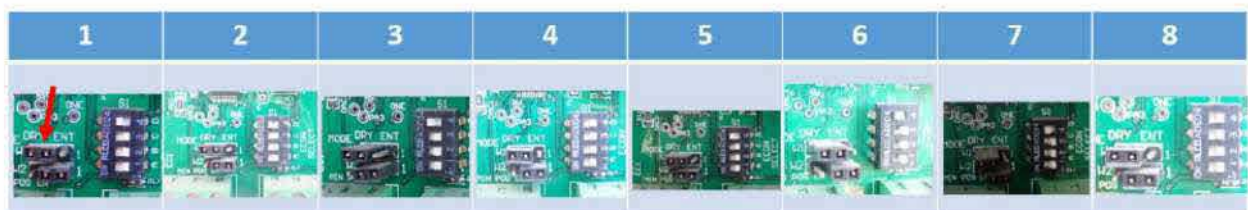


Figure 88 Photographs of all eight HVAC economizer control boards showing they were configured to receive dry bulb temperature sensor signals.

A liquid water leak may have occurred if outside rain entered the BESS, if a blockage in an HVAC condensation drain port resulted in an overflow condition, or if another abnormality in the HVAC system occurred.

Evidence of liquid marks were observed on the inside face of the HVAC #3, which mates with the exterior wall of the BESS (see Figure 89). Additionally, below the same return air cutout, drip marks were observed on the inside wall of the BESS (see Figure 90). The drip marks on the inside wall of the BESS appear to align with the spout formed by the bend in the corner flashing in the HVAC. This bend likely occurred as a result of the explosion, and therefore the drip marks on the inside wall of the BESS likely occurred after the incident. Dried liquid marks were also seen underneath Rack 15 (see Figure 92 and Figure 93) and along the same wall towards the corner of the container (see Figure 91). Figure 93 shows what appears to be rust residue on the floor. If standing water is present in the BESS, it will tend to evaporate provided

the air is not already saturated with water vapor, which in turn will be a source of water vapor which may condense onto electronics. It reportedly rained and water entered the BESS in the days following the event, although no documentation has been provided regarding those observations. This may explain those water marks. Figure 94 shows the top of HVAC #3, where it mates with the container. The black marks above the HVAC flange in areas between flange screws suggest egress of soot during the event. Those also may also have occurred as a result of the explosion, although it does not preclude a leak in this area prior to the event.

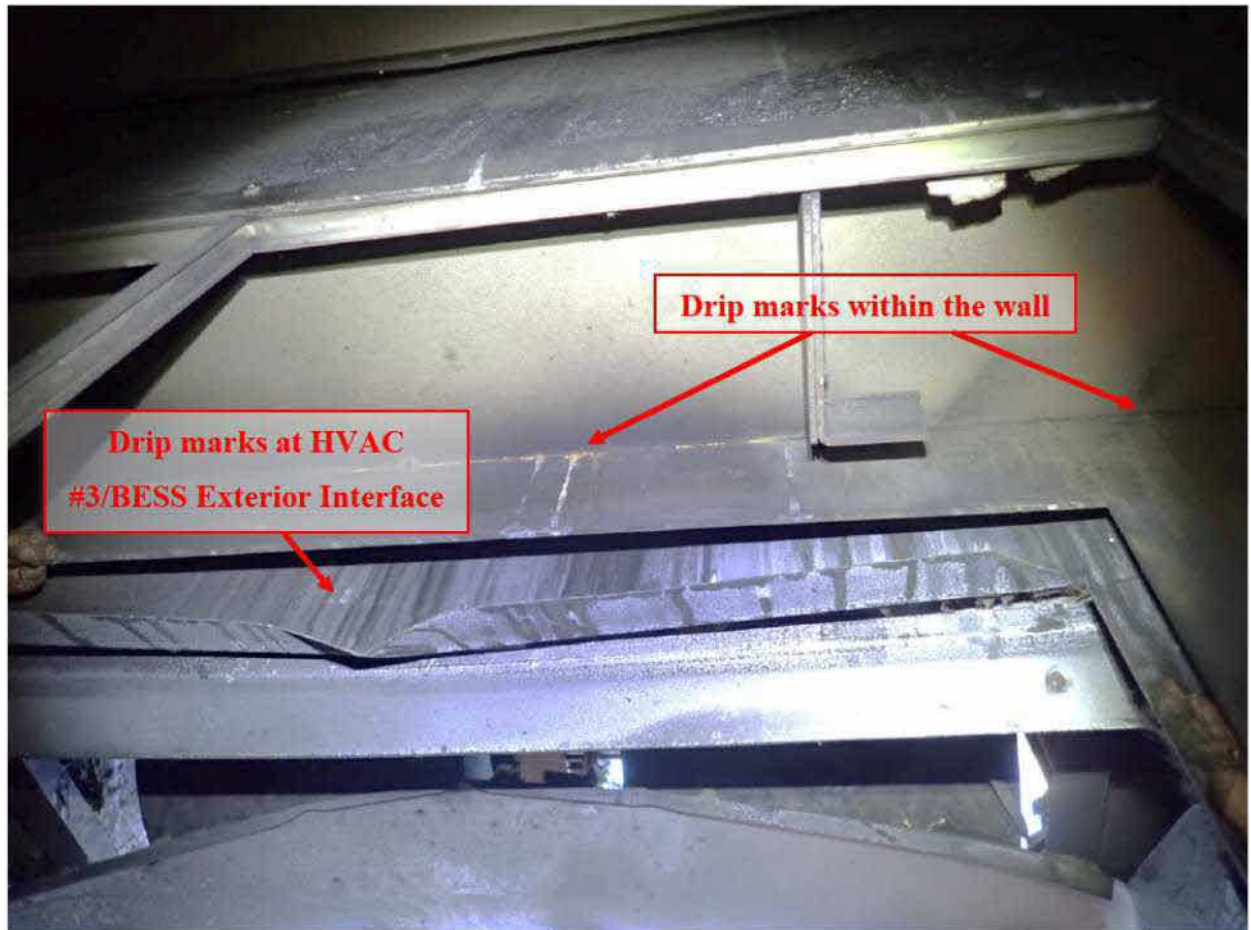


Figure 89 Evidence of liquid marks observed on the inside face of the HVAC #3, which mates with the exterior BESS wall. This photograph was taken as viewed through the return air cutout in the wall, adjacent to Rack 15.

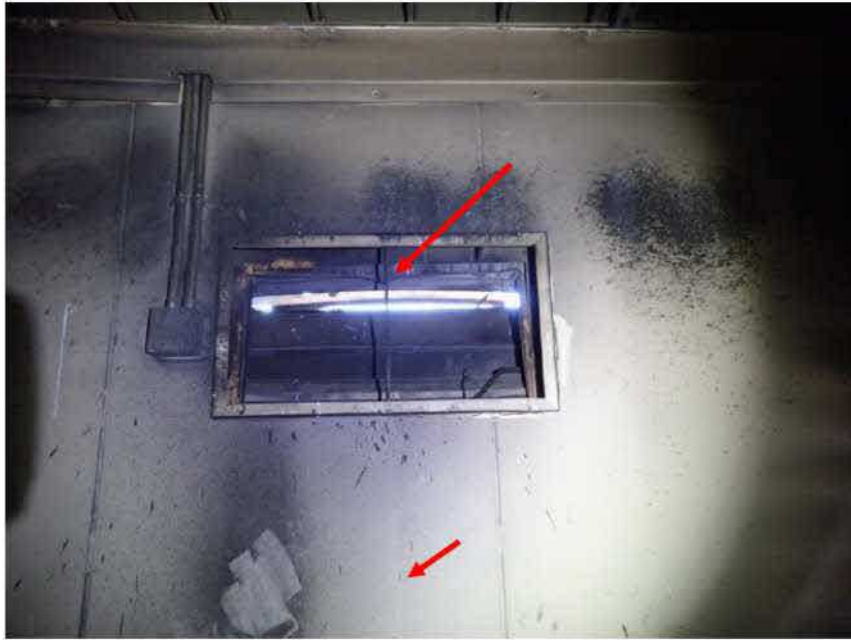


Figure 90 Liquid drip marks observed on the BESS inside wall, adjacent to Rack 15.



Figure 91 Dried liquid marks on the same inner wall of the BESS towards the corner.



Figure 92 Photograph showing the floor underneath Rack 15.



Figure 93 Photograph showing liquid marks and what appears to be residue of rust on the floor underneath Rack 15.

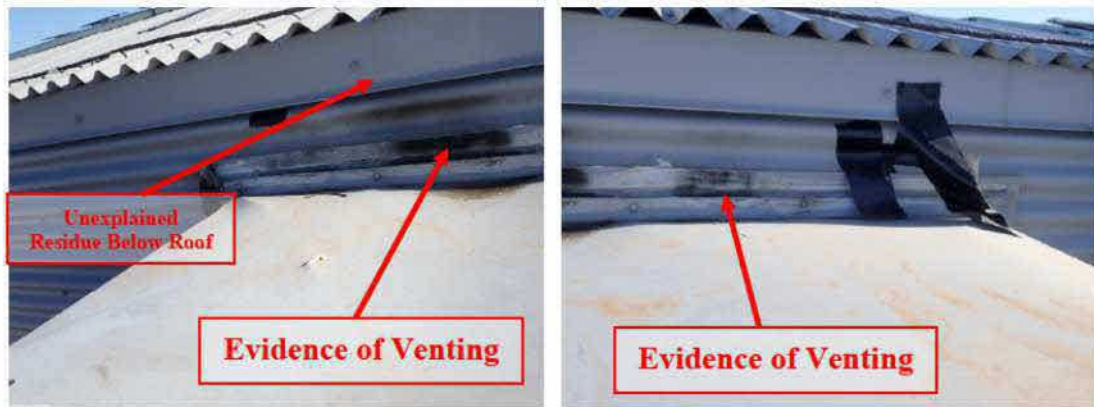


Figure 94 Photographs taken at the top of HVAC #3 where it mates with the BESS. Black residue is observed adjacent to the flange which is likely due to venting during the event, but there is also an unexplained residue dripping from underneath the corrugated roof.

Evidence of liquid intrusion into the BESS which is not readily explained by damage sustained during the incident was identified. Liquid residue was observed indicating that rainwater penetrated the room and walls of the BESS.

The BESS has a sloped, corrugated steel roof with the highest elevation on the southwest side, and the lowest elevation on the northeast side (the side with Rack 15). The roofing on the lowest elevation side includes an overhang so rain water runs off the roofing materials and falls to the ground (or onto the HVAC units, where it then falls to the ground; see Figure 95 showing the overhang).

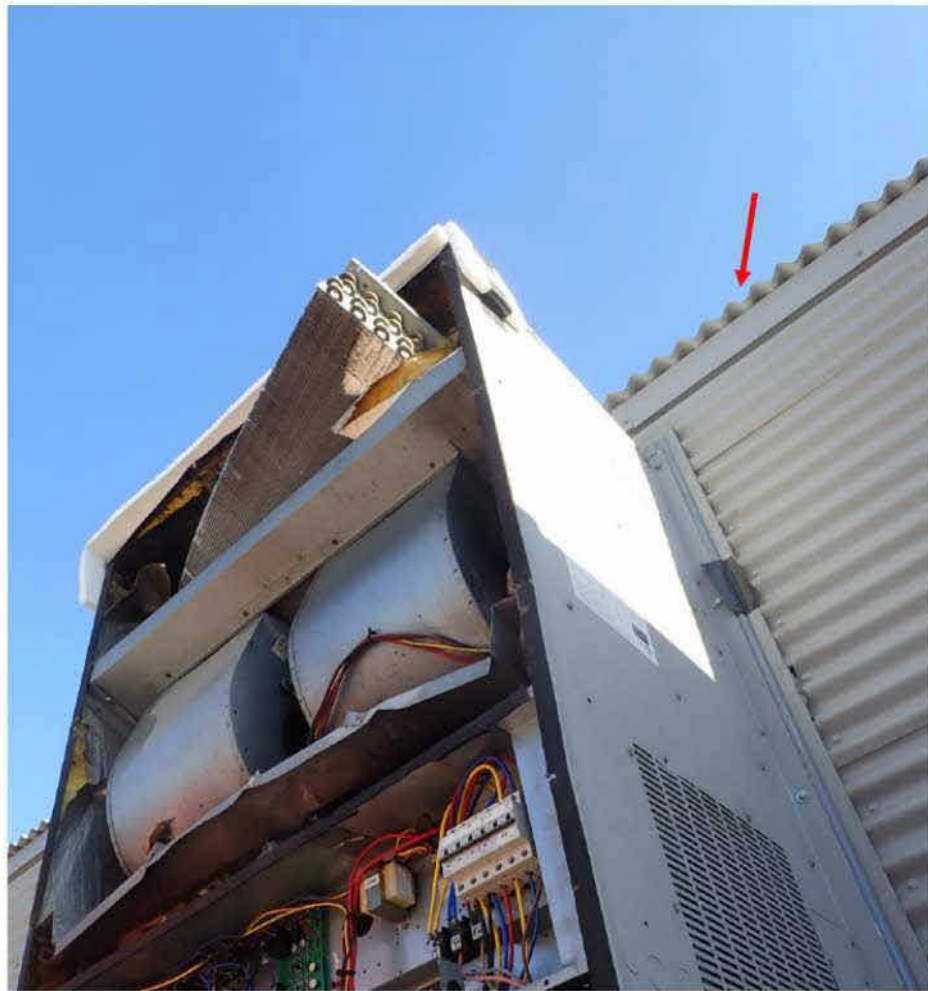


Figure 95 Photograph showing HVAC #3, and the overhang of the corrugated steel metal roof.

Figure 96 shows a zoomed in view of the left photograph in Figure 94. In this photograph, liquid residue can be seen emanating from underneath the corrugated roof cladding and running down the flashing. Liquid water leaks generally tend to follow gravity (except in some circumstances when high winds can push water). This residue indicates that rainwater penetrated the roofing material somewhere above the BESS, and that at least some water flowed down the underside of the roof to create this residue pattern.



Figure 96 Zoomed in view of the left photograph in Figure 94. There is an unexplained residue emanating from underneath the corrugated steel roofing material.

In instances like this, it is recommended to either remove the roof cladding to look for additional residue, and/or remove BESS ceiling materials to look for residue and ingress points. This way, the penetration points in the roof, moisture barrier (if any), and into the container can potentially be identified, and the likelihood of these factors existing prior to the incident or being created during the incident can be evaluated. At the time of this report, these inspections and investigative steps have not been done. There was, however, evidence that liquid was present within the wall of the BESS (see Figure 89). As a result, a liquid water leak in the roofing material and into the container cannot be ruled out as contributing moisture to the container environment.

Exponent was provided with documentation that indicates that the Punkin Center BESS had a water leak issue which reportedly resulted in a ground fault.<sup>27</sup> Exponent does not currently have any information regarding the root cause of the water leak, or the ground fault condition, which would be useful to compare against observations of the McMicken BESS for similarities and differences.

Heat damage to HVAC #3 precluded an analysis of whether a blockage occurred in the condensation drain tubing. Polymeric drain tubing was consumed by fire.

Abnormal operation of the HVAC units may also have played a role in contributing moisture to the BESS. Marvair has reportedly indicated to LG Chem that if the temperature set point is set below 20°C (68°F), there is a strong probability of having the HVAC coils freeze.<sup>28</sup> The data presented in Figure 83 show that temperatures reached approximately 17°C in the area near the HVAC #3 supply duct, suggesting that the set point may very well have been below 20°C. Accordingly, based on this information, there is a strong probability that ice was forming on the evaporator coil which may result in melting and dripping into the blowers. This water may not have been discharged to the outside (e.g. if it melted and dripped onto the blowers) and may have contributed moisture to the BESS.

Although the measurements at the five discrete locations do not indicate that condensation occurred on surfaces in the vicinity of the sensors, the spatial resolution is inadequate for a more detailed assessment to be made. Therefore, the role of condensation on electronics in the BESS cannot be ruled out as a root cause of the initial failure. For example, the water vapor concentration will be higher closer to the source, and since the sensors are not located at the source of the water vapor, higher water vapor concentrations than shown in the data may be feasible elsewhere in the container. In the days leading up to the incident, the relative humidity data (measured at the sensor locations) reached 70-75% inside the container. At typical temperatures in the container, this moisture can condense in air and on surfaces 5-6°C cooler (see Psychrometric chart in Figure 97). Similar to the water vapor concentration phenomenon,

---

<sup>27</sup> 2018-11-29 – FR & McM – FPS testing CT mount and PCS replacement v2, p2

<sup>28</sup> Email from Kevin Fok to Michael Cundy on 11/5/2019, at 8:47pm.

the temperatures may be colder in locations closest to the cooling source. There is a cold air supply duct blowing down onto the front face of Racks 13 and 15 and the nearest environmental sensors are affixed to Rack 19 and Rack 16, so the area in front of Rack 15 could be one of the colder locations within the container when HVAC #3 is running.

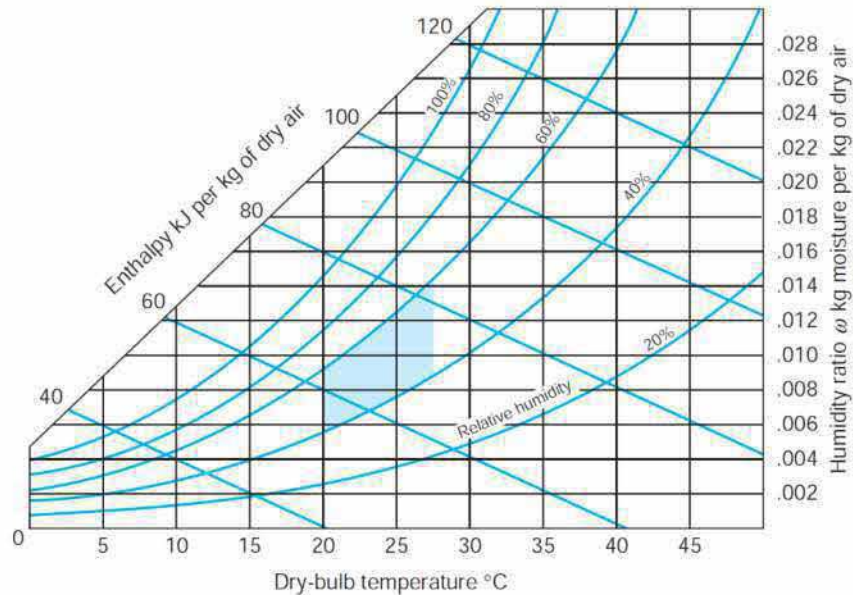


Figure 97 Psychrometric chart.

The battery module temperatures recorded by the BMS are influenced by the sensor locations, thermal properties of adjacent materials, heat generation within the modules, and the thermal inertia of the modules. The module temperature sensors are sandwiched between foam panels, which are compressed between the two submodules in the module. These temperatures will change at a slower rate than ambient air temperatures and will be influenced by heat generation and thermal transport of neighboring battery cells. Considering these effects, it is noteworthy that the measured data shows that the minimum module temperature in Rack 15 is lower than the nearby environmental sensor #3 measurement (see Figure 98) at times. If warmer, moist air from some location within the BESS were to enter colder modules, this would potentially result in condensation within the modules.

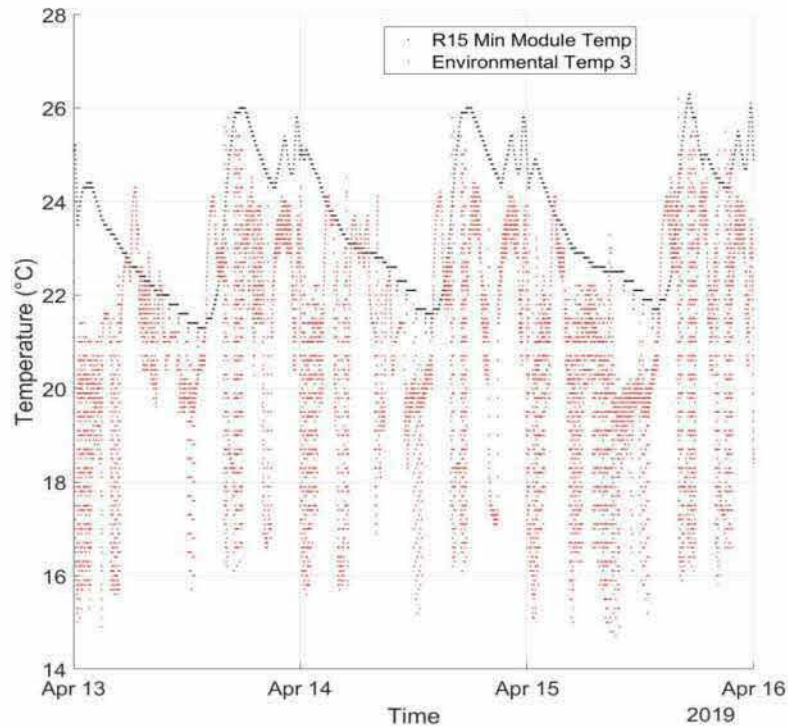


Figure 98 Plot showing that the temperature measured at the sensor three location is higher than the minimum module temperature at times.

The effects of high humidity on the electronics has also not been ruled out as a potential cause or contributor to the initial failure event. Historically, the container reached relative humidity between 80-90%, including at the location of environmental sensor #3. Figure 99 shows relative humidity measurements from June 2018 up until the incident. At these relative humidities, it would only take a drop in temperature of approximately 2°C - 4°C for water to begin condensing out. For example, if 80% relative humidity air were to migrate from the environmental sensor location #3 to the colder area below the HVAC #3 cold air supply duct, condensation may occur.

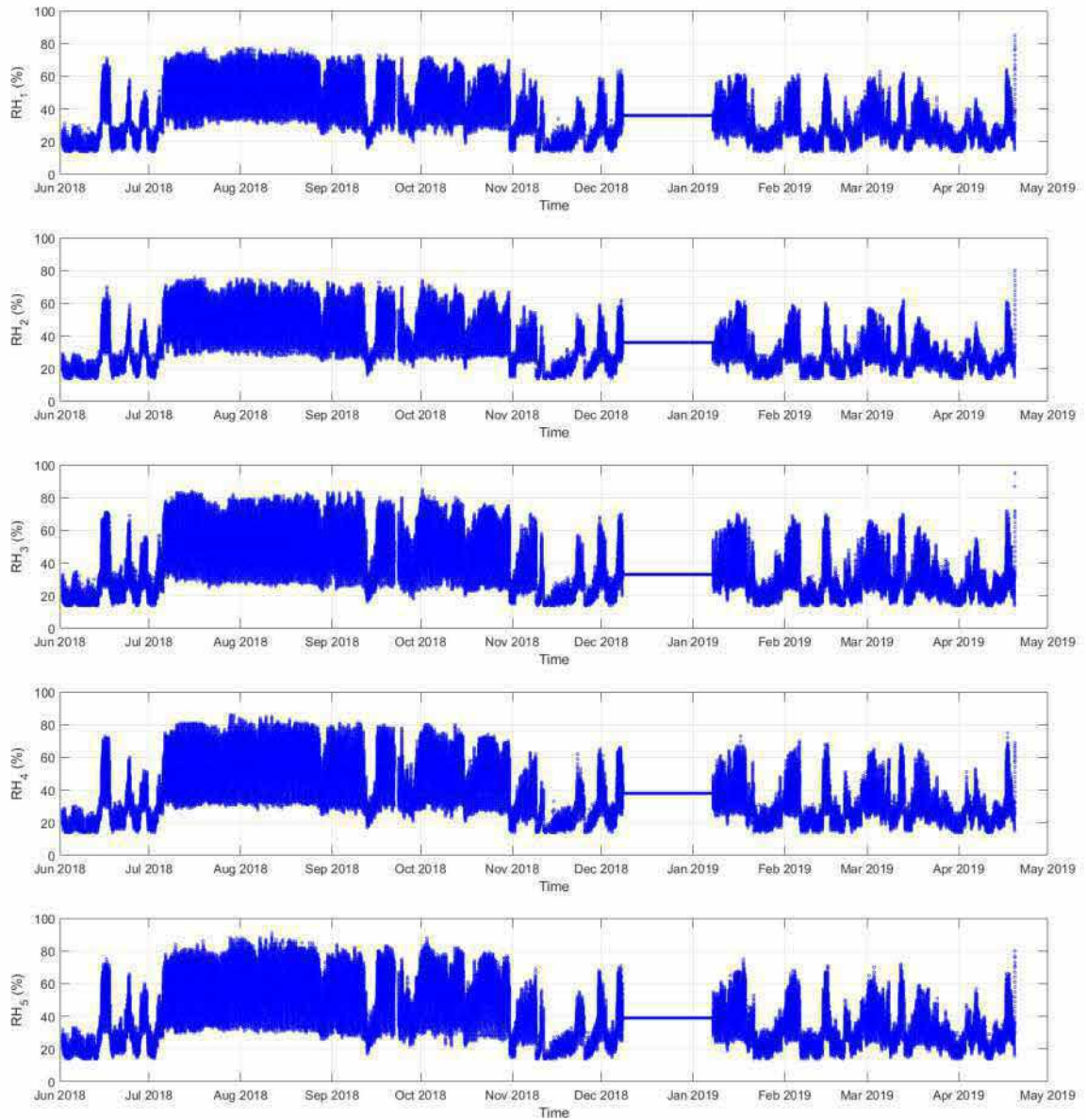


Figure 99 Relative humidities measured at each of the five measurement locations between June 2018 and the incident. Note that relative humidities regularly reached to between 80-90%, including at locations near Rack 15.

## Key Observations

- The sensor locations are not located at locations where the coldest air enters the BESS or where the moisture source is, and therefore the extremes of the temperature and humidity are not captured in the data set (poor spatial resolution).
  - As a result, the temperature and relative humidity extremes are unknown.
- Despite the poor spatial resolution, large temperature differences were still measured at the same point in time.
- The dew point temperature repeatedly increased following cooling cycles prior to the incident, indicating that the system was not a closed system and that there was a source of water vapor.
- The HVAC systems were not configured per the manufacturer's specifications, and it is currently not known if the economizer doors were open at any time during the BESS operation.
- The data that is available showed that, over the history of operation of the BESS, the relative humidity consistently reached 80% or higher. The temperature at the front face of Rack 15 will be lower than what is measured at nearby environmental sensors when HVAC #3 is running because it is below the HVAC #3 cold air supply duct. This would facilitate bulk condensation or corrosion on electronics.
- The source of water vapor has not been identified to-date.
  - Liquid marks were identified emanating from underneath the roof cladding and within the BESS wall in the vicinity of Rack 15 which are not readily explained by explosion damage and rain following the event.
  - Liquid marks were observed between the HVAC #3 and the exterior BESS wall, on the interior wall of the BESS below, along the base of the same wall, and below Rack 15. In the latter area, there appeared to be rust residue. These may have been associated with overpressure damage followed by rain after the event, given the formation of a spout on the HVAC flashing.
- The role of high relative humidity and/or condensation on electronics in the BESS cannot be ruled out as a contributor to the root cause of the initial failure.

- Localized, adverse environmental conditions may affect all modules, electronics, or components within that zone. Therefore, adverse environmental conditions are not inconsistent with a single-point initial failure or a two-point failure.

## Summary of Observations

---

Based on the system log data received, site inspections; module inspection, cell and CT analysis, and Exponent test data evaluated to date, Exponent made the following preliminary observations:

- The cell voltage and rack current measurements may not be accurately reconstructed due to the low data sample rate and likely signal aliasing. Thus, the failure analysis may not solely rely on the minimum voltage signal as a potential failure origin and failure mechanism indicator.
- Parallel cell level and module level thermal runaway characterization tests have shown that the incident voltage profile and duration are not consistent with the Cell 7 pair voltage excursion profile. This observation suggests the incident BESS failure mechanism is not associated with a single cell failure mechanism. In addition, the Rack 15 voltage dropped from 799.9V to 796.1V, ten seconds after the first voltage excursion and then recovered again to 798.9V eight seconds later and remained at this voltage for another 29 seconds before dropping to 796V again – this is not consistent with the timing of the Cell 7 pair voltage excursion. In addition, and also not consistent with the cell pair voltage behavior of a cell pair going into thermal runaway. This voltage deviation is also not consistent with the parallel cell test data.
- The suspected arcing at the edges of the Module 2's, parallel Cell 7 pair, shows that the rack electrical insulation in a different location were also compromised prior to or at the time of the arcing events and that the cells in the rack were not electrically isolated from the rack. This event likely enabled the observed electrical arcing from Module 2's, parallel Cell 7 pair to the module enclosure. This failure mechanism requires a double point electrical isolation failure mechanism.
- Currently, a low frequency parallel cell pair with a single cell thermal runaway failure event cannot explain the following:
  - The rate at which the Module 2, Cell 7 pair voltage decayed,
  - Account for the various inconsistent voltage parameters stored,
  - The rack DC voltage recovery,
  - The rack DC discharge current,

- The arcing at the edge of the two parallel cells at location 7 in Module 2,
  - Arcing at Module 2, parallel cell pair 14 to the enclosure,
  - The arcing at Module 3 positive power terminal,
  - IMD electrical isolation anomalies prior to the cell pair voltage excursion.
- There was no evidence in the cell analysis to show that Module 2 Cell 7 pair was the initiating cell.
  - The temperature and humidity extremes were not captured in the data recorded during the incident because the sensors are generally not spatially aligned with the sources of cold air and the source of water vapor. As a result, Exponent was not able to rule out if bulk condensation or corrosion occurred within or on electronics which contributed to the initial failure event. It is not known whether the environmental excursion 3 days prior to the incident played a contributing role in the failure event.

At this stage of the investigation, a single cell failure was ruled out and a double point electrical isolation failure mechanism is the most likely cause of the fire event. Given the investigation is not complete, the root cause initiating event has not yet been determined. Further analysis and additional experimental and characterization testing need to be conducted to determine which likely failure mechanism is representative of the observed data and evidence. Should additional information become available, Exponent may change these preliminary conclusions.

## Limitations

---

This is a progress report. Exponent does not consider this investigation complete, and accordingly the root cause of the incident has not yet been determined. This is not a final report and significant changes may be made to the content of the report, including observations, analysis, and conclusions, until a final report is issued. The findings presented herein are made to a reasonable degree of engineering certainty. We have made every effort to accurately and completely investigate all areas of concern identified within the scope of our investigation. However, the extent of Exponent's investigation is limited because of limited access to inspection of the remaining evidence, additional documentation review, and subsequent investigation paths including testing that may arise from further investigation.

The purpose of this report is to communicate Exponent's observations to-date based on the visual inspection of the incident BESS; modules; cells; and HVAC systems involved in the incident; as well as analysis of test data, system data, and literature. The scope of services performed during this investigation to-date may not adequately address the needs of other users of this report, particularly because the investigation is not complete, and any re-use of this report or its findings, conclusions, or recommendations presented herein are at the sole risk of the user.

Exponent was retained on behalf of LG Chem to inspect the site, observe the discharge of the battery modules and investigate the likely cause of the battery failure incident. The observations and analysis presented in this update report are based on information available at the time this update report was written. No guarantee or warranty as to future life or performance of any reviewed condition is expressed or implied. In the analysis, we have relied on our current understanding of the logged files, technical explanations by LG Chem, material samples, testing performed and information provided by LG Chem and other parties. We cannot verify the correctness of this input and rely on those parties for accuracy.

When new information becomes available or if there are perceived omissions or misstatements in this report regarding any aspect of those conditions, we ask that they be brought to our attention immediately so that we have the opportunity to fully address them.

## Appendix A – Resume for Jan Swart

---



**Exponent**<sup>®</sup>  
Engineering & Scientific Consulting

**Jan Swart, Ph.D., CFEI, CVFI**

Principal | Vehicle Engineering  
23445 North 19th Ave | Phoenix, AZ 85027  
(623) 587-4113 tel | jswart@exponent.com

### Professional Profile

Dr. Swart applies engineering and science principals in the analysis, investigation, understanding, and prevention of automotive, industrial and consumer product failures. His vast failure analysis investigation experience helps his clients to quickly and efficiently understand failure modes, failure mechanisms and failure trends. This information is then used to evaluate safety risks as well as drive product design improvements.

Dr. Swart is also internationally recognized as a battery expert. Battery technology is complex and multidisciplinary. Due to his extensive background in electronic and electrical failure analysis, Dr. Swart is unique in that he can combine his battery design knowledge with his failure analysis knowledge and thus provide his clients with in-depth and unique technical consulting services.

Dr. Swart has successfully supported many clients by providing new technology battery system consulting support by assisting his clients to rapidly build a technology knowledgebase, evaluate their current designs against state of the art in the industry, develop robust specifications, provide manufacturing support through auditing manufacturing processes and evaluating vendor failure analysis capabilities and processes.

Dr. Swart offers his client's expertise in three areas, namely, failure analysis, safety design consulting and new technology consulting support.

He is currently providing consulting services to the Automotive industry, Electronic Nicotine Delivery System (ENDS devices or eCigarettes) Industry, Portable consumer product industry, Telecommunication Industry and Utility industry

Prior to joining Exponent, Dr. Swart presented lectures on Electronics and Control Systems in South Africa and served as a member of a tertiary College Executive Council. He spent two years in renewable energy research in South African and Germany. He has held various technical and research positions in South Africa, Germany and the USA.

## **Academic Credentials & Professional Honors**

Ph.D., Engineering Management, California Coast University, 2011

Masters Diploma, Technology, Cape Peninsula University of Technology, South Africa, 1996

National Higher Diploma, Electrical Engineering, Cape Peninsula University of Technology, South Africa, 1992

National Diploma, Electrical Engineering, Cape Peninsula University of Technology, South Africa, 1991

## **Licenses and Certifications**

Certified Fire and Explosion Investigator, CFEI

Certified Vehicle Fire Investigator, CVFI

## **Professional Affiliations**

IEEE Senior Member - 2018

## **Patents**

Six patents recognized at Dell Computers.

United States Patent Application United States Patent Application 20100065637: Testing protocols for extended functionality cards.

## **Publications**

### **Books**

Loznen S, Bolintineanu C, Swart J. Electrical Product Compliance and Safety Engineering. Artech House. ISBN 13:978-1-63081-011-5, 2017.

### **Book Chapters**

Arora A, Medora NK, Livernois T, Swart J. Safety of lithium-ion batteries for hybrid electric vehicles. In: Electric and Hybrid Vehicles Overview Power Sources, Models, Sustainability, Infrastructures and the Market. Pistoia G (ed), Elsevier B.V., in press 2010.

### **Selected Publications**

Swart J. Lithium Ion Batteries and Fires Investigations. International Symposium on Fire Investigation (ISFI), Itasca, Illinois, 2018.

Swart J, Harrington R, Rajamani V, Kingsley D. The quiet transformation of vehicles without computers, to computers on wheels. IEEE Symposium on Product Compliance Engineering, San Jose, CA, 2017.

Dalal S, Swart J, Pinnangudi B. IEEE 1625 and battery powered products. IEEE Symposium on Product Compliance Engineering, San Diego, CA, 2011.

Pinnangudi B, Dalal SB, Medora NK, Arora A, Swart J. Thermal shutdown characteristics of insulating materials used in lithium ion batteries. IEEE Symposium on product compliance engineering, Boston, MA, October 2010.

Dalal S, Swart J, Pinnangudi B. IEEE 1725 and battery powered products. IEEE Symposium on Product Compliance Engineering, Toronto, Canada, 2009.

Swart J, Slee D, Loud J. Arcing and fires — Case studies. IEEE Symposium on Product Compliance Engineering, Toronto, CA, 2009.

Slee D, Stepan J, Wei W, Swart J. Introduction to printed circuit board failures. IEEE Symposium on Product Compliance Engineering, Toronto, CA, 2009.

Swart J, Slee D. Failure analysis methodology for battery powered product incidents. IEEE Symposium on Product Compliance Engineering, Austin, TX, 2008.

Arora A, Medora N, Swart J. Failures of electrical/electronic components: Selected case studies. IEEE Symposium on Product Compliance Engineering, Longmont, CO, 2007.

Swart J, Edmonds J, Arora A, Dalal S. Case studies of electrical motor and generator failures. Failures 2007, South Africa, 2007.

Swart J, Arora A, Megerle M, Nilsson S. Methods for measuring the mechanical safety vent pressure of lithium ion cells. IEEE Symposium on Product Safety and Compliance Engineering, Irvine, CA, 2006.

Swart J, Arora A, Nilsson S, Ross B. Case studies of electrical component failures. Failures 2006, South Africa, 2006.

Swart J, Arora A, Nilsson S. Characterizing the performance of battery chemistries used to power a single-person vehicle. 6th International Advanced Automotive Battery and Ultracapacitor Conference, Baltimore, MD, 2006.

Swart J, Arora A, Nilsson S, Xu Y. Going beyond industry standards in critically evaluating Lithium-ion batteries. Advancements in Battery Charging, Monitoring and Testing, Vancouver, Canada, 2005.

Swart J, Arora A, Nilsson S, Xu Y. Characterizing the vent operation of Lithium-ion cells and battery packs. 5th International Advanced Automotive Battery (and Ultracapacitor) Conference, Hawaii, 2005.

Swart J, Arora A, Nilsson S, Xu Y. Lithium-ion batteries for hybrid electric vehicles. A safety perspective. 5th International Advanced Automotive Battery (and Ultracapacitor) Conference, Hawaii, 2005.

Swart J, Wu J, Zumwalt R, Birdsley J. Case studies of IR based rapid PC motherboard failure analysis. ISTFA, Phoenix, AZ, 2002.

### **Selected Posters and Presentations**

Swart J. Lithium Ion Batteries and Fires Investigations. International Symposium on Fire Investigation (ISFI), Itasca, Illinois, 2018.

Swart J. Five good practices to minimize your lithium ion battery failure risks. Battery Power 2017, Dallas TX, 2017.

Swart J, Harrington R, Rajamani V, Kingsley D. The quiet transformation of vehicles without computers, to computers on wheels. IEEE Symposium on Product Compliance Engineering, San Jose, CA, 2017.

Swart J, Bourton D. Electronic cigarettes and battery standards. IEEE Symposium on Product Compliance Engineering, Anaheim, CA, 2016.

Swart J, Spray R. Float charging and its effects on lithium-ion cells - What can we learn? 18th International Meeting on Lithium Batteries, Chicago, 2016.

Swart J. Electronic Product Component Failure Mechanisms. IEEE EMC Society Symposium, Dresden, Germany, 2015.

Swart J, Spray R. Float Charging and its Effects on Lithium Ion Cells - What can we learn? Battery Power 2015, Denver CO, 2015

Swart J, Spray R. Latent defect characterization using Lithium ion cells. IEEE Symposium on Product Compliance Engineering, San Jose, CA, 2014.

Swart J. Lithium ion batteries 101 - What drives the safety design? Battery Power 2014, Denver CO, 2014.

Yount L, Swart J. The strive for Zero Defect — How to design fail safe control systems in critical subsystems. IEEE Symposium on Product Compliance Engineering, Austin, TX, 2013.

Swart J. Large format batteries and latent defect testing. Battery Congress 2012, Ann Arbor, MI, 2012.

Swart J. Lithium ion batteries and safety: What can we learn? MD&M West 2012, Conference, Anaheim, CA, 2012.

Swart J. Electric vehicles - A view from the past. IEEE Symposium on Product Compliance Engineering, Portland, OR, 2012.

Swart J. Battery failures: A perspective on battery system failures and test development. MD&M Minneapolis 2011 Conference, Minneapolis, MN, 2011.

Swart J, Dalal S, Pinnangudi B. Custom cell abuse tests. The Battery Show, Detroit, MI, 2011.

Swart J, Shkolnikov Y. Electrical shock and the electric powered vehicles — An introduction. IEEE Symposium on Product Compliance Engineering, San Diego, CA, 2011.

Swart J. Battery failures: A perspective on battery system failures and test development. 8th MIT Workshop on Fracture Mechanics and Battery Modeling, MIT Cambridge, MA, 2011.

Swart J, Dalal S. Custom cell abuse testing — How were the tests performed? Advanced Automotive Battery Conference, Mainz, Germany, June, 2011.

Swart J. Panel 2: Emerging battery technologies and stationary applications. 15th Annual Battcon ® 2011 International Battery Conference, Orlando, FL, 2011.

Swart J. The electrification of vehicles: An introduction into Lithium ion batteries. IEEE PSES Symposium, Boston, MA, October, 2010.

Swart J. The battery in your product failed — What now? The Battery Show, San Jose, CA, October, 2010.

Dalal SB, Swart J. Your product's battery failed — What now? Battery Power Conference 2010,

Dallas, TX, October, 2010.

Swart J, Dalal S, Pinnangudi B, Medora NK, Arora A. Lithium ion battery standards. 10th Annual International Advanced Automotive Battery Conference and Symposia, Orlando Florida, May 17-21, 2010.

Stewart S, Horn Q, Budiansky N, White K, Mikolajczak C, Wu M, Swart J. Optimizing design, charging algorithm and predicting useful life by electrochemical modeling. AABC 09 - Advanced Automotive Battery & EC Capacitor Conference, Long Beach CA, 2009.

Swart J, Arora A. Characterizing regenerative braking in a micro hybrid vehicle. AABC 09 - Advanced Automotive Battery & EC Capacitor Conference, Long Beach CA, 2009.

Arora A, Medora N, Swart J. Arc faults in hybrid and high voltage automotive electrical systems. AABC 09 - Advanced Automotive Battery & EC Capacitor Conference, Long Beach CA, 2009.

Swart J, Slee D. Failure analysis methodology for battery powered product incidents. IEEE Symposium on Product Compliance Engineering, Austin, TX, 2008.

Swart J. Constraint based product component safety evaluation. IEEE Symposium on Product Compliance Engineering, Longmont, CO, 2007.

Arora A, Swart J. Design review of a lithium-ion battery powered product. IEEE Symposium on Product Compliance Engineering, Longmont, CO, 2007.

BenKinney M, Arora A, Swart J. The influence of regulatory changes on unique product designs. IEEE Symposium on Product Compliance Engineering, Longmont, CO, 2007.

Swart J, Edmonds J, Arora A, Dalal S. Case studies of electrical motor and generator failures. Failures 2007, South Africa, 2007.

Swart J, Arora A, Nilsson S. Lithium ion batteries for micro photovoltaic power systems. Lithium Mobile Power, San Diego, CA, 2007.

Arora A, Megerle M, Swart J, Nilsson S. Methods for measuring the mechanical safety vent pressure of lithium ion cells. IEEE Symposium on Product Safety and Compliance Engineering, Irvine, CA, 2006.

Swart J, Arora A, Nilsson S, Ross B. Case studies of electrical component failures. Failures 2006, South Africa, 2006.

Swart J, Arora A. Is lithium ion chemistry viable as a renewable energy storage medium in a micro photovoltaic power system? Advancements in Battery Charging, Monitoring and Testing, Chicago, IL, 2006.

Swart J, Arora A, Nilsson S, Xu Y. Lithium-ion batteries for hybrid electric vehicles: A safety perspective. 5th International Advanced Automotive Battery (and Ultracapacitor) Conference, Hawaii, 2005.

Swart J, Arora A, Nilsson S, Xu Y. Going beyond industry standards in critically evaluating lithium-ion batteries. Advancements in Battery Charging, Monitoring and Testing, Vancouver, Canada, 2005.

Arora A, Swart J, Nilsson S, Xu Y. Characterizing the vent operation of lithium-ion cells and battery packs. 5th International Advanced Automotive Battery (and Ultracapacitor) Conference, Hawaii, 2005.

Swart J, Wu J, Zumwalt R, Birdsley J. Case studies of IR based rapid PC motherboard failure analysis. ISTFA, Phoenix, AZ, 2002.

Swart J. The unexploited low-heat hydro power in Germany using existing weirs. Karlsruhe University, Germany, 1994.

## **Project Experience**

Vehicle sensor failure investigations.

Electric vehicle fire investigations.

Defense Advanced Research Projects Agency, Tactical Technology Office, Solicitation Number: BAA-15-27. Title: Portable/Automotive Lithium Ion Battery Fire Virus.

Consumer product and hybrid vehicle battery consulting and failure analysis.

Cell, battery, and system safety testing of Lithium ion cells and battery packs.

Development of safety testing protocols of pre-production lithium ion cells and lithium ion battery packs.

Development of thermal chamber thermo electric heat pumps.

Development of safety testing protocols for pre-production power supplies, i.e. switch mode, fly-back, DC-DC.

Safety testing and analysis of pre-production power supplies, i.e. switch mode, fly-back, DC-DC.

Electronic component failures and circuit board combustion failure analysis.

Electrical house fire investigations; household electrical product fire investigations.

Electrical outdoor fire investigations.

Power supply testing and failure analysis.

Computer equipment testing and failure analysis.

Laboratory inspections of failed products and equipment.

Power failure investigations.

Stray Voltage, shock, and electrocution investigations.

Chiller fire investigations.

CPSC investigations - product safety testing and evaluation.

MIL STD 217-stress analysis on electronic components.

Design of specialized electronic testing and measuring equipment.

Evaluating and writing specifications and safety specifications for products.

CTIA BCRO and CATL Battery testing.

IEEE 1725 and IEEE 1625 conformance testing.

UN (section 38.3 - Lithium Batteries) compliance testing.

## Appendix B – Resume for Kevin White

---



**Exponent**<sup>®</sup>  
Engineering & Scientific Consulting

**Kevin C. White, Ph.D.**

Principal Scientist | Polymer Science & Materials Chemistry  
1075 Worcester St. | Natick, MA 01760  
(508) 652-8575 tel | [kwwhite@exponent.com](mailto:kwwhite@exponent.com)

### Professional Profile

Dr. White's core discipline is chemistry with emphasis on electrochemistry, polymer chemistry and the intersection of the two fields. Dr. White has extensive experience in electrochemical energy conversion, chemical/material interactions and diffusion and migration based mass transport in liquids and solids. His specialties include battery science, mass transport in polymers and interfacial chemistry/electrochemistry.

Dr. White addresses challenges related to battery technology, including: battery-device relationships, cell design, manufacturing and evaluation, performance degradation, cell safety, accelerated lifetime testing, failure analysis, and due diligence technology evaluation. His skills are applied to a range of cell chemistries including: lithium-ion, lithium primary, lead acid, nickel-metal hydride, nickel cadmium, and alkaline primary. Dr. White has extensive experience consulting across multiple industries utilizing small and large format batteries including the consumer electronics, electrified clothing, medical device, industrial equipment, power tool, automotive and aerospace industries. He has developed particular experience with complex large format battery failure analysis through direct involvement with several high profile incidents.

His polymer science practice includes processing, chemical resistance, material selection, mass transport evaluation (with particular emphasis on electric voltage driven mechanisms resulting in metal dendrite formation), and failure analysis.

Prior to joining Exponent, Dr. White was a Principal Research Scientist at Physical Sciences Inc. (PSI). His research and development efforts focused on novel architectures and materials for advanced lithium ion batteries, chemistry, and coatings for corrosion inhibition in harsh environments and novel polymer processing techniques. His research yielded a patent for an electrochemical energy device with power density characteristic of electrochemical capacitors and energy density characteristic of lithium ion batteries, and patent applications for a high energy metal oxide/conducting polymer composite cathode system for lithium ion batteries and novel structural electrode designs for lithium-ion batteries. In addition, Dr. White advanced anti-corrosion coatings for mild steel reinforcement in concrete for marine environments and the processing of polymers in functional, application driven nanoscale geometries.

Dr. White is a former NASA Fellow, an active member of the Electrochemical Society (ECS) and former Chairman of the New England Section of ECS.

## Academic Credentials & Professional Honors

Ph.D., Electrochemistry, University of Wyoming, 2000

B.S., Chemistry, Michigan State University, 1994

Visiting Scholar, University of Sao Paulo, Brazil, 1999

NASA Space Grant Fellowship, 1996-1997

## Professional Affiliations

Member of the Electrochemical Society, 1996-present

New England Section of the Electrochemical Society, 2005-present

## Patents

United States Patent 7,709,139 B2: Three Dimensional Battery, May 4 2010.

Patent Application No. 20100124702: High Energy Composite Cathodes for Lithium-ion Batteries, Published June, 2010.

Patent Application No. 20090291368: Carbon Foam Based Three-Dimensional Batteries and Methods, Published November 2009.

## Publications

Mikolajczak C, Kahn M, White K, Long RT. Lithium-ion batteries hazard and use assessment. The Fire Protection Research Foundation, July 2011.  
<http://www.nfpa.org/assets/files/PDF/Research/RFLithiumIonBatteriesHazard.pdf>

Horn Q, Hayes T, Slee D, White K, Harmon J, Godithi R, Wu M, Megerle M, Singh S, Mikolajczak C. Methodologies for Battery Failure Analysis. In: Handbook of Batteries, 4th edition. Thomas Reddy (ed), McGraw-Hill, October 2010.

Mikolajczak C, Harmon J, Hayes T, Megerle M, White K, Horn Q, Wu M. Li-ion battery cell failure analysis: The significance of surviving features on copper current collectors in cells that have experienced thermal runaway. Proceedings, 25th International Battery Seminar & Exhibit for Primary & Secondary Batteries, Small Fuel Cells, and Other Technologies, Fort Lauderdale, FL, March 17-20, 2008.

White K, Miller J, Lennhoff J. Electrospun nanofiber reinforcement of gossamer space structures. *Nonwovens World* 2004; 13(1):46.

Pope J, Sato T, Shoji E, Oyama N, White K, Buttry D. Organosulfur/conducting polymer composite cathodes II. Spectroscopic determination of the protonation and oxidations of 2,5-Dimercapto-1,3,4-thiadiazole. *Journal of the Electrochemical Society* 2002; 149(7):A939.

White K, Buttry D. An electrochemical and FTIR spectroscopic study of the aqueous oxidation of

quadricyclane and noritricyclanol. *Journal of the Electrochemical Society* 2000; 147(1):266.

### **Presentations and Published Abstracts**

White K. Predicting Long term lithium-ion battery performance through the application of chemical kinetics. MedTech Innovate Seminars at MD&M West, February, 2013.

White K, Somendapalli V, Mahr K, Horn Q. Combustion properties of Li-ion battery vent gases. IEEE Product Safety Symposium, Portland, OR, November 2012.

White K. Battery standards, regulations and beyond. The Battery Show, Detroit, MI, November 2012.

White K. Battery standards, industry best practices and achieving true battery safety. Invited Speaker at the Electrochem Symposium on Batteries for Critical Applications, Boston, MA, April 2012.

White K, Horn Q. Quantifying lithium-ion battery safety. IEEE Product Safety Symposium, San Diego, CA, November 2011.

Horn Q, White K, Spray R. Mapping thermal stability of lithium-ion cells. Invited presentation at the Dow-Kokam Advanced Battery Technology Exchange, Lee's Summit, MO, October 20, 2011.

Mikolajczak C, Harmon J, White K, Horn Q, Wu M. Detecting lithium-ion cell internal faults in real time. *Power Electronics Technology*, March 2010.

White K, Horn Q, Singh S, Spray R. Thermal stability of lithium-ion cells as functions of chemistry, design and energy. Invited Presentation, International Battery Association Conference, Kona, HI, January 2010.

White K, Horn Q. Evaluating performance, reliability and safety in lithium-ion battery cells. IEEE International Conference on Technologies for Practical Robot Applications, Waltham, MA December 2009.

Horn Q, White K. Characterizing performance and determining reliability for batteries in medical device applications. ASM Materials and Processes for Medical Devices, Minneapolis, MN, August 13, 2009.

Stewart S, Horn Q, Mikolajczak C, White K, Budiansky N, Wu M. Optimizing design, charging algorithm, and predicting useful life by electrochemical modeling. Proceedings, 9th International Advanced Automotive Battery & EC Capacitor Conference, Long Beach, CA, June 10-12, 2009.

Mikolajczak C, Harmon J, Stewart S, Arora A, Horn Q, White K, Wu M. Mechanisms of latent internal cell fault formation, screening and real time detection approaches. Proceedings, Space Power Workshop, Manhattan Beach, CA, April 20-23, 2009.

White K, Horn Q. Lithium-ion cell overcharge in the absence of battery management unit failure. 214th Meeting of the Electrochemical Society, Honolulu, HI, October 2008; and 2008 Battery Power Conference, Dallas, TX, November 2008.

Myers T, White K, Xu T. Did a dust explosion occur? Microscopic and thermogravimetric techniques to determine if dust participated in an explosion event. Proceedings, International Symposium on Fire Investigation Science and Technology, Cincinnati, OH, 2008; and Proceedings, Mary Kay O'Connor Process Safety Center Symposium, College Station, TX, 2008.

Horn Q, White K. Advances in characterization techniques for understanding degradation and failure modes in lithium-ion cells: Imaging of Internal Microshorts. Invited presentation, International Meeting on Lithium Batteries 14, Tianjin, China, June 27, 2008.

Horn Q, White K. Novel imaging techniques for understanding degradation mechanisms in lithium-ion

batteries. Presented at the Advanced Automotive Battery Conference, Tampa, FL, May 13, 2008.

Horn Q, White K. Understanding lithium-ion degradation and failure mechanisms by cross-section analysis. 211th Electrochemical Society Meeting, Chicago, IL, Spring 2007.

White K, Newman A, Boehme J, Middleton C, Pawle R, Middleton E, Lennhoff J, Horn Q, Shao-Horn Y. Anode and cathode templated three-dimensional lithium-ion batteries based on nano-fibrous electrodes. Invited presentation, 208th Electrochemical Society Meeting, Los Angeles, CA, Fall 2005.

White K, Horn Q, Newman A, Salley E, Lennhoff J. Lithium-ion batteries based on polymer modified  $V_2O_5$  cathode materials. Presented at the 206th Electrochemical Society Meeting, Honolulu, HI, October 2004.

White K, Lennhoff J, Salley E, Horn Q, Pasco-Gardner S, Racoveanu A. Advanced materials for battery applications. Invited Speaker, 8th Electrochemical Power Sources R&D Symposium, Portsmouth, VA, July 2003.

White K, Horn Q, Salley E, Lennhoff J. Three-dimensional cathode materials from electrospinning. 204th Electrochemical Society Meeting, Orlando, FL, Fall 2003.

Horn Q, White K, Shao-Horn Y, Lennhoff J. Three dimensional lithium-ion batteries based on non-woven carbon fabrics. 204th Electrochemical Society Meeting, Orlando, FL, Fall 2003.

White K, Salley E, Jayne K, Lennhoff J. Application of electrospinning to the fabrication and reinforcement of gossamer space structures. Annual Technical Conference of The Fiber Society, Natick, MA, October 2002.

White K, Buttry D, Torresi R, Bruno R. Novel  $v_2o_5$  composites for secondary lithium-ion battery application. 196th Electrochemical Society Meeting, Honolulu, HI, October 1999.

White KC, Shouji E, Buttry DA. New approaches to lithium-ion battery cathode materials. 50th Pittsburgh Conference, Orlando, FL, 1999.

White K, Buttry D, Torresi R, Torresi S. Sol-gel synthetic routes to novel lithium ion intercalation materials. Presented at the 217th national meeting of the American Chemical Society, Anaheim, CA, March 1999.

White K, Buttry D. Basic electrochemistry of some highly strained hydrocarbons. 189th Meeting of the Electrochemical Society, Los Angeles, CA, May 1996.

## Appendix C – Resume for Michael Cundy

---



**Exponent**<sup>®</sup>  
Engineering & Scientific Consulting

**Michael E. Cundy, Ph.D., P.E., CFEI**

Managing Engineer | Thermal Sciences  
23445 North 19th Ave | Phoenix, AZ 85027  
(623) 587-6783 tel | [mcundy@exponent.com](mailto:mcundy@exponent.com)

### Professional Profile

Dr. Cundy is a licensed Mechanical Engineer who utilizes his skillset in the analysis and investigation of complex mechanical and electrical systems, with an emphasis on thermal and fluid events such as the investigation of fires, explosions, carbon monoxide exposures, and water losses. His work spans different industries and often involves the investigation of vehicle systems, oil & gas processes, industrial facilities and equipment, and commercial and residential building systems, including heating, ventilation, and air conditioning (HVAC) equipment. Dr. Cundy has performed fire and explosion cause and origin investigations involving on-road and off-road vehicles, electric and hybrid vehicles, forklifts, houses, warehouses, at industrial facilities such as oil refineries and hydraulic fracturing well pads, and with industrial equipment, including boilers. He has investigated water loss claims involving hydraulic transients (water hammer) and large-scale water distribution systems. Dr. Cundy also has experience investigating the condition of industrial equipment subjected to a fire and subsequent repairs. His research and testing activities are broad and include the development and utilization of a large-scale oxygen depletion calorimeter to measure heat release rates and total heat release from large format lithium ion battery cells, flammable refrigerant testing, explosion testing of gas and electrical appliances, failing airbag inflators, and heat transfer testing in clothing. He is a resident of and actively utilizes Exponent's 147 acre Test & Engineering Center in Phoenix, Arizona, and he has worked in areas of product development, third-party validation, and product safety.

Prior to joining Exponent, he was a member of the Quantitative Laser Diagnostics Laboratory in the Walter E. Lay Automotive Laboratory at the University of Michigan in Ann Arbor, Michigan, where he developed and applied various novel laser-based spectroscopy and optical measurement systems to study combustion in internal combustion engines. His work included developing and applying temperature field diagnostics, based on laser-induced fluorescence, to evaluate heat transfer from hot gases to the engine block; utilizing particle-image velocimetry to study flow patterns in engines; and developing and applying fuel concentration diagnostics to study combustion stability, including misfires and partial burns, in an advanced internal combustion engine.

While at the University of Michigan, Dr. Cundy was an instructor for a laboratory course that focused on experimental data collection, analysis, data presentation, and error analysis.

Dr. Cundy also performed fluid mechanics research in the Non-equilibrium Thermodynamics Laboratory at The Ohio State University in Columbus, Ohio. He worked on a project funded by the U.S. Air Force

where he developed a laser diagnostic tool to measure density fluctuations in the boundary layer of a supersonic flow.

## **Academic Credentials & Professional Honors**

Ph.D., Mechanical Engineering, University of Michigan, Ann Arbor, 2012

M.S.E., Mechanical Engineering, University of Michigan, Ann Arbor, 2008

B.S., Mechanical Engineering, The Ohio State University, with distinction, with honors, 2005

Voting Member - ASTM Committee E58 on Forensic Engineering, and member of subcommittees on Electrical Incidents, Industrial Processes, and Product Defect Incidents

Alternate - National Fire Protection Association (NFPA) Technical Committee on Recreational Vehicles, 2012-2014

## **Licenses and Certifications**

National Association of Fire Investigators Certified Fire and Explosion Investigator (CFEI), #21707-12362

Licensed Professional Mechanical Engineer, Arizona, #55526

Labview Associate Developer (lapsed), #100-310-1923

Fire Investigation 1A: Fire Origin and Cause Determination; accredited by the California State Fire Marshal

Fire Investigation 1B: Techniques of Fire Investigation; accredited by the California State Fire Marshal

## **Professional Affiliations**

National Fire Protection Association - NFPA

Society of Automotive Engineers - SAE

American Society of Mechanical Engineers - ASME

ASTM International

National Association of Fire Investigators - NAFI

## **Publications**

Jokar A, O'hern S, Anderson D, Cundy M, Ogle R. Flammable Refrigerants: Efficiencies, Safeties, and Lessons Learned. Proceedings of the 2019 ASHRAE Winter Conference, Atlanta, GA, 2019.

Morse T, Cundy M, Kytomaa H. Vehicle fires resulting from hot surface ignition of grass and leaves. SAE Paper 2017-01-1354, 2017.

Colwell JD, Cundy M. Full-scale burn test of a 1992 compact pickup truck. SAE Paper 2013-01-0209, 2013.

Cundy ME. Development of high-speed laser diagnostics for the investigation of scalar heterogeneities in engines. Ph.D. dissertation, University of Michigan, 2012.

Cundy ME, Trunk P, Dreizler A, Sick V. Gas-phase toluene LIF temperature imaging near surfaces at 10 kHz. *Experiments in Fluids* 2011, DOI 10.1007/s00348-011-1137-8.

Cundy ME, Sick V. Hydroxyl radical imaging at kHz rates using a frequency quadrupled Nd:YLF laser. *Applied Physics B* 2009; 96(2):241-244.

Cundy ME, Schucht T, Thiele O, Sick V. High-speed laser-induced fluorescence and spark plug absorption sensor diagnostics for mixing and combustion studies in engines. *Applied Optics* 2009; 48(4):B94-B104.

Cundy ME. Detection and measurement of density fluctuations induced by a magnetohydrodynamic force in a supersonic boundary layer. Undergraduate Honors Thesis, The Ohio State University, 2005.

Meyer R, Nishihara M, Hicks A, Chintala M, Cundy M, Lempert WR, Adamovich IV, Gogineni S. Measurements of flow conductivity and density fluctuations in supersonic nonequilibrium MHD flows. *AIAA Journal* 2005; 43(9):1923.

## Conference Presentations

Cundy M, Bennett T. Breathing Easier: Evaluating Carbon Monoxide Injury Claims. DRI Product Liability Seminar, Austin, TX, 2019.

Cundy M, Schucht T, Thiele O, Sick V. Novel optical diagnostics for mixing and combustion studies in engines. Poster presented at the University of Michigan Graduate Student Symposium, Ann Arbor, MI, November 2008.

Cundy M, Sick V. Misfire analysis techniques in a direct injection engine. Presented at the Gordon Conference on Laser Diagnostics in Combustion, Oxford, UK, August 2007.

Cundy M, Lempert W. Study of the effect of electromagnetic fields on density fluctuations in a supersonic boundary layer. Presented at the Denman Undergraduate Honors Research Forum, Columbus, OH, May 2004.

Cundy M, Sick V. Hydroxyl radical imaging at kHz rates using a frequency quadrupled Nd:YLF laser. Presented at the University of Michigan Graduate Student Symposium, Ann Arbor, MI, November 2009.

Drake MC, Fansler TD, Cundy M, Sick V. High-repetition-rate Mie scattering and particle-image-velocimetry for flow and combustion diagnostics in a direct-injection gasoline engine. Presented at the 6th U. S. National Combustion Meeting, Ann Arbor, MI, May 2009.

Cundy M, Schucht T, Thiele O, Sick V. Novel optical diagnostics for mixing and combustion studies in engines. Presented at the University of Michigan Graduate Student Symposium, Ann Arbor, MI, November 2008.

## Appendix D

---

The single cell pair voltage excursion cannot be accounted for, for the following reasons:

- At 19:54:30 rack voltage was 798.9V, the cell sum voltage was 800.4V and the cell voltage averaged 4.083V. When a calculation is performed, the average cell voltage should be 4.0825V. It is not known how many decimals after the comma is considered for the calculation. Also at the point the rack voltage dropped by 0.3V and the cell sum voltage remained the same, the possible loss voltages of the minimum cell of approximately between 0.069V (4.061V-3.992V) or 0.106V (4.098V-3.992V) cannot be accounted for.
- At 19:54:32 rack voltage changed from 798.9 to 799.6V – a 0.7V jump, the cell sum voltage dropped from 800.4 to 800.2V, the maximum cell voltage dropped from 4.098V to 4.097V. The average cell voltage remained at 4.083V. The possible loss voltages of the minimum cell of approximately between -0.01V (3.992V-4.002V) and 0.095V (3.992V-4.097V) cannot be accounted for.

The same observation can be made for the other available CAN BUS data of the event.

## Appendix E

---

It was noted in two previous charge cycles, that the rack DC voltage will relax by about 2V, immediately after the charge current has stopped. However at the time of the failure event the rack voltage relaxed by approximately 3.8V, nearly twice the normal relaxation voltage (see Table 2, at 19:54:38 and 19:55:40) and then recovered again after approximately eight seconds at 19:54:48 to 798.9V (with a discharge current). As the rack discharge current increased, the rack voltage dropped again to 796V. This suggests that more than one cell voltages in the rack recovered to pre-voltage excursion levels. This is not consistent with the parallel cell failure testing voltage profile. This observation also suggests that the cause for the rack DC volt drop, relaxation and hence the rack voltage recovery was not due to a single parallel cell failure. A rack DC discharge current of 3.6A was noted shortly after charging. This current is abnormal. A normal end of charge profile is shown in Figure 39 and (see bottom red arrow), after the charge current stopped, the DC discharge current remained 0A through the current transducer.